Study of molecular matter wave interferometers in Ramsey and Ramsey-Bordé configuration

Von der Fakultät für Mathematik und Physik der
Gottfried Wilhelm Leibniz Universität Hannover

zur Erlangung des Grades

Doktor der Naturwissenschaften
Dr. rer. nat.

genehmigte Dissertation
von

Dipl.-Phys. Sha Liu
geboren am 29.12.1980 in Hunan, China
2009

Referent: Prof. Dr. Eberhard Tiemann

Koreferent: Prof. Dr. Jan Arlt

Tag der Promotion: 15.January.2010

To my Parents and Arnaud Lecallier

Abstract

Study of molecular matter wave interferometers in Ramsey and Ramsey-Bordé configuration - Sha Liu

This thesis deals with the characterization of matter wave interferometers with laser induced beam splitters in a supersonic K_2 beam, and with the investigation of the suitability of their applications in high precision measurements. Two kinds of interferometer configurations are implemented. One is the Ramsey interferometer, with two identical laser beam splitters across the molecular beam in the same direction, which result in transversally partial overlap of the matter waves. The other is the Ramsey-Bordé interferometer with two pairs of counter-propagating laser beam splitters across the molecular beam, which result in transversally fully overlapped wave packets.

First experiments were done by comparing the interference fringes detected from the excited state and ground state exits of the Ramsey-Bordé interferometer. Different molecular transitions are probed for the ground state detection. Data analysis reveals the signal from an embedded Ramsey interferometer. A model of propagation and interference of matter wave packets for the interferometers is developed to explain the phenomena in our special experiment situation.

A Ramsey interferometer is constructed with phase stabilization. After the analysis of its phase stability, it was used to compare the different detection schemes, which reveals the ground state as the more suitable detection channel. This Ramsey interferometer with ground state detection is used for observing the change of the interference contrast with modification of the transversal coherent length. The observation is consistent with the wave packet model.

The Ramsey interferometer is also applied to measure molecular transition dipole moments. For that purpose the molecular ground state is coupled with a near resonant light field to an excited state by AC-Stark effect. The imprinted phase on the matter wave is read out by the interferometer and will allow to derive the transition dipole moment of the coupling transition.

An extension of the earlier work for a systematic analysis of the cold collision between the molecules and ground state atoms is done with Ramsey-Bordé interferometer. The density of the collisional medium is changed by deflecting atoms out of the molecular beam. The phase shift derived from the measurement is too small to identify undoubtedly the collisional effect.

Keywords

Ramsey interferometer, Ramsey-Bordé interferometer, AC-Stark effect, cold collision between atoms and molecules

Zusammenfassung

Studium eines molekularen Materiewellen- Interferometers in Ramsey - und Ramsey-Bordé Konfiguration - Sha Liu

Die Dissertation handelt von der Charakterisierung von Materiewellen- Interferometern mit Lichtfeldern als Strahlteiler für die Materiewelle in einem Überschallstrahl von K2, sowie von der Untersuchung ihrer Eignung für die Anwendung in hochgenauen Messungen. Zwei Typen von Interferometer-Konfigurationen wurden realisiert. Eins ist das Ramsey-Interferometer, mit zwei identischen Laserfeldern gleicher Ausbreitungsrichtung als Strahlteiler am Molekülstrahl, die einen teilweise Überlapp der Materiewellen in transversaler Richtung erzeugen. Das andere ist ein Ramsey-Bordé Interferometer mit einem Paar von Laserfeldern gleicher Ausbreitungsrichtung und einem Paar von gleichgerichteten Laserfeldern entgegen gesetzter Richtung als Strahlteiler auf dem Molekülstrahl, welches transversal vollständig überlappende Wellenpakete ergibt. In ersten Experimenten werden die beobachteten Interferenzen des Interferometer-Ausganges mit Molekülen im angeregten Zustand mit solchen des Ausganges mit Molekülen im Grundzustand verglichen. Verschiedene Molekülübergänge werden für den Grundzustandsnachweis untersucht. Die Datenanalyse zeigt, dass die Beobachtungen zusätzlich ein Signal von einem Ramsey- Interferometer enthalten. Es wird ein Modell der Ausbreitung und Interferenz der Materiewellenpakete entwickelt, um die Beobachtungen in unserer speziellen experimentellen Situation zu erklären. Es wird ein Ramsey-Interferometer mit einer Phasenstabilisierung konstruiert. Nach der Analyse seiner Phasenstabilität wird es zum Vergleich der verschiedenen Nachweisschemata verwendet, was den Grundzustand als den besser geeigneten Nachweiskanal offenbart. Dies Ramsey-Interferometer mit Grundzustandsnachweis wird für die Beobachtung der Änderung des Interferenzkontrastes bei Änderung der transversalen Kohärenzlänge verwendet. Die Boebachtungen sind konsistent mit dem Wellenpaket-Modell. Das Ramsey-Interferometer wird auch eingesetzt für Messungen von molekularen Übergangsdipolmomenten. Zu diesem Zweck wird der molekulare Grundzustand mit einem nah-resonanten Lichtfeld und einen angeregten Zustand mit dem dynamischen Starkeffekt gekoppelt. Die auf die Materiewelle aufgeprägte Phase wird durch das Interferometer ausgelesen und und erlaubt die Bestimmung des Übergangsdipolmomentes des koppelnden Übergangs. Eine Erweiterung früherer Arbeiten für eine systematische Analyse von kalten Stößen zwischen Molekülen und Atomen im Grundzustand mit dem Ramsey-Bordé Interferometer wird durchgeführt. Die Dichte des stoßenden Mediums wird durch Ablenkung der Atome aus dem Molekülstrahl verändert. Die aus den Messungen bestimmte Phasen-

verschiebung ist zu klein, um den Effekt eindeutig zu identifizieren.

Schlagworte

Ramsey Interferometer, Ramsey-Bordé Interferometer, dynamischer Starkeffekt, kalte Stöße zwischen Atomen und Molekülen.

Contents

Contents

1. Introduction

One of the fundamental presentation of quantum mechanics is the wave-particle dualism. This macroscopically not directly observable phenomenon has led to a series of basic experiments in understanding the interplay between wave and particle character since the introduction of quantum mechanics. An experiment like Compton scattering effect proves the particle characteristics of the electromagnetic wave, recognized through the equation $p = h/\lambda$, p is the momentum and λ is the wavelength of the photon. De Broglie was the first person who came to the idea that the relationship between momentum and wavelength is valid not only for classical waves like light but also for particles. Typical wave phenomena like diffraction and interference should also be observed on matter waves. To get stable interference pattern, the interfering matter wave packets need to have constant phase difference. In order to get the ideal case of identical stable sources, people come to the idea of coherently splitting the main source into multiple secondary sources. In order not to wash out the interference pattern, the whole particle ensemble representing the wave needs to have a narrow velocity distribution like the coherence condition of light beams.

The high momentum due to the large particle mass leads to short de-Broglie wavelength, which requires a comparable scale to observe the wave characteristic. For example, the typical light wavelength is several hundred nanometers for visible region, while the typical atomic wavelength is several picometer at room temperature. Diffraction and interference experiments were first realized by well collimated electron beams and highly collimated neutron beam on crystals as beam splitters. The extension to experiments with matter waves of complex particles like atoms and molecules came much later. The problem for long time was how to split and recombine the matter wave with the short wavelength of 10^{-12} m at room temperature [1].

The developments of nanotechnology and laser physics provide new possibilities to realize atom and molecule interferometers. Periodical structures at nanometer scale can be used to deflect the matter wave working as beam splitters [2], [3] and [4]. With a series of gratings a complete interferometer can be constructed. These methods are especially useful for large molecules, because this mechanically splitting avoids dealing with complex internal energy levels

[5] [6].

To access the inner degrees of freedom of the particles is also important. A certain quantum state can be addressed by implementing a resonant laser field working as the beam splitter. Through the absorption or emission process, the photon momentum is transferred to the particle. By the unique choice of the interaction parameters, a beam splitter will fix not only the inner state of a matter wave but also the momentum. By this way, an interferometer comparable to the one mentioned before with gratings can be constructed by a series of laser beam splitters.

The detection of interference is normally done by measuring the particle number. Different particle detectors are implemented in different experiments. Laser spectroscopy is the natural method if laser beams are already used as beam splitters.

In our experiment, resonant laser fields are used as the beam splitters to build an interferometer on a supersonic K_2 beam. The simplified molecular potential scheme of K_2 is presented in figure 1.1. The molecular beam out of an oven prepares for example a population of K_2 in vibrational level $v'' = 0$ and $J'' = 25$ in the molecular ground state.

The beam splitters work with the resonant transition $R(25)$ in the $(27-0)$ band of the $b^3\Pi_u \leftarrow X^1\Sigma_g^+$ transition. The transition moment for this transition, in zero order forbidden, stems from mixing of the $b^3\Pi_{u0^+}$ state with the $A^1\Sigma_u^+$ state by spin-orbit interaction. Because of this weak interaction the life time of state b is fairly long, i.e. in the order of microseconds. Due to the high molecular velocity around 1000 m/s, a separation of less than 1 mm inside the interferometer results in a time of flight less than one microsecond. This allows the coherence built up by the laser beam splitter not to be destroyed by the spontaneous decay. Another characteristic of the molecular potential is the richness in vibrational and rotational energy levels. The probability to reach the original ground state from spontaneous decay is small. Due to the long lifetime of the ground state levels, the interference information carried in the ground state molecular population can be preserved, which enables the comparison of detection of interference patterns from ground and excited states simultaneously.

Various physical effects like collisions between atoms and molecules, interaction between monochromatic field and particles e.g. coupling the state $X^1\Sigma_g^+$ through the transition $Q(25)$ $(4-0)$ $B^1\Pi_u \leftarrow X^1\Sigma_g^+$ in figure 1.1 can be studied between the pair of laser beams. All these effects will contribute to the phase of the matter wave. If one of the matter waves is influenced differ-
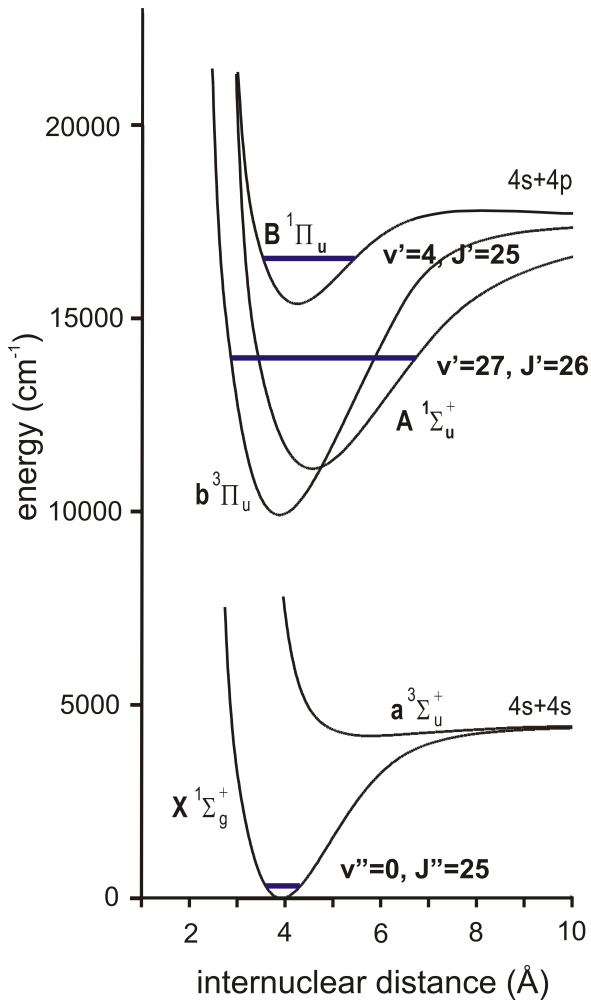
Figure 1.1.: Simplified molecular potential scheme of K_2.

ently than the other, the phase difference results in the shift of the interference pattern. The topic of this thesis is to measure the different physical properties using a matter wave interferometer.

Chapter 2 describes the theoretical background to understand the Ramsey interferometer and Ramsey-Bordé interferometer. The phase accumulation of a matter wave through a number of laser beam splitters is explained with a schematic view. The physical interactions introduced along the traveling paths can add an additional phase to the matter waves and appear as a shift of the interferogram.

Chapter 3 describes the experimental components for building the interferometers: the vacuum apparatus, the diode laser system and its stabilization scheme.

Chapter 4 gives a detailed description of the Ramsey interferometer embedded in the Ramsey-Bordé interferometer, the detection of interference fringes in the ground state and excited state exits simultaneously, the data analysis and a discussions of the results.

In chapter 5, the relative phase of the laser beam splitters of Ramsey interferometer is stabilized and the resulting stable Ramsey fringe is applied for a series of characterizing experiments, like the relaxation of the population in the molecular ground state and the modification of the coherence length of the matter wave.

Chapter 6 is based on chapter 5, using the stabilized Ramsey interferometer to measure molecular transition dipole moments by the AC-Stark effect.

Chapter 7 is an example of the usage of a Ramsey-Bordé interferometer to study a cold collision process between molecules in different internal states and ground state atoms within the molecular beam.

2. Theory of matter wave interferometer

The theory of matter wave interferometer is discussed already in different books like [7] and theses like [8] [9]. Here I just try to give the reader necessary information to understand the interferometer experiments in our group. In the following part, a schematic view of the interferometer will be given.

2.1. Beam splitter

The laser beam splitter used in our experiment can be understood as a traveling wave interacting with a two-level system. The traveling wave is a laser beam composed of photons. Each photon is with energy $E = \hbar\omega_L$ and momentum $\vec{p} = \hbar\vec{k}$. The two level system denotes that there is only one resonant transition with the laser field, with lower energy level as ground state $|g>$ and higher energy level as excited state $|e>$, the transition frequency between $|g>$ and $|e>$ is $\omega_0/2\pi$.

According to energy and momentum conservation, before and after the absorption of a photon, the total energy is described in equation 2.1

$$\frac{\vec{p_0}^2}{2M} + \hbar\omega_L = \frac{(\vec{p_0} + \hbar\vec{k})^2}{2M} + \hbar\omega_0 \tag{2.1}$$

$\vec{p_0}$ is the initial momentum of the molecule, M is the molecular mass, $\hbar$ is the Planck constant. The left side of the equation is the total energy before absorption, which comprises the kinetic energy of the molecule in ground state $\vec{p_0}^2/2M$ and the energy of the photon $\hbar\omega_L$. The right hand side describes the situation after the absorption, which is the kinetic energy of the molecule in the excited state $(\vec{p_0} + \hbar\vec{k})^2/2M$ and the internal energy $\hbar\omega_0$ of the molecule due to the transition.
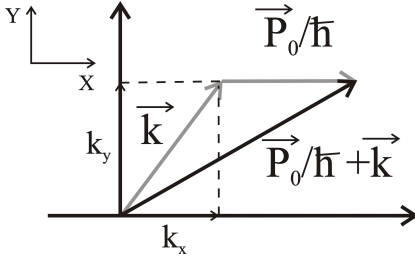
Figure 2.1.: Scheme of the wave vector construction for photon absorption

Equation 2.1 can be simplified to [9],

$$\frac{\vec{k} \cdot \vec{p_0}}{M} = \Delta - \delta \quad \text{with photon recoil } \delta = \frac{\hbar k^2}{2M}, \quad \text{laser detuning } \Delta = \omega_L - \omega_0$$
$$(2.2)$$

Figure 2.1 shows the scheme of the wave vector construction for the photon absorption process. The coordinate system drawn in figure 2.1 with the molecular beam in x direction will be used for the whole thesis unless especially specified in some sections. The photon with wave vector $\vec{k}$ interacts with the molecule with momentum $\vec{p_0}$ at a certain angle, such that the scalar product fits equation 2.2. The result is the molecular matter wave with wave vector $\vec{P_0}/\hbar + \vec{k}$. $\vec{k}$ has component k_x parallel to x direction and k_y parallel to y direction. Due to momentum conservation, after absorbing a photon, the molecule will be accelerated in x direction with momentum $\hbar k_x$ and in y direction with $\hbar k_y$, which leads to a shift in x and a displacement in y, respectively. The k_x can be written out explicitly as

$k_x = \frac{M}{p_0}(\Delta - \delta) = \frac{1}{v_0}(\Delta - \delta)$, v_0 is the initial molecular velocity.

The excitation happens with a certain transition probability P_t according to the transition moment and laser intensity. After the interaction, the molecule is in a superposition of ground state with probability $1 - P_t$ and excited state with probability P_t. A simple plane wave picture will be used to describe the matter wave because the spatial divergence in transverse direction is small due to narrow velocity distribution in transverse direction. The collimation ratio of transverse to longitudinal is 1/1000, and the additional transverse velocity due to photon absorption is 5 orders of magnitude smaller than the original transverse velocity. A matter wave in ground state can be described by $\Psi \propto e^{ik_0 x} \cdot |g>$, where $k_0 = p_0/\hbar$ is the initial wave vector of a molecular matter wave. Starting at the first laser beam splitter x = 0, at the point x = L the
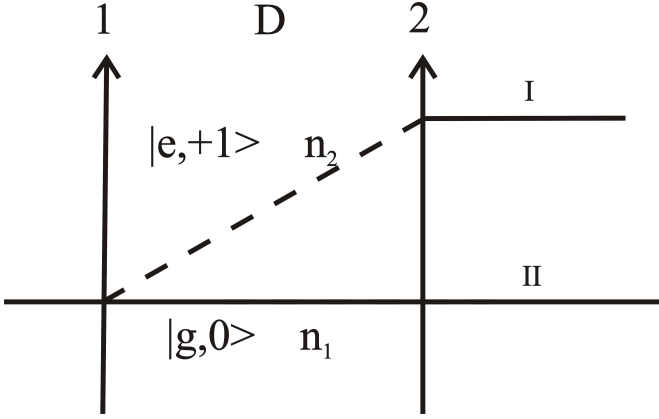
Figure 2.2.: The splitting of molecular matter wave in different internal states with different index of refractions n_i. By a pair of co-propagating laser beams, the Ramsey interferometer is built from the overlap of matter waves from path I and II.

forward traveling wave functions can be written as

$$\Psi_e \quad \propto \quad \sqrt{P_t} \cdot e^{i((k_0+k_x)L+\phi_1)} \cdot |e> \qquad (2.3)$$

$$\Psi_g \quad \propto \quad \sqrt{1-P_t} \cdot e^{ik_0L} \cdot |g> \qquad (2.4)$$

ϕ_1 is the phase of the electro-magnetic wave added on the matter wave by the induced electric dipole, $|g>$ and $|e>$ denote the ground and excited states respectively.

A new wave vector $k = nk_0$ with complex index of refraction n can be introduced. Any physical properties introduced at the traveling path of the interferometer can be described by n macroscopically. For more theory on the index of refraction picture please refer to paper [2] and thesis [9].

2.2. Ramsey interferometer by two laser beam splitters

Laser fields are used to split and to recombine the matter waves to form an interferometer. Figure 2.2 shows the basic scheme of a Ramsey interferometer

with two laser beam splitters. The solid lines represent traveling molecules in the ground state, the dashed lines molecules in the excited state. The arrows with numbers 1 or 2 are the laser beams acting as beam splitters that the molecules encounter. The space between them is called dark zone with the length D. The state $|g/e, m>$ labels by g or e the molecular state, and by m the number of the transferred photon momenta in units of $\hbar k$, where $\vec{k}$ is the photon wave vector. When molecule does not absorb the photon, it is in the state $|g,0>$, which experiences an index of refraction n_1 in the dark zone. When a molecule absorbs one photon, the traveling direction is changed due to additional momentum and the molecule in state $|e,+1>$ sees an index of refraction n_2, because the excited state molecules are in a different electronic state. The laser beam 2 is identical to laser beam 1 in frequency, power and geometry. For a molecule in the excited state, the transition probability for a stimulated emission is also P_t if spontaneous emission is neglected and the quantum state prepared by laser beam 1 is preserved through the travel from laser beam 1 to 2. After beam splitter 2, there are four possible matter waves, two are in the ground state, another two are in the excited state. In figure 2.2, only the pair in the ground state is kept for illustration, the different paths are marked by I and II. Molecular waves in the same state can interfere with each other depending on their phase difference and coherence properties if the waves overlap. The phase will be calculated in the coming paragraph. The contrast is a function of P_t, for $P_t = 50\%$ the contrast is highest[10]. So in the following paragraph, A $= \sqrt{P_t} = \sqrt{1 - P_t}$ is used to denote the wave amplitude for both ground and excited state. The contrast is also determined by the overlap of the matter waves in transverse direction which depends on the deflection angle and dark zone length. For the signal contrast detected in reality, the spontaneous decay also needs to be taken into consideration.

The detected signal strength of the matter waves in the ground state is proportional to the population probability of this state

$$\text{I} \propto |Ae^{i\phi_{12}^I} + Ae^{i\phi_{12}^{II}}|^2 = 2A^2 cos(\phi_{12}^I - \phi_{12}^{II}) + 2A^2$$

For the matter wave through path I, the molecule absorbs and emits one photon, the phase ϕ_{12}^I of the matter wave acquired between beam splitter 1 and 2 can be written as

$$\phi_{12}^I = n_2(k_0 + k_x)D + \phi_1 - \phi_2 \tag{2.5}$$

Through path II the phase of the matter wave in the ground state is

$$\phi_{12}^{II} = n_1 k_0 D \tag{2.6}$$

the phase difference between the two wave packets is

$$\Delta\phi = \phi_{12}^{I} - \phi_{12}^{II} = (n_2 - n_1)k_0 D + n_2 \frac{D}{v_0}(\Delta - \delta) + \phi_1 - \phi_2 \tag{2.7}$$

If $n_1 = n_2 = 1$ for example, there is no potential, no collision, not any physical interaction with the matter wave traveling through the dark zone length D, the phase difference between the matter waves will be

$$\Delta\phi = \frac{D}{v_0}(\Delta - \delta) + \phi_1 - \phi_2. \tag{2.8}$$

This first term in equation 2.8 is a linear function of the laser frequency detuning Δ, where the Doppler effect from the velocity component in direction of the laser beam is neglected. The second term comes from the phases of the laser fields. The oscillation pattern appears as the laser frequency tunes linearly.

Experiments on the Ramsey interferometer are described in chapter 4, 5.

If $n_1 \neq n_2$ comparing the situations described by equations 2.8 and equation 2.7, the interference fringe will have a shift of $(n_2 - n_1)k_0 D$. Such an experiment situation will be discussed in in chapter 6, where a near resonant laser field coupled to ground state of interferometer is introduced in the dark zone.

In principle, for any Ramsey interferometer, the two matter waves leading to interference only partially overlap. Depending on the geometry, this can give high interference contrast as in the case of microwave fields as beam splitters, or low contrast or even no interference at all, if the lateral overlap of the two waves vanishes. The Ramsey setup is an example of an interferometer, where the paths are not spatially closed.

2.3. Spatially closed interferometer

″Because of recoil, this interferometer (Ramsey interferometer) can not be closed in space and the fringes result from only a partial transverse overlap of the wave packets″ [7]. If we want to close the interferometer in space, we need to deflect the paths back for full spatial overlap. General schemes of possible closed interferometer geometries are shown in figure 2.3 using three

or four diffractive elements. The bottom one is the one that we applied for our experiment.
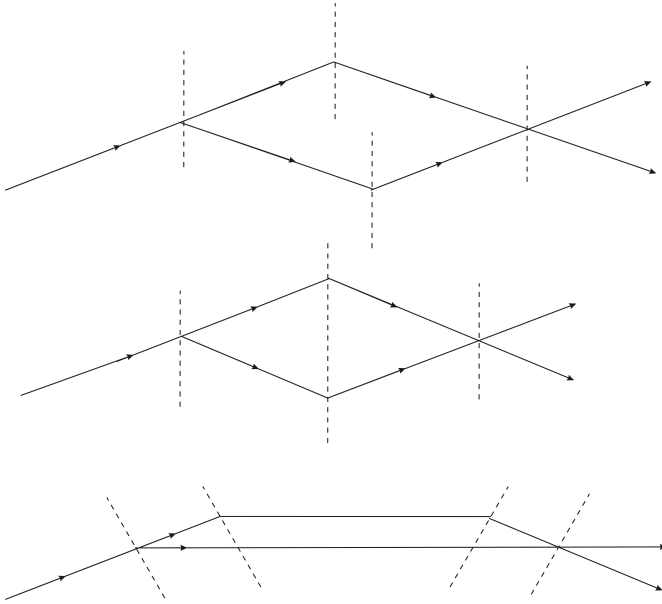
Figure 2.3.: General schema of interferometer geometries. The dashed lines stand for the diffractive field, the solid lines stand for matter wave, arrows indicate the travelling direction (cited from book [7]).

In order to simplify the alignment, $90°$ is used for the crossing angle between molecular beam and laser beam. This setup is called Ramsey-Bordé interferometer. The detailed scheme of this interferometer is shown in figure 2.4. The solid lines with arrows indicate laser beams. This construction is two pairs of identical laser beams with distance D counter-propagating with separation D' across the molecular beam. The solid lines stand for molecules in ground state, dashed lines stand for molecules in excited state. There are two closed interferometer paths indicated by the circles.

In our experiment, the upper interferometer as drawn in figure 2.4 is lost, due to the spontaneous decay of the excited state at large separation D'. ($D' \approx 15mm, D \approx 500\mu m$). The indexes of refraction for the matter wave in different inner states are marked in figure 2.5. The nomenclature is the same
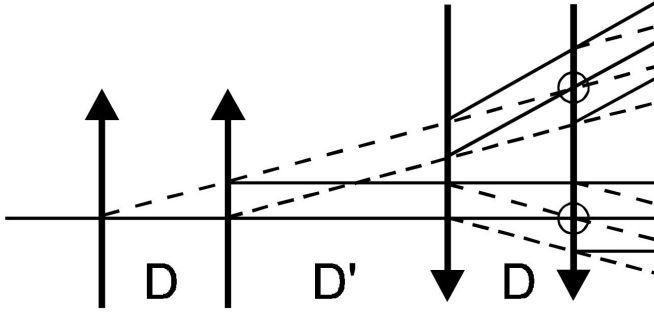
Figure 2.4.: Ramsey-Bordé interferometer setup, it is cited from [9].

as in figure 2.2.
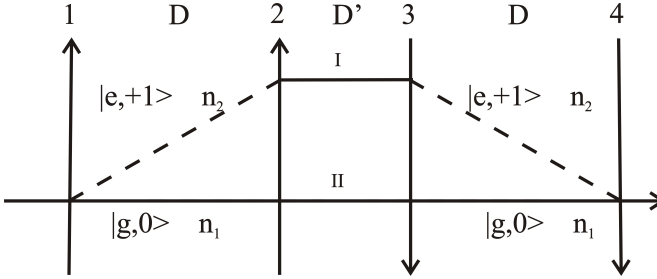
Figure 2.5.: Ramsey-Bordé interferometer with index of refraction n_i for molecules in different internal states.

For matter wave traveling through path I ending in ground state, the additional phases of the matter wave accumulated through path I are

$$\phi_{23}^{I} = n_1 k_0 D' \tag{2.9}$$

$$\phi_{34}^{I} = n_2(k_0 D + k_x D) + \phi_3 - \phi_4 \tag{2.10}$$

and in total from 1 to 4:

$$\phi_{14}^{I} = n_2(k_0 D + k_x D) \cdot 2 + n_1 k_0 D' + \phi_1 - \phi_2 + \phi_3 - \phi_4 \tag{2.11}$$

For path II, the accumulated phase of ground state matter wave is

$$\phi_{14}^{II} = n_1 k_0 (2D + D') \tag{2.12}$$

23

2. Theory of matter wave interferometer

The total phase difference results in

$$\Delta\phi = \phi^I - \phi^{II} = 2k_0 D[(n_2 - n_1) + n_2 \frac{1}{k_0 v_0}(\Delta - \delta)] + \phi_1 - \phi_2 + \phi_3 - \phi_4 \quad (2.13)$$

Because of ϕ_i, the stability of the interference pattern depends on the optical stability of the laser beams. If a single retro reflector is used, this contribution cancels out in first order. The retro reflector transfers beam 1 to beam 4 and beam 2 to beam 3, changes of ϕ_1 will be transferred in an opposite change of ϕ_4, so the net phase change by such instability is ideally zero.

Setting $n_1 = n_2 = 1$ when there is no interaction with the matter waves at the path, the equation 2.13 can be simplified to

$$\Delta\phi = \frac{2D}{v_0}(\Delta - \delta) \quad (2.14)$$

This experimental case is described in chapter 4.

Now when we consider closely the physical effect introduced during the traveling paths, not only the phase of the matter wave changes, but also the matter wave amplitude can be attenuated. After propagating the distance L, the phase shift and attenuation of the matter wave are written out explicitly as [2],

$$\Psi(x = L) = A \cdot e^{ik_0 L} e^{i\phi NL} e^{-\frac{\sigma}{2}NL} \quad (2.15)$$

Here N denotes the density of the medium, $\frac{\sigma}{2}NL$ and ϕNL are attenuation and phase shift accumulated on distance L. This can be collected as an index of refraction

$$n = 1 + \frac{N}{k_0}(\phi + i\sigma/2) \quad (2.16)$$

A new paramter ϵ can be introduced to denote $n_i = 1 + \epsilon_i$, then according to equation 2.16, $\epsilon \propto N$.

$$\Delta\phi(\epsilon_i = 0) = \frac{2D}{v_0}(\Delta - \delta) \quad (2.17)$$

$$\Delta\phi'(\epsilon_i \neq 0) = 2k_0 D[(\epsilon_2 - \epsilon_1) + (1 + \epsilon_2)\frac{\Delta - \delta}{k_0 v_0}] \quad (2.18)$$

When the density of the medium changes from N to ηN ($0 \leq \eta \leq 1$), $\epsilon'_i = \eta\epsilon_i$.

Δ is the detuning at density N

Δ' is the detuning at density ηN.

$\Delta' = \Delta + \gamma(1 - \eta)$, γ is the collision induced resonant frequency shift due to the different medium density.

For Ramsey-Bordé interferometer, the interference fringe will have a phase shift due to different medium density by

$$2k_0 D(1 - \eta)\left[(\varepsilon_2 - \varepsilon_1) - \frac{1 + \varepsilon_2}{k_0 v_0}\gamma + \frac{\varepsilon_2}{k_0 v_0}(\Delta - \delta)\right] \qquad (2.19)$$

This is used for the experiment in chapter 7. The medium density is changed by delfecting the ground state atoms out of the molecular beam. The shift of the interference pattern is used to calculate $\varepsilon_2 - \varepsilon_1$, which supplies the information of different collision cross-sections of excited state and ground state molecules with ground state atoms.

2. Theory of matter wave interferometer

3. The experimental components

In this chapter all experimental components to build molecular Ramsey and Ramsey-Bordé interferometers will be described and the applications for the related experiments using these interferometers in later chapters will also be shortly mentioned here. I will start from the molecular beam apparatus, then describe the diode laser system with frequency stabilization scheme, afterwards I will present the arrangement of the diode laser beams crossing the molecular beam as an example of the molecular beam splitter, the key and basic element of the interferometer. Finally, a general frequency stabilization scheme via an iodine stabilized Helium-Neon laser for other lasers will be explained.

The whole interferometer experiment takes place inside a vacuum chamber. The main chamber for the molecular beam was built by Christian Lisdat and described in his thesis [9]. Later deflection of ground state atoms was introduced by Sebastian Jung and details are given in his diploma work [11]. Ivan Sherstov implemented the second observation zone and magnetic shielding by a μ-metal box, the modifications are in thesis [12]. During my diploma work, the laser system is improved and characterized and new programs are written for the data acquisition [10]. I collect all the necessary information from former works and add the new modifications of the chamber to give the reader a complete overview to understand the experiments described in this thesis.

3.1. Vacuum apparatus for molecular beam

The K_2 molecular beam is produced by a $''$ free jet source $''$, which means that the molecular beam is a neutral beam extracted from an underexpanded, supersonic, continuum jet expansion from a high-pressure gas source into a low-pressure ambient background [13]. The $''$ free jet source $''$ fulfills two key requirements of the K_2 beam: a continuum source with sufficiently high density to have enough molecules for a significant signal-to-noise ratio, and a narrow velocity distribution to avoid the smear out of the interference patterns from different velocity components, or more specific to get a sufficient
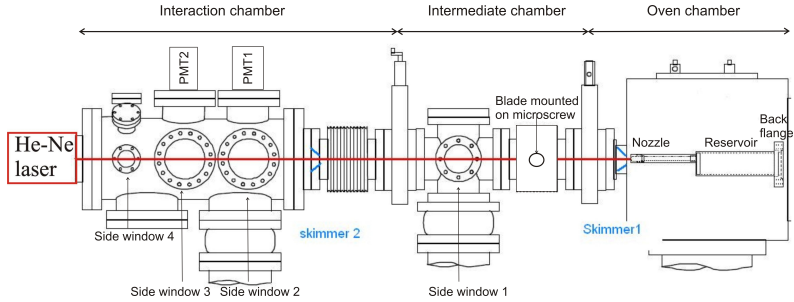
coherence length.

Figure 3.1.: Scheme of the vacuum system, a He-Ne laser is used to align the nozzle and two skimmers, this defines the molecular trajectory

The vacuum system is composed of three chambers as shown in Figure 3.1. Starting from right hand side, the first chamber is for the oven. Evacuated by a ″Varian DS602″ (a rotary Vane Vacuum pump) to 10^{-4} mbar as the prevacuum, two water cooled diffusion pumps further reduce the pressure to 10^{-8} mbar during oven operation. Since potassium is a very reactive material, the requirement on the diffusion pump oil is high. Santovac 5 Polypheny is an advanced high purity diffusion pump fluid used in critical applications requiring contamination free ultra-high vacuum environments. The middle part acts as a differential pumping stage. It is evacuated to 10^{-8} mbar by a turbomolecular pump, backed by a membrane pump at $1mbar$. In this stage, some physical interactions with the molecular beam can be introduced, like the resonant light pressure force of a laser field to deflect atoms out of the particle beam. The left hand side is the interaction chamber, where interferometers and detections are set. The same type of pumps as in the intermediate chamber are used here, typically the pressure is 10^{-8} mbar. In stand-by mode (no experiment running), the chambers are separated by high vacuum valves, so each chamber can be vented separately. Between oven chamber and interaction chamber, there are two skimmers with an opening of 2mm and a distance of 1m. This defines the axis of the molecular beam, and gives a collimation ratio of $1/1000$. By using a Helium-Neon laser, the oven is aligned to this axis. (Details of alignment see appendix A)

The oven is composed of three parts, a back flange, an oven reservoir and a nozzle at the tip of a long small tube as shown in Figure 3.1. There is a groove at the ring of the back flange to mark the position of oven. The reservoir has

a volume of about $50cm^3$, and around 5 gram pure potassium is filled for each experiment run (around ten hours). The nozzle has an opening of $200\mu m$. The first skimmer is 2 cm away from the nozzle.

The circuits for heating are separated, so the temperatures can be set differently, the typical temperature settings for the particle beam source are shown in Table 3.1. The back flange of the oven is not heated, so there is a temperature gradient from nozzle to the back flange to avoid the clogging of the nozzle.

	current /A	Temperature /°C
nozzle	0.275	492-528
oven	1.8	374-400
skimmer	3.4	250-265

Table 3.1.: Typical operational settings for the particle beam source

The potassium is liquid in the oven, the vapor pressure is approximately 10^{-2} bar [12]. The pressure difference inside and outside the oven induces an underexpanded, supersonic, continuum jet expansion. K_2 molecules and clusters K_n are produced by collision during expansion, and the K_2 abundance is estimated to be a few percent [9], the main contribution in the particle beam is K atoms. Because the mean free path inside the reservoir is smaller than the size of the nozzle, multiple collisions during the expansion leads to a rearrangement of the internal energy of the sample particles [13] and low vibrational levels of molecular electronic ground state are populated. Because it is a supersonic expansion [13], the core of the expansion is in a quiet environment, and it is selected by the first skimmer, this leads to the narrow velocity distribution in longitudinal direction.

When the molecules fly through the intermediate chamber, first they encounter a pair of blades, which can be symmetrically moved to delimit the molecular beam. They are used in the Ramsey interferometer experiment to modify the transverse momentum distribution of the K_2 (see chapter 5). One of the blades is also used in the experiment for deflecting K atom (see chapter 7). A pair of side windows (marked as side window 1) in the intermediate chamber provide optical access for laser beams to use the resonant light pressure force to deflect the atoms. Directly above this laser-particle interaction area there is the view port for observation. Typically a camera is mounted here to observe the spatial distribution of the fluorescence of potassium D_2 line for the deflection experiment.

The pair of side windows 2 in figure 3.1 is for the laser beams of the interferometer setup. The observation here can be done either in the excited state exit or in the ground state exit of the interferometer, the fluorescence is recorded by photomultiplier tube 1 (PM1). The pair of side windows 3 is for the observation of interference pattern in ground state exit, the fluorescence is recorded by photomultiplier tube 2 (PM2). The experiment of using PM1 and PM2 to observe the interference fringe is first introduced in chapter 4, and then used as a standard technique for the later experiments.

In the interaction chamber, the velocity was measured at the place where the interferometer is located. By means of the Doppler effect, the most probable longitudinal velocity was measured to be $v_{prob} = 912 \pm 30 m/s$, and the velocity width $\Delta v = 120 m/s$ for the applied beam [9]. Because of uncertainties in the temperature setting and the long time drift in the flux density of the particle beam, velocity measurements at different days differ and the accuracy is within 10%.

The high collimation ratio of 1/1000 by the two skimmers results in a velocity distribution with a width of 1.2 m/s in the direction perpendicular to the molecular beam. The density of the particles is estimated to be in the order of $10^{13} cm^{-3}$ at the interferometer location [12].

The magnetic field inside the vacuum at the interferometer area is shield by a μ-metal box. The attenuation in the center of the μ-metal box is 20 dB and residual magnetic field gradient is less than 2 μT [12].

The small windows at the tail marked as side window 4 can provides some possibilities for quality check. e.g. check the deflection efficiency of atoms.

3.2. Diode laser system for interferometer setup and detections

In order to use the matter wave interferometers for sensitive measurement on a long time scale, there are several requirements for the laser beam splitters: stable central frequency, narrow laser linewidth and constant power at least for the whole measurement time (ten hours). This is realized by stabilizing an external cavity diode laser to a moderate finesse cavity, which is locked to a Rubidium hyperfine transition via another diode laser. The principle scheme of the optical setup is given in thesis [9] and thesis [12], here just the conception of the stabilization is introduced.

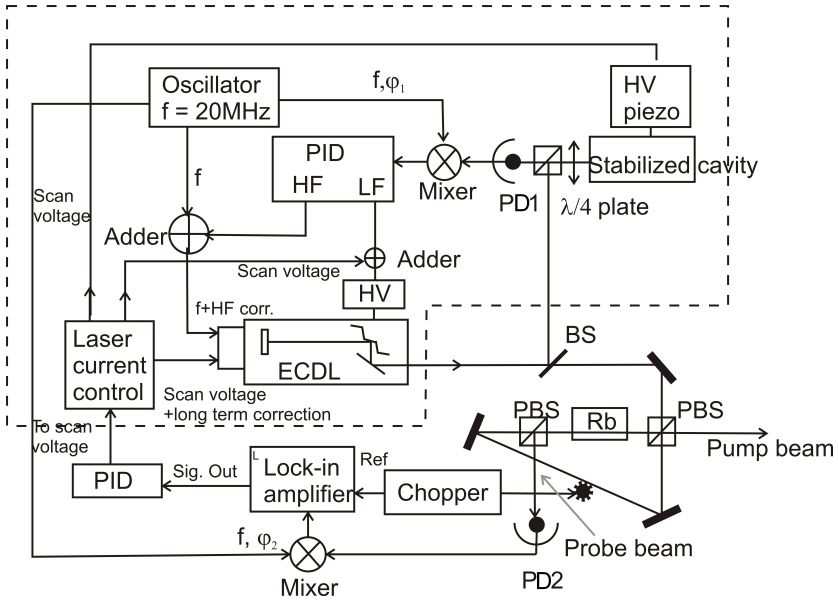The concept of locking a cavity to an atomic transition is given in Figure 3.2.

Figure 3.2.: Stabilization scheme for an optical cavity. Enclosed in the dashed lines is the diode laser locked to the optical cavity via the Pound-Drever-Hall (PDH) technique. The bottom part is the laser plus cavity unit locked to a Rb hyperfine component via a saturation setup.

3. The experimental components

The central unit is the external cavity diode laser (ECDL). The part enclosed in the box by the dashed lines represents the diode laser stabilized to the cavity via the Pound-Drever-Hall technique (PDH).

The optical arrangement is simple: the beam out of laser head (ECDL) as indicated by the arrow is reflected from beam splitter (BS) to the cavity and back reflected from the cavity and to the photo diode (PD1).

The servo loop to stabilized the laser to the cavity consists of the following parts. There is one 20MHz oscillator used for the modulation of the whole experiment. A laser diode is normally lasing at a wavelength defined by temperature, current and settings at the grating. Out of laser diode the first diffraction order of the reflection grating is coupled back to the laser diode, so grating and laser diode represent an extended cavity and this reflected mode is amplified, the laser frequency is selected by the angle of the grating. When the laser current is modulated, the side bands can also be detected by the PD1. The signal from PD1 goes to a mixer which multiplies the signal with the 20MHz reference signal with an adjustable phase delay φ_1 from the same oscillator, which provides the modulation to the laser diode current. The error signal goes to proportional-integral-derivative controller (PID). The high frequency part of the error signal is added together with the 20MHz modulation to the laser current. The low frequency part is fed back to the high voltage amplifier (HV) to control the grating in the ECDL. With this setup the laser is stabilized to the cavity. Adding a tuning voltage to all elements determining the laser frequency, the unit, laser plus cavity, can be scanned continuously.

The lower part of figure 3.2 shows the saturation spectroscopy on Rubidium. The laser beam out of ECDL through BS is split by polarizing beam splitters (PBS) into a pump beam and a probe beam. The pump beam has high intensity to saturate the transition, and probe beam has low intensity to resolve the saturation dip on top of the Rb transition profile. The two laser beams overlap counter-propagating through the Rubidium cell, the probe laser beam is detected by the photo diode 2 (PD2). The laser frequency is set resonant with the Rb D_2 line, this Doppler-free saturation spectroscopic setup resolves a single hyperfine component.

For the serve loop, the signal from PD2 multiplied with the 20MHz reference signal with a proper phase delay φ_2 gives the error signal at the hyperfine components of the Rb D_2 line. These error signals sit on a background of the Rb absorption profile. To get rid of the background, a lock-in technique with a chopper for the pump beam is introduced. After the lock-in amplifier, the error signal is amplified by PID and fed back to the current control of the diode laser. Any deviation of the frequency of the stabilized ECDL from the

Rb resonance results in a correction voltage to the laser plus cavity unit and pulls it back to the Rb frequency. As a result we have a cavity with good long term frequency stability. The long term frequency stabilization is 300 Hz/min [10].

The diode laser system for the matter wave interferometer is realized in a master-slave configuration. The master laser is locked to the same cavity as mentioned above via PDH stabilization method. So it inherits the long term stability of the cavity. The sharp slope of the error signal results in a greatly reduced laser bandwidth, when the electronic is sufficiently fast. For our experiment, the laser linewidth is reduced to 30 kHz for a detection time of seconds. This master laser beam goes two times through an acoustic-optical modulator (AOM) for adjusting the desired frequency or producing a frequency scan. Then it is directed into a laser diode which is used as an injection locked slave laser. The long term stabilization and narrow linewidth of the slave laser are inherited from the master laser. The AOM is driven by a RF syntheziser with a precision better than 10^{-7}.
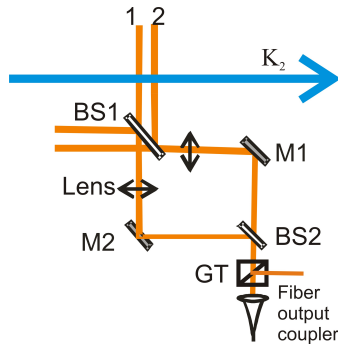
Figure 3.3.: Optical alignment for laser beam splitters

To build a Ramsey interferometer, it requires two laser beam splitters to split the molecules. So in this section we will discuss how to split one laser beam into two identical ones. The method was previously described in [9]. Figure 3.3 shows the modified optical setup. The collimated laser beam out of a fiber coupler with diameter of 4mm is purified in polarization by a Glan-Taylor crystal(GT). The polarization direction afterward is parallel to the optical table in the plane of the drawing. The optical beam splitters BS1, BS2 and mirrors M1 and M2 are arranged symmetrically. The laser beam either goes

through BS2 reflected from M1 and BS1 marked as laser beam 2 or is reflected from BS2, M2 and goes through BS1 marked as laser beam 1. If both optical beam splitters have reflectivity R, transmittance T = 1-R, the power of laser beam 1 and 2 after BS1 is P = R(1-R). The experimental value is P = 2.5mW (measured directly before the laser beams enter the vacuum chamber), which fulfills the $\pi/2$ condition of Rabi oscillation for the chosen transition in K_2. It means the laser beam works as a 50% splitter for the molecular matter wave. The wave fronts of the laser beam 1,2 are adjusted parallel. Because of the symmetrical arrangement, the two laser beam paths have almost equal length. This simplifies the stabilization of the phase difference between the two laser beams during the laser frequency tuning described in chapter 5. After BS1, the pair of laser beams 1 and 2 enters through the side window 2 marked in figure 3.1 the interaction vacuum chamber and crosses the molecular beam.

Matter wave interference fringes appear only within the homogeneous width of a transition line. Focusing lens with a focal length of 45 cm are introduced for getting sufficient transit time broadening to observe several fringes for a single transition. The focus plane lies at the point where the laser beam crosses the molecular beam. The laser beam waist is $\sigma = 200\mu m$.

In chapter 4, for building Ramsey-Bordé interferometer, two pairs of counter-propagating laser beams will be obtained by introducing a retro reflector, which images the laser beams 1 and 2.

The practical procedure for the alignment of the laser beam splitters is described in the appendix A.

3.3. The stabilization scheme for a laser by applying an iodine stabilized HeNe laser

For different experiments, various laser systems were used, e.g. dye lasers or titanium-sapphire lasers, to control the physical conditions on the traveling path of matter wave. For our experiment, the long term stability of the physical effect introduced by the laser field is important. So they need to have proper power and frequency stabilization. Here I schematically describe one of the general methods for the long time frequency stabilization of lasers. The stabilization scheme was previously described in details in thesis [15].

Similar to section 3.2, an ultra stable cavity is realized by stabilizing it to an iodine hyperfine transition via a Helium-Neon laser. Any other laser locked to the cavity inherits this long term stability. This iodine stabilized He-Ne

laser is a commercial product with an accuracy of 10^{-11}. The frequency of the He-Ne laser coupled to this cavity is tunable by an AOM. The tuning range is larger than the free spectral range (FSR) of the cavity to match the frequency difference between the optical mode used for stabilizing a second laser and the optical mode used for the HeNe stabilization. The requirement on the laser to be stabilized is that they need to have an external voltage input which can tune the laser frequency selecting elements properly. Such modifications are built into all our lasers.

3. The experimental components

4. Ramsey-Bordé interferometer and embedded Ramsey interferometer with molecular matter waves of $^{39}K_2$

This chapter describes the building up of a Ramsey-Bordé interferometer and the detection of interference fringes. Due to the configuration, there is a Ramsey interferometer embedded inside it. In the data treatment, the separation of signals of Ramsey-Bordé interferometer from those of the embedded Ramsey interferometer is introduced. This chapter gives the motivation to analyze and to apply the Ramsey interferometer in chapter 5 and chapter 6. This chapter will also work for chapter 7, where the Ramsey-Bordé interferometer is used to measure the collision induced phase shift. The whole chapter is a manuscript already submitted for publication [16].

4.1. Introduction

A Ramsey-Bordé matter wave interferometer (MWI) employing a beam of $^{39}K_2$ molecules has been realized [17]. The matter wave interferometry will be used as a sensitive method for various investigations, e.g. study of molecular transition dipole moments 6 and detection of collisions between atoms and molecules 7.

In the experiment the atoms and molecules are prepared in a particle beam formed by supersonic expansion. The abundance of the molecules in the beam is a few percent, so that the physical situation can be described as K_2 molecules being diluted in a medium of K atoms. The influence of the medium being present or absent will result in phase and amplitude changes of the matter wave interferences, due to the change of index of refraction of the medium, in which the matter wave propagates. Pioneering experiments using this index of refraction picture for matter wave propagation have been performed by the
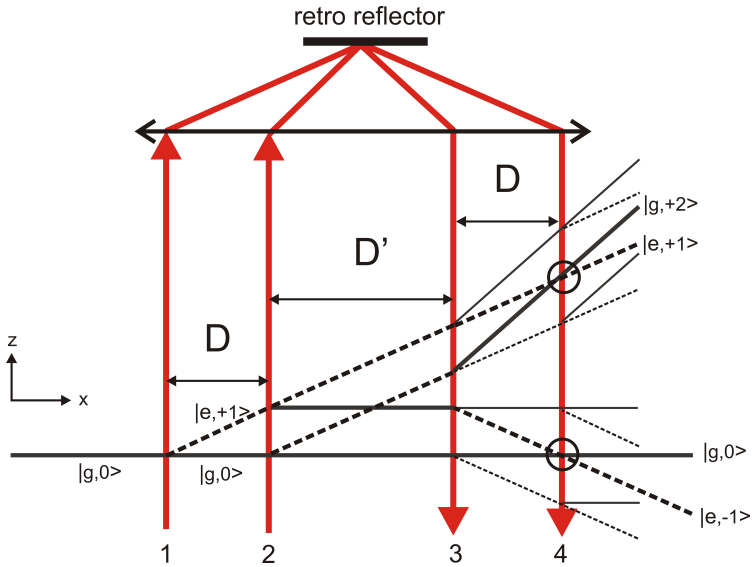
Figure 4.1.: Scheme of the Ramsey-Bordé interferometer: the molecular state ($|g, e, \pm m\rangle$) is marked by g, e for ground and excited states respectively, and by $\pm m$ for the number of photon momenta transferred. The separation between each pair of laser beams (arrows) is called dark zone D. Only within this chapter, the z direction is defined as the laser running direction.

Pritchard group [3, 4, 2], while substantial contributions for the theoretical description have been made by Vigué [18].

Another topic will be the determination of molecular transition dipole moments with the matter wave interferometer as the measuring device. Applying a laser field near resonant to a molecular transition between two levels, one of which is shared by the beam splitter transition of the matter wave interferometer, will introduce a phase shift and a change of the contrast of the matter wave interferences, and will allow to determine the transition moment of the "near resonant" transition.

While matter wave interferometers with atoms have been realized more frequently [19], such interferometers with molecules are rarely studied. SF_6 is used in the infrared in a Ramsey interferometer employed as frequency standard [20] and the iodine molecules was used for demonstrating a Ramsey-Bordé matter wave interferometer [21]. Presently the Vienna group led by Arndt (e.g. [22]) is driving forward investigations of matter wave interferometry on molecules with gratings as beam splitters. One of their main issues is increasing the mass of the molecules to find out how far matter wave interferences can be observed or when decoherence by the high number of internal degrees of freedom in a big molecule might smear out the interference.

The experimental details of our matter wave interferometer have been described in detail previously in [17, 9, 12] and some parts in chapter 3. Various approaches of modulation techniques were reported for improving the detection of the matter wave interferences [23].

The basic scheme of the present interferometer with four traveling wave fields in a Ramsey-Bordé setup is drawn in figure 4.1. A set of four laser beams acts as beam splitters which coherently split and recombine the molecular matter wave, yielding essentially two closed interferometer paths, whose exits are encircled in figure 4.1 for easy identification. The solid lines stand for paths of the molecular matter wave in the ground state, while the dashed lines stand for paths in the excited state. The state $|g/e, m\rangle$ labels by g or e the molecular state, and by m the number of the transferred photon momenta in units of $\hbar\mathbf{k}$, where $\mathbf{k}$ is the photon wave vector. A retro reflector images the copropagating pair of laser beams 1 and 2 (left arrows) into the opposite direction, beams 4 and 3 are mirror images of 1 and 2, respectively.

The time of flight for molecules through the zone marked by D' in figure 4.1 is much larger than the life time of the excited molecular state. The molecules in the excited state paths have spontaneously decayed after passing this zone. Thus the upper closed interferometer is lost, which simplifies the interference pattern observed when tuning the laser frequency, because the over-

lap of the two recoil components does not appear. Additionally, the excited state molecules decay according to the Franck-Condon principle to a series of ground state levels. The probability to repopulate the initial rovibronic ground level is low. These molecules are completely lost for the detection and will not add incoherent background to the lower interferometer path in figure 4.1.

Another consequence of the finite excited state life time is the applicable length of dark zone D. By a proper selection of the upper molecular level of the $b^3\Pi_{0_e^+}$ state, the lifetime can be chosen in the order of μs [17]. Within a lifetime τ of the upper state of e.g. ≈ 1.5 μs the molecule travels about 1.4 mm. For sufficient contrast of the interferences, D is practically limited to below 1 mm, while D' is chosen between 10 mm and 20 mm. Such small value D leads to small transverse spacings in the order of few nanometers between the two coherently propagating matter waves after the zone D. We will show later that this results in an additional interference pattern related to the Ramsey interference applied in spectroscopy with radio or microwave fields see frequency standard with Cs [24].

As indicated in figure 4.1, for the lower closed interferometer path, the encircled area has an exit where molecules are in the excited state labeled by $|e, -1\rangle$ and a complementary exit with the ground state labeled by $|g, 0\rangle$. The matter wave interference can be detected by observing the fluorescence out of the upper molecular state $|e, -1\rangle$. This detection principle will be called in the following observation the "excited state exit" of the interferometer and was used in our first demonstration [17]. The exit $|g, 0\rangle$ can be inspected by the remaining population in the ground state and its change due to the matter wave interference. The observation of this exit, further on called "ground state exit" of the matter wave interferometer, has been realized in this work. Its properties will be compared with those of the excited state exit.

In section 4.2 we shall give our considerations of the special properties of the present matter wave interferometer. Then we will in section 4.3 describe the modifications of the experimental setup compared to the one used in Ref. [17], in order to put into operation the ground state exit. Section 4.4 gives details on the selected molecular transitions and the corresponding observations. The analysis of the observed signals as overlapping of two interferences will be described in section 4.5 and consequences for precision measurements are presented in section 4.6.

4.2. Propagation of matter wave packets

In our interferometer we have due to experimental requirements special conditions, which are not common with other interferometer setups. Therefore, we discuss them here in more detail.

By means of the Doppler effect the molecular velocity distribution has been determined for the applied beam, giving the most probable longitudinal velocity $v_{prob} = 912 \pm 30$ m/s, and the velocity width $\Delta v = 120$ m/s [17] for a Maxwell distribution

$$n(v) \propto v^2 e^{-(\frac{v-v_{prob}}{\Delta v})^2} \tag{4.1}$$

In the transverse direction, the beam is highly collimated with a collimation ratio of 1/1000. Thus the residual transverse velocity distribution is scaled by this factor, resulting in a velocity distribution in a direction perpendicular to the molecular beam with a width of 1.2 m/s. These widths translate to corresponding coherence lengths of the matter wave packets according to $l_c = \hbar/2\Delta P$ [7], where ΔP is the particle's linear momentum spread. This gives for K_2 molecules under the conditions mentioned above $l_c = 3.4$ pm in the longitudinal and 3.4 nm in the transverse directions. Thus the spatial shape of the wave packet can be imagined as a very thin disk with a large extension perpendicular to the molecular beam axis.

In figure 4.2 we show how the wave packets propagate through the interferometer. For simplicity the wave packet is represented by a rectangle, which is narrow in x direction corresponding to the beam direction and wider in z direction. The interaction between the molecule and laser beams is assumed to fulfill the $\pi/2$ condition for the Bloch vector, so the molecular matter wave is coherently split into two parts of equal amplitude at each laser interaction. The degradation from strong to light color of the wave packets indicates the different losses of amplitude because of the four acting beam splitters.

As indicated by solid and dashed lines in figure 4.2, after the first laser beam splitter the molecule is in a superposition of excited state and ground state. Due to the momentum transfer in the splitting process, the matter wave packets of molecules in the different inner states are split laterally in space. The additional transverse momentum $\hbar k$ yields on a typical length $D \approx 600$ μm of the zone between two beam splitters a transverse spatial shift of the deflected part of the matter wave of $\delta \approx 3.4$ nm. When the laser frequency is tuned off resonant from the molecular transition, the molecules in the excited state will also be accelerated or decelerated due to a momentum transfer in the longitudinal direction and thus accumulate a longitudinal phase shift during the
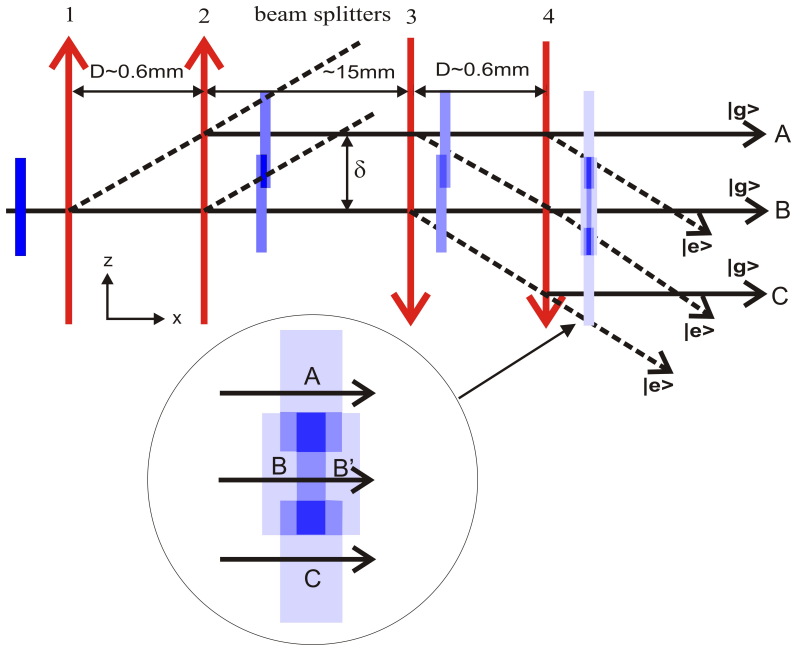
Figure 4.2.: Schematics of the propagation of the wave packets through the Ramsey-Bordé interferometer. The ground state wave packets are indicated by their estimated coherence lengths in the direction of the molecular beam, *x* and perpendicular to it, *z*. The inset shows an enlarged view of the wave packets after beam splitter 4.

dark zone D. After the interaction zone 2 the two wave packets travel parallel. They overlap spatially in the longitudinal and also in the transverse direction and have a phase shift in the longitudinal direction depending on the detuning of the beam splitters.

This is indicated in figure 4.2 by the dark overlap areas. In this region both matter wave packets interfere with each other. The matter wave interference can already be observed with a pair of only two laser beams as beam splitters, when the laser is tuned. This is a similar situation as in the case of Ramsey interferometers in the microwave or infrared region. However, the lateral displacement of the matter waves is negligible in these cases according to the small momentum transferred. In the text below we will address interferences resulting from two beam splitters as "Ramsey interferences". The traveling time, in which the phase shift is build up, is determined by the length of the dark zone D and the longitudinal speed v_l of the molecules

$$T = \frac{D}{v_l} \tag{4.2}$$

and gives also the period T of the observable interference pattern while tuning the laser [7], i.e. the reciprocal $1/T$ gives the magnitude of the detuning of the laser for which the phase shift varies by 2π. An example of such Ramsey interference   is given later in figure 4.4.

For each wave packet in the ground state, the pair of beam splitters 3 and 4 works exactly as the beam splitters 1 and 2 before, each producing parallel traveling matter wave packets with lateral overlaps in the ground state (labeled by A, B, C in figure 4.2) and similarly in the excited state not shown in the figure. Due to the equal separation D of the laser beam pairs, the wave packets of B and B' form the closed path of the Ramsey-Bordé interferometer with full lateral overlap of the wave packets. They accumulate phase shifts in longitudinal direction during the first and the second dark zone labeled D, thus the interference period T' is given by

$$T' = \frac{2 \cdot D}{v_l} \tag{4.3}$$

In figure 4.2, the resulting superpositions of the wave packets behind the beam splitter 4, are drawn in detail in the inset for the ground state molecule to give an imagination of the transverse and longitudinal overlaps, which result in interferences. The shaded areas are shifted against each other to indicate the longitudinal phase shift for an arbitrarily chosen detuning of the laser. Wave

packet B has no phase shift, wave packet B' has a phase shift according to equation 2.14, wave packet A and C have phase shift according to equation 2.8.

One can expect a Ramsey interference signal between the laterally displaced wave packets from the overlap of pair A B, A B' and of pair B C, B' C, and the interference pattern is governed by T. The overlap of the two ground state wave packets B and B' result in the Ramsey-Bordé interference governed by T'. The degradation from strong to light color of the wave packets in figure 4.2 indicates the different losses of amplitude because of the four acting beam splitters. In addition, there is another group of wave packets in the excited state (not shown) at beam splitter 4, where similar spatial overlaps are present, which are observable in the excited state exit.

By increasing the length D of the dark zones, the transverse separation between the coherent paths is increased and the lateral overlap of the wave packets between different paths decreases. Therefore, the contrast of the Ramsey interference with period T will decrease. The contrast of the Ramsey-Bordé interference which results mainly from the lifetime of the upper state and the traveling time in D, will also change by varying D, but in a different manner than for the Ramsey interference .

Now we will turn to a detailed discussion of the influence of the phases of the laser fields on the interference pattern. When the molecules interact with the laser beams, the phases φ_i ($i = 1, 2, 3, 4$) from the lasers beams are added to that of the matter wave by the induced electric dipole; i marks the different laser beams acting as beam splitters. The total phase accumulated by the interaction with the beam splitters of two interfering matter wave packets in the Ramsey-Bordé setup between B and B' is [7]

$$\varphi_{1-4} = \varphi_1 - \varphi_2 + \varphi_3 - \varphi_4, \tag{4.4}$$

while for packets after traversing a pair of laser beams of the same direction we have [7]

$$\varphi_{1-2} = \varphi_1 - \varphi_2 \tag{4.5}$$

for A B, and B' C. or

$$\varphi_{3-4} = -\varphi_3 + \varphi_4, \tag{4.6}$$

for A B' and B C.

Pairs of A with B and A with B' give Ramsey interference   according to Eqs. 4.2, with additional phase differences from the laser interactions through 4.5, and 4.6. Similarly, interferences result from the pairs C with B and C

with B'. The same discussion can be made for the excited state exit, given by dashed lines in figure 4.2. The resulting interference pattern is complementary, but will show different background signals, through the different detection schemes, which are discussed in the following sections. Thus the visibility of the interference can be significantly different.

In the Ramsey-Bordé interferometer , phase drifts of the beam splitters 1 or 2 are compensated according to Eq. 4.4 by an opposite phase shift for splitter 4 and 3, respectively, due to the retro reflector, if no additional phase difference is built up by it. This gives a good internal stability with respect to mechanically induced phase changes in the four beam splitter setup. Such favorable condition is not present in the two beam splitter arrangement. The aspect of phase compensation plays an important role for high precision phase measurements using a matter wave interferometer.

4.3. Setup for simultaneous excited and ground state detection

The principal optical layout is similar to that shown in the figures 4.1 and 4.2. The laser system for the beam splitters of the interferometer part is described in detail in chapter 3. The master laser was improved compared to [17] regarding its long term stability to a drift of less than 300 Hz/min by thermal shielding of the container of the offset-lock cavity and by careful adjustment of the mode matching condition for both the Rb-stabilized reference laser and the master laser beams. The spectral width of the laser radiation is less than 30 kHz. The light of the master laser is frequency shifted by an acousto-optic modulator (AOM) and used for injection lock of a slave diode laser which provides the required output power for the matter wave beam splitters. The AOM is driven by a RF-synthesizer, whose frequency setting is synchronized with the data acquisition system. The laser beams of the beam splitters are focused by cylindrical lenses to a width in x direction of ≈ 100 μm, so that the spectral lines are broadened by time-of-flight broadening. This is necessary for a sufficiently wide homogeneous line width, on which several fringes of the matter wave interference are observed.

Another part of the master laser beam is frequency shifted in a similar way by a second AOM and used for injection lock of a second slave diode laser, which is employed to probe the population of the molecular ground state behind the matter wave interferometer on the $b - X$ transition of K_2 (see below).

Photomultiplier PM1 is installed above the crossing of laser beam 4 with the molecular beam (see figure 4.2). The observation area of the optics is about 2 mm × 2 mm wide at the position of the molecular beam. The distance D of the pair of laser beams is always less than 1 mm, fluorescence from beam splitter 3 is present in this area, and thus fluorescence excited by the laser beams 3 and 4 is observed simultaneously. The excitation laser for the detection of the ground state exit (laser beam 5, not shown in figure 4.2) crosses the molecular beam about 300 mm downstream of laser beam 1. The laser induced fluorescence is detected by a second photomultiplier (PM2).

The laser beam 5 can also be directed to cross the molecular beam close to beam splitter 4. Then the fluorescence is detected by PM1. Such arrangement can be used for investigation if repopulation of the ground state and thus loss of contrast of the interferences on the long path from the beam splitters to the detection occurs. During the traveling time of 300 μs for the length of 300 mm the molecules in the excited state have certainly decayed when they arrive at beam 5. After beam 4, the interference signal is imprinted in the population of the ground state level. Collisions between particles, however, could change the population in the ground state and thus reduce the interference contrast. In an experiment using only a Ramsey interferometer setup, signals of the ground state exit were detected switching fast (to avoid influence of drifts of the laser phases) between detection directly behind the interferometer beams with PM1 and further downstream with PM2. Comparing the resulting spectra no reduction of the interference contrast was observed.

The currents from both photomultipliers are converted to voltages and recorded by the data acquisition system. While the laser creating the beam splitter fields is tuned step wise, the signals at each frequency setting are typically averaged for 100 ms up to 1 s with 1 ms as sampling rate and then stored in a computer. For a sufficient number of points on a spectral feature frequency steps of the synthesizer of about 10 kHz are typically used, the number of points for one record are between 500 and 1000. Due to the high stability of the laser system and the well controlled RF-tuning of the frequency, the signal-to-noise ratio (S/N) can be readily improved by averaging several of such records.

4.4. Molecular transitions and observations

Following our earlier spectroscopic investigations [25] of this range of the $b - A$ complex of K_2, the selected level $J = 26$, $v = 27$ of the upper b state has a lifetime of 1.5 μs [17], allowing for sufficiently large dark zones D of

the interferometer setup. The $b^3\Pi_{u0^+}$ has predominantly magnetic hyperfine structure with a splitting of few MHz [26] while the hyperfine splitting in the ground state is less than 100 kHz from quadrupole and nuclear spin-rotation interaction [27]. Thus in general each $b - X$ rovibronic line is split into either 6 hyperfine components for even J'' or into 10 components for odd J'', due to the nuclear spin of 3/2 for ^{39}K and thus total nuclear spins of $I = 0$ and 2 or of 1 and 3 for the different classes of J (see e.g. [26], figure 1, 2) and due to the selection rules for the electric dipole transition.

The $R(25)$ line displays a pattern of 7 hyperfine components (compare figure 1 in Ref. [26]), of which the 3 central ones have roughly twice the intensity compared to the lower two or the upper two components, as they are blends of two. The following experiments will concentrate on the two single components in the high frequency part of the hyperfine structure, which are well resolved when excited by an unfocused laser beam. Under the focusing conditions of the matter wave interferometer (see section 5.1) the hyperfine structure is no longer well resolved, but an overlapping structure of the incoherent background appears on which the interference patterns at the positions of the hyperfine components are sufficiently separated. A typical complete spectrum can be found in figure 7 of Ref. [17].

4.4.1. Probing the ground state exit of the MWI with excitation on the $B - X$ transition of K$_2$

At first glance, a strong probe transition could be preferable for high detection efficiency. The $B^1\Pi$ state is in a convenient energy range just above the $b - A$ system and the $B - X$ transition is known to be strong (arrow A in figure 4.3). The spectrum of the $B - X$ band system has been analyzed in [28]. The transition $Q(25)$ $(4 - 0)$ $B^1\Pi_u \leftarrow X^1\Sigma_g^+$ at 15655.36 cm^{-1} was chosen due to its favorable Franck-Condon factor. It shares the ground state level $v'' = 0$, $J'' = 25$ with the $R(25)$ $(27 - 0)$ $b^3\Pi_u \leftarrow X^1\Sigma_g^+$ transition employed in the matter wave interferometry. A dye laser with DCM dye was employed for excitation of this transition. It was frequency stabilized by locking it to a confocal Fabry-Pérot transfer cavity, which itself is locked to an iodine stabilized HeNe laser. The spectral line width of this laser is about 2 MHz.

For the B state the hyperfine splitting is known to be small [28], single hyperfine components are not resolved in the spectrum. Thus an excitation involves all the hyperfine components simultaneously. Manipulation of the population of one of the 10 ground state hyperfine levels while leaving the
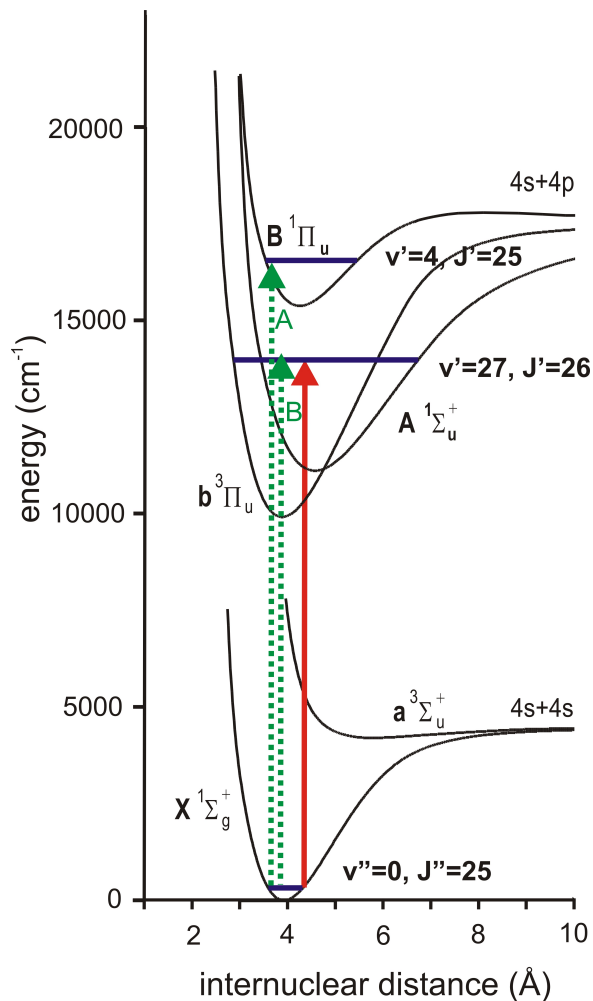
Figure 4.3.: Simplified molecular potential scheme of K_2. The excitation (solid) and detection (dashed) transitions are indicated by vertical arrows: detection by exciting to the $B^1\Pi_u$ state (case A) or to the $b^3\Pi_{u0^+}$ state (case B).

other ones unchanged will accordingly lead to a maximal change of 1/10 of the whole laser induced fluorescence on the $B - X$ transition.

In figure 4.4 simultaneous records of interference patterns observed with PM1 for the excited state exit of the MWI and with PM2 for the ground state exit are shown. For good signal-to-noise ratio we employed a notch filter for PM2 to suppress residual scattered light from the exciting laser. In the experiment only beam splitters 3 and 4 were used, so the interference is a Ramsey interference when tuning the interferometer laser. The central fringes of two hyperfine components are located at about 614 MHz and 621.5 MHz in the diagram. The other fringes are partly overlapping, because the short dark zone of $D \approx 200$ μm leads to a wide interference period of about 4.5 MHz at each hyperfine component. This distance was selected to achieve a good contrast of the interferences for demonstration.

On the high frequency end in the diagram, the excited state signal is close to zero while the ground state exit shows maximum intensity. This is expected because, the interferometer laser is not resonant and the molecular ground state population is preserved at the detection zone for the ground state exit. When the beam splitter laser is tuned closer to resonance, the ground state levels are depopulated, resulting in a reduced fluorescence at the ground state exit. From the upper trace it is obvious that the signal contrast is much lower compared to the lower one.

The middle trace shows the rescaled upper trace where the signal is magnified and shifted down to have similar interference amplitude as the lower trace for better visibility of the complementarity of the structure. The signal-to-noise ratio for this type of observation of the ground state exit is worse compared to the excited state exit. The reason for the noise is the high fluorescence background and intensity fluctuations of the dye laser applied.

As a conclusion, using the $B - X$ transition the matter wave interferences are observable on the ground state exit, but due to the signal properties like high background and small contrast, and due to intensity fluctuations of the exciting laser there is no advantage compared to the previous detection method employing directly the fluorescence from the beam splitters. A better control of the intensity of the dye laser would improve the situation, but the high background is unavoidable.
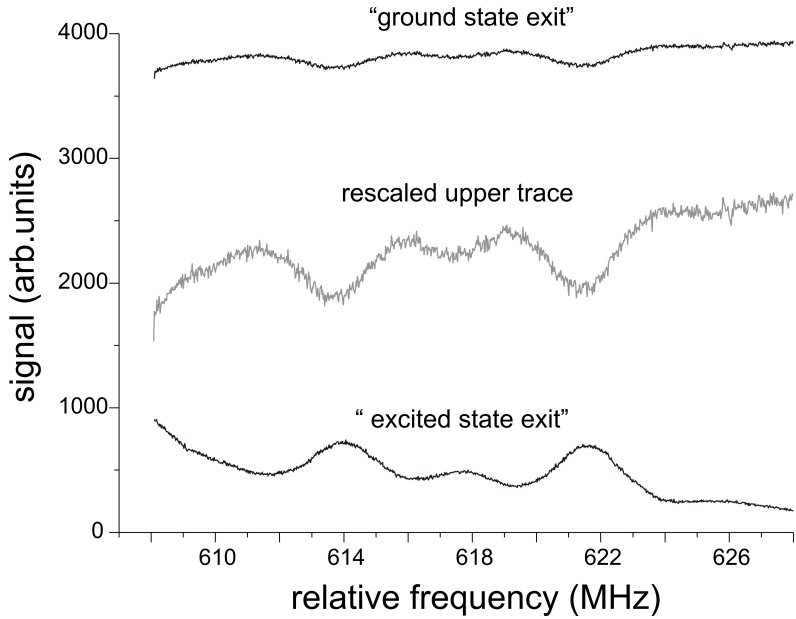
Figure 4.4.: Simultaneous spectra of the interference patterns for the excited state (lower trace) and ground state (upper trace) exits using excitation on the $B - X$ $Q(25)$ $(4 - 0)$ transition of K_2 with the configuration of beam splitters 3 and 4 only and a distance $D = 200\,\mu$m. The middle trace is a scaled replica of the upper one to get the same amplitude of the fringes as in the lower trace for direct comparison of the two exits with respect to the S/N ratio achieved.

4.4.2. Probing the ground state exit of the MWI with excitation on the $b - X$ transition

In spite of having a much smaller transition moment than the $B - X$ transition the $b - X$ transition for detection has one intriguing speciality, namely the hyperfine splitting can be readily resolved in this transition. Thus, the detection of a single hyperfine component is possible, if a laser beam with a diameter for sufficiently small transit time broadening is employed. Therefore, the fluorescence will show changes only when the interferometer laser is acting on the same hyperfine level of the ground state which is detected in the ground state exit. In this way a method is at hand which offers to detect matter wave interferences from a single hyperfine level of the ground state, in contrast to the excited state exit.

For probing the $b - X$ transition (arrow B in figure 4.3) we used the second, independently tunable slave laser as described above. The frequency of this slave can be tuned across the same transition that is used in the interferometer. For detection of the ground state population it is set to the center frequency of the hyperfine component chosen to be detected. In figure 4.5 the simultaneous records for both interferometer exits are shown. The interferometer laser was tuned, while the probe laser frequency was fixed at the peak of the fluorescence profile of the hyperfine component of highest frequency.

While the excited state exit shows clearly matter wave interferences for two hyperfine components on top of the overall fluorescence profile, the signal from the ground state exit shows the interference pattern in a dip corresponding to the transition of a single hyperfine component. Essentially the interferences of excited state and ground state exit are opposite in phase with a period of about 1.2 MHz corresponding to $D = 650\ \mu$m (compare equation 4.3 for a Ramsey-Bordé interferometer). But for the ground state exit it appears very pronounced that the interferences are a superposition of the Ramsey-Bordé interferences and Ramsey interferences with twice the period of the former. We found, that the signal-to-noise ratio of the ground state exit detection is similar compared to that for the excited state exit. This is not obvious from figure 4.5 because different kinds of amplifiers with different bandwidths were used in the fluorescence detection, but it was checked separately. As only one hyperfine component is involved in the ground state detection, the signal appears symmetric on the background, which promises great advantages for high precision determination of phase changes.

According to the selectivity for a single hyperfine component and good signal-to-noise ratio, probing the ground state exit with the $b - X$ system was
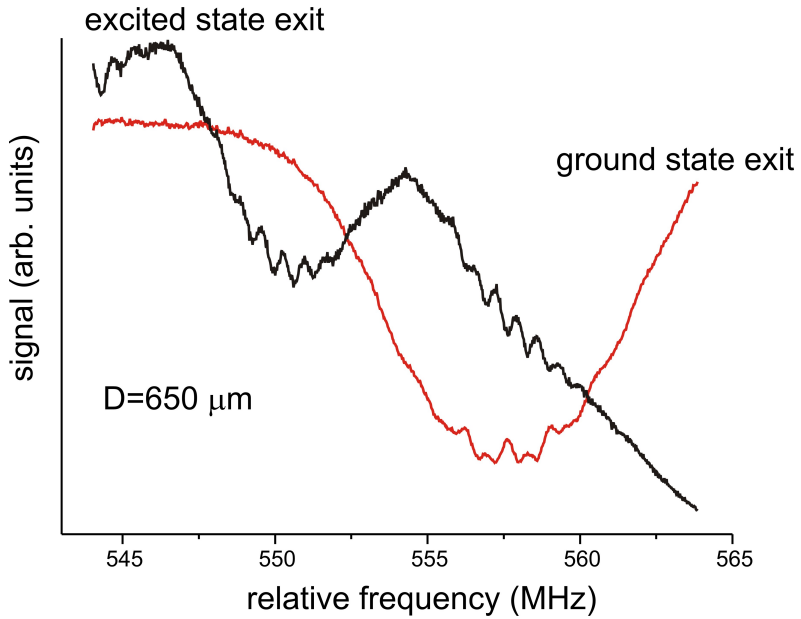
Figure 4.5.: Simultaneous records of matter wave interferences from ground state exit, detected by laser induced fluorescence on the highest frequency hyperfine component of transition $R(25)\,(27-0)\,b-X$, and from the excited state exit. The configuration is the Ramsey-Bordé interferometer with dark zone size $D = 650\ \mu$m. Note that the ground state exit shows the interference pattern and the background due to only one hyperfine component.

further used instead of the $B - X$ transition for signal comparison with that of the excited state exit.

4.5. Analysis of the signals

While for the ground state exit the structure is already reduced to a single hyperfine component, for the excited state exit we have an overlap of more than one hyperfine component sitting on an asymmetric background. The signals (see e.g. figure 4.5) for both exits are a superposition of an incoherent background and interference fringes from different interference phenomena with interference periods differing by a factor of two. For analysis of the content and comparison of the phases of the interference patterns of the different exits it is necessary to disentangle the interferences from the background and from each other.

As a convenient approach we employ digital filtering by Fourier transformation. In this discussion, in order to simplify the terminology, we regard the spectra as being recorded linearly in time, i.e. the frequency scale underneath the spectra being linear in time and the frequency steps during the recording are the steps in time. Then the Fourier transform can be regarded as a power spectral density as usual with a frequency scale according to the step unit in time.

First, spectra like those shown in figure 4.5 are made symmetric by creating an image mirrored at the vertical axis at the start point of frequency scan. Then this symmetric structure is Fourier transformed. The corresponding power spectrum for the example in figure 4.5 is shown by figure 4.6 for both traces, vertically shifted for better comparison. The frequency scale is arbitrary by the chosen time for the frequency step during the recording. The spectra typically show a low frequency increase for the slowly varying profiles and two main peaks on a noisy background structure. The center frequencies of the peaks differ by the expected factor of 2. They are labeled in figure 4.6 as corresponding to the Ramsey or Ramsey-Bordé interferences. In this Fourier transformation the two frequency components clearly appear, which directly proves that also for the excited state exit the Ramsey interferences are observed, which was not obvious from the trace shown in figure 4.5.

Digital filtering is performed by selecting an appropriate interval around one of the peaks, then setting the remaining parts of the Fourier spectrum to zero and transforming back to obtain the filtered structure. This is equivalent to applying a narrow band pass filter with rectangular shape tuned to the frequency
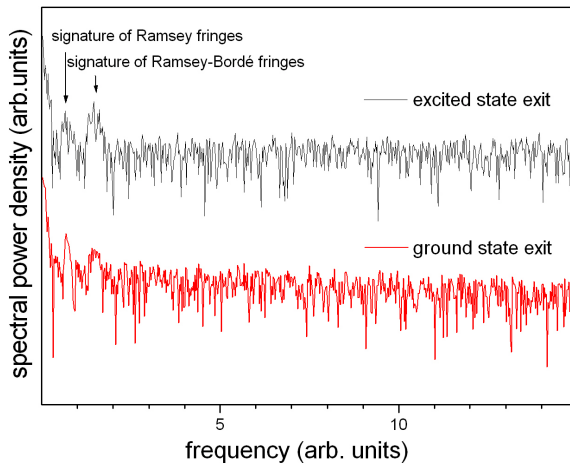
Figure 4.6.: Fourier transformation of the Ramsey-Bordé signals of both inter-
ferometer exits from figure 4.5. The power spectrum of the ground
state exit is vertically shifted allowing better comparison with the
excited state spectrum D = 650 *μm*.

of the Ramsey or the Ramsey-Bordé interferences. The background structure and the high frequency noise can be suppressed by this filtering process. This procedure works well with the signals of both exits. As an example the result of such filtering is shown in figure 4.7.
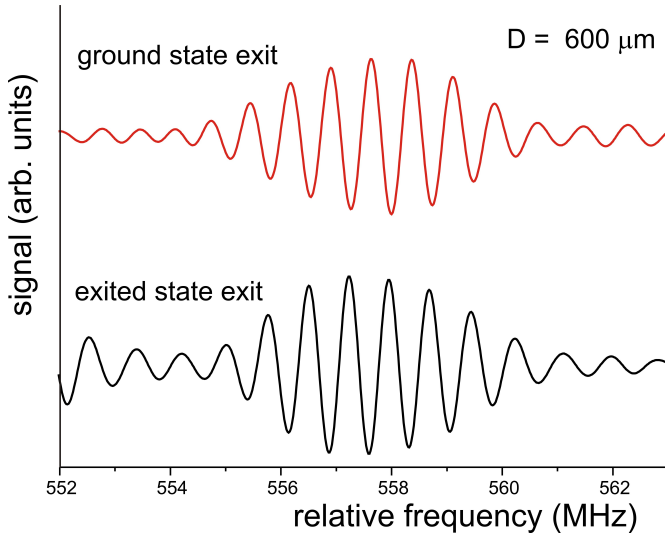

Figure 4.7.: Result of narrow-band Fourier-filtering of the Ramsey-Bordé interferences of both interferometer exits

The central parts of the interferences can be well recognized. The non zero amplitudes to higher and lower frequencies stem from the noise power within the filter bandwidth, which remains from the total noise. For the excited state exit, at low frequencies side the amplitude raises again due to the interference pattern of the next coming hyperfine component in figure 4.5. Such part is not visible in the signal of the ground state exit as it contains only the signal of a single hyperfine component.

For the signals from the Ramsey interferences a similar approach can be used to separate them from background and from the other interferences, by centering the filter around the first peak in the Fourier spectrum of figure 4.6. Apart from the different period, the result looks similar to the one shown.

4.6. Discussion and conclusions

This section describes the extension of a Ramsey-Bordé interferometer for simultaneous observation of both interferometer exits. The operational conditions of the interferometer imply simultaneous observation of Ramsey interference and Ramsey-Bordé interference in this matter wave interferometer with laser beam splitters. This appearance is related to the short dark zone required because of the short life time of the molecular excited state and the long transversal coherence length due to collimation of the molecular beam.

For the detailed study of the interferometer we employed both interferometer exits for both cases, Ramsey interference and Ramsey-Bordé interference . The installation of the ground state detection provides advantages over observation of excited state molecules. We demonstrate by using the $b - X$ transition with well resolved hyperfine structure, that this detection scheme offers additional spectral selectivity which is not available at the excited state exit.

The ground state detection requires an additional, independently tunable laser, which also must be frequency stabilized within a small fraction of the line width of a hyperfine component. With our present setup this requirement could be readily fulfilled due to the master-slave configuration of diode lasers used already for the beam splitters.

Both interferometer exits show interference structures, which comprise different amounts of Ramsey and Ramsey-Bordé interference contributions depending on the distance D between the beam splitters of the matter wave. In figure 4.5 an example is given. While the excited state exit seems to reflect only Ramsey-Bordé patterns, the signal of the ground state exit shows a beat structure of oscillating signals. Fourier analysis of both interference signals shows, however, substantial amounts of Ramsey and Ramsey-Bordé structures in each case.

In a previous paper [23] various modulation techniques were presented, among them a method which is also able to separate a single hyperfine component from the blended spectral profile at the excited state exit. This is achieved by depletion of the population of undesired hyperfine sublevels in the ground state through optical pumping before the particles reach the interferometer zone. This method requires also an additional laser fulfilling the requirements above, but does not yield the complementary interference signal like the ground state exit does, which contains valuable information regarding the presence of Ramsey interferences.

The application of the Ramsey interferometry for comparison of phases is an interesting issue, as it needs only two beam splitters, and the contrast can

be higher compared to the Ramsey-Bordé case, depending on the separation of the beam splitters. So for our case of low contrast Ramsey-Bordé interferences, the observation of the Ramsey interferences could give an improvement for phase measurements.

However, caution is advisable. From formulas 4.4 to 4.6 it is obvious that the requirement of phase stability of the laser fields for the beam splitters is very high for the Ramsey setup compared to the Ramsey-Bordé interferometer with its intrinsic phase shift cancellation. Any phase shift in one of the optical beams with respect to the other will immediately appear as a phase shift of the matter wave interference pattern. For the Ramsey-Bordé setup, using a cats eye which transfers beam 1 into 4 and beam 2 into 3, any phase shift in beam 1 will be compensated by the same shift opposite in sign in beam 4, the same arguments applying to beams 2 and 3 as well (assuming that the optical set-up is stable enough within the time the molecules need to propagate through the MWI.)

Thus the phase stability of the Ramsey interferences is only as good as the relative phase stability of both beam splitter fields for the Ramsey arrangement.

The high sensitivity on the phases for the Ramsey interferences suggests to work on improvement of the stability of the phases of the beam splitter fields. Presently, the suitability of our Ramsey-Bordé configuration for phase comparisons is limited by the drift of the optical phases. Reduction of the collimation of the molecular beam would reduce the coherence length of the wave packets in transverse direction yielding a smaller contribution of Ramsey interference.

A more promising approach will be to design a scheme which will provide stable relative optical phases for the beam splitters. This would allow to employ the Ramsey scheme for phase measurements, which would yield better contrast of the interferences. First experiments were started, and the preliminary observations are quite promising as described in chapter 5. We do not expect that we can suppress the Ramsey part completely due to our limitations in the lifetime of the molecular state used, thus phase determinations from the spectra will always suffer from the phase sensitivity of the Ramsey contribution.

Thus the success in phase stabilization of the laser beams will allow to extend our experiments to applications of Ramsey interferences like the observation of phase shifts by near resonant laser fields to study molecular transition moments or intra-beam atom-molecule collisions where the atoms are prepared in a specific quantum state. This will allow the observation of quantum

state specific collisions, both collision partners would be prepared in a selected quantum state. Such experiments will be described in chapter 6 and 7.

5. Ramsey IM stabilization and application

A Ramsey interferometer is a useful tool and widely applied in the high precision measurement of quantum metrology, like the atomic clocks with Cs and Rb [29]. Compared to other interferometer configurations, the Ramsey interferometer uses the lowest number of beam splitters, thus it is comparatively easy to realize and the signal amplitude is large. But comparing with a Ramsey-Bordé interferometer, where the paths are closed in space and the phase variations introduced by the lasers are compensated, the Ramsey interferometer has transversally only partial overlap of the wave packets and any laser phase variation shows up on the interference pattern. This chapter is about the building up and characterizing of a Ramsey interferometer.

5.1. Experiment

First the experimental setup of the Ramsey interferometer by employing two laser beam splitters is described and the stabilization scheme of the phase difference between the two laser beams is explained. Then the repopulation process of the ground state will be analyzed by comparing the interferograms both from ground state exits, but separated far away. Further the experiment will be modified for the comparison of interferograms from ground state exit and exited state exit at the same separation as before but using a modulation method to suppress the background. Finally, the transverse coherence length of the matter wave will be modified to see the change of the interference contrast. This modification of transverse coherence length is used to verify our wave packet model of the Ramsey interferometer.

5.1.1. Phase stabilization

As discussed in the theory chapter 2, for a Ramsey interferometer composed of two laser beams, the phase difference between the two tansversally partially

overlapped wave packets is in equation 5.1

$$\Delta\phi = T(\Delta - \delta) + \phi_1 - \phi_2 \qquad (5.1)$$

$T = D/v_0$ is the traveling time of the matter wave between both laser beam splitters, Δ is the frequency detuning of the laser and δ is the effective detuning by the photon recoil $\delta = \hbar k^2/2M$. Because of energy and momentum conservation, the phase part $T(\Delta - \delta)$ is fixed for a given detuning Δ. ϕ_i is the phase added from the laser beam wave front on the molecular matter wave during the interaction. The phase ϕ_i depends strongly on the mechanical stability of the optical components which direct the laser beam. The short term mechanical stability is influenced by the vibration on the optomechanical parts, transfered from the vacuum pump system to the optical table, although a damping stage is built in between. The long term influence comes from the thermal expansion of optomechanical material, following the temperature changes induced by the air conditioning system. Any change of the laser beam path length will shift the wave front crossing the K_2 beam, thus imprint a different phase on the matter wave. This variation of $\phi_1 - \phi_2$ leads to a shift of the Ramsey interference pattern. In order to obtain stable Ramsey fringes for sensitive phase measurements, interferometric stability for optical beams is required. This can be achieved by stabilizing the phase difference between the two laser beams. For this purpose the two laser beams are focused by a lens to form a spatial optical interference pattern which provides local interference maxima, whose positions are sensitive to the phase difference between the two wave fronts. By fixing the optical interference pattern spatially, the phase difference between the laser beam splitters can be stabilized.

In the figure 5.1, the scheme of the phase stabilization is shown. The two laser beams 1 and 2 for Ramsey interferometer are separated by the dark zone of length D. They are focused by a lens with focal length f, such that the two laser beams cross at an angle Θ. The right side of figure 5.1 shows the enlarged top view of the crossing of the laser beams. A plane wave approximation of each optical beam is used for easier illustration. The thick lines stand for laser beams which cross at angle Θ. Perpendicular to each laser beam, the array of thin lines represent its wave fronts. The distance between two thin lines is the wavelength λ. The crossing points of wave fronts form interference maxima as marked by black dots with transverse separation d and vertical distance L. A screen placed behind the focal point of the lens can get a spatial resolved optical interference pattern as indicated by the dashed line along the black dots a, b and c, the interference maxima. A phase shift of 2π of laser beam 1 would move the interference maximum at dot a in transverse direction to the position
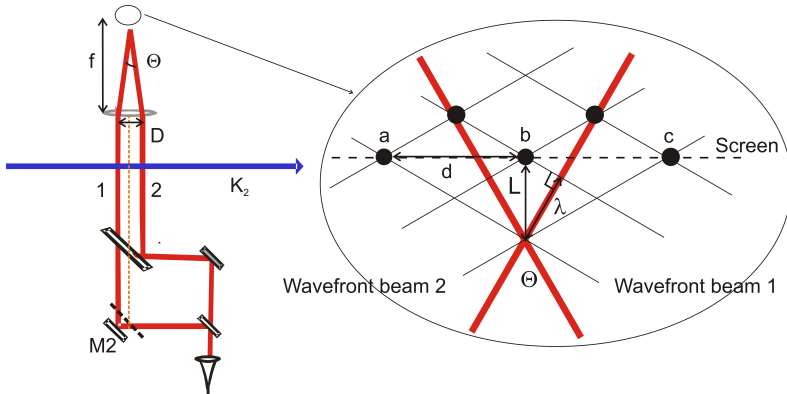
Figure 5.1.: The optical setup for the stabilization of the phase difference be-
tween the two laser beams 1 and 2. The enlarged circle shows the
crossing of the wave fronts at a moment of time, which forms a
spatial optical interference pattern. The screen can be put at a dis-
tance of NL/2 (N is an integer number) behind the focus point to
get a spatially well resolved optical interference pattern.

of dot b in the screen. When the observation is spatially limited to a small area,
the optical intensity at this point can be used to monitor the intensity change
by the shift of phase difference. A piezo is mounted to the mirror M2 which
reflects the laser beam 1. Any relative phase change of lasers leading to the
change of the optical intensity locally can be converted to a voltage to drive
the piezo to stabilize the position of the optical interference pattern, thus to
compensate this phase shift. When the piezo moves, it will also change the
distance D and Θ between a pair of laser beams as shown in figure 5.1. This
will have no influence on the intensity for observation, because the change of
separation between two interference maxima is negligible. This can be proved
by the following considerations. The distance d between adjacent interference
maxima on the screen can be derived from

$$figure 5.1 \quad left \quad side \qquad tg\frac{\Theta}{2} \;=\; \frac{D/2}{f} \tag{5.2}$$

$$figure 5.1 \quad right \quad side \qquad cos\frac{\Theta}{2} \;=\; \frac{\lambda}{L} \tag{5.3}$$

$$tg\frac{\Theta}{2} \;=\; \frac{L}{d} \tag{5.4}$$

$$d \;=\; \lambda\sqrt{1+(\frac{2f}{D})^2} \approx 2\lambda\frac{f}{D} \tag{5.5}$$

With a laser wavelength λ of 818nm, a separation D of $500\mu m$, and a focal length f of 50cm, d = 1.6 mm. The reduction of D by $\lambda/2 \approx 400$ nm leads to a change Δ d = 130 nm according to formula 5.5. This is indeed negligible compared to d. But this variation in phase leads to a shift of optical interference pattern by $\approx 800 \ \mu$m in transverse direction between point a and b. A small detail in figure 5.1 should be emphasized here: this is the symmetrical arrangement of the laser beam out of the fiber coupler. The nearly equal optical lengths of laser beam 1 and 2 make sure no relative phase shift due to laser frequency tuning.

The complete servo loop for stabilization of the relative phase of the two laser beams is drawn in the left part of figure 5.2. Coming out of the lower fiber coupler, the laser beam is polarization purified by a Glan-Taylor crystal(GT). By mirrors and beamsplitters, it is divided into laser beam 1 and 2 with equal intensity and adjusted with parallel wave fronts. They cross the molecular beam of K_2 forming the beam splitters of Ramsey interferometer. The pair of laser beams at the left hand side of BS1 are used for phase stabilization. They are superimposed by a lens on a photo diode (PD1) which is placed behind a diaphragm to detect the optical interference pattern. A pin hole with diameter smaller than d in equation 5.5 is installed on PD1 to limit the detected area to enhance the interference contrast. The PD1 with the pinhole is built on a two dimensional translational stage to adjust the position. When a linear voltage is applied to the high voltage amplifier (HV) to drive the piezo at M2, as the wave front of laser beam 1 runs continuously, PD1 observes an oscillation pattern on the intensity. The part of laser beam reflected by GT to photo diode 2 (PD2) is used to normalize the signal from PD1. Both photo diodes signals are processed by an analog divider and are adjusted such that the error signal (PD1-PD2)/PD2 is nearly symmetric to 0 as shown in figure 5.2 before the Proportional-Integrator (PI).
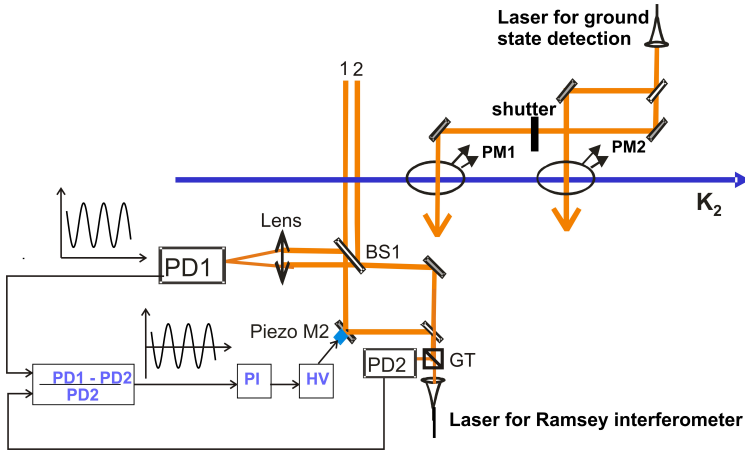
Figure 5.2.: Servo loop of the phase stabilization and the detection scheme of interference patterns. The right side shows the detection scheme to investigate possible relaxation effects in the ground state population

The PI has a proportional part with cutoff frequency 5kHz, and the integration part is set to a time constant of 2.5s. The error signals with open and closed servo loop were recorded for half an hour and are compared in figure 5.3. For the error signal recorded without phase stabilization, the spikes of the noise structure correspond to the short time instability, and the periodical structure represents the long time drift of the optical phase. For the error signal recorded with closed servo loop, the residual phase shift is less than 0.1 radian and there is no obvious long time drift.

5.1.2. Application to the investigation of relaxation effects in the ground state population

After the two laser beam splitters, the result of the coherent interference of the matter waves is preserved in the population of the ground state. We use some method downstream to read out this information carried by the molecule population. In order to investigate the question whether there occurs repopulation of the ground state levels and thus loss of interference contrast on a long path, we compare two observation zones separated by 30cm as shown in figure
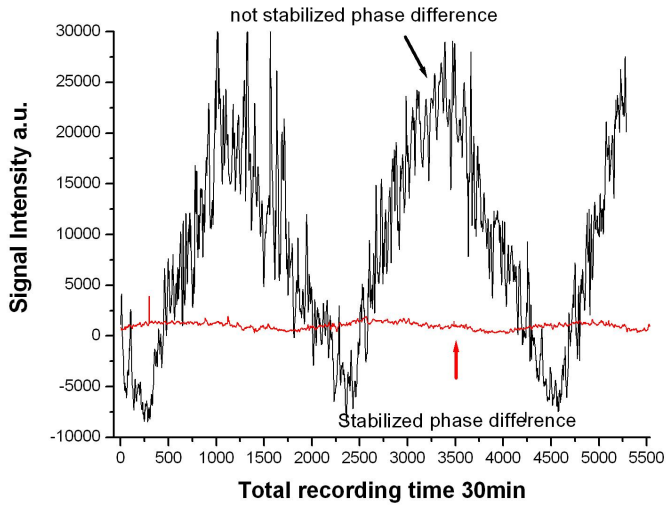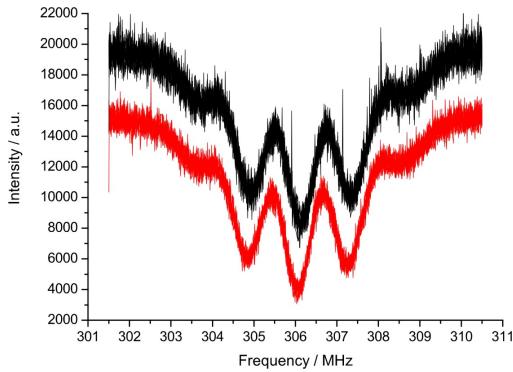
Figure 5.3.: The comparison of error signals with open and closed servo loop for a total recording time of 30 minutes. The x axis represents the data point. The error signal for the open servo loop is not symmetric to zero because the amplification setting of signal from PD2 was not perfect.

(a) A long time recording of interference patterns to test the phase stabilization setup. The upper curve is recorded from PM1, the lower is from PM2. The recording time is 90 min, overlap of 10 scans to give a direct impression of the stability.
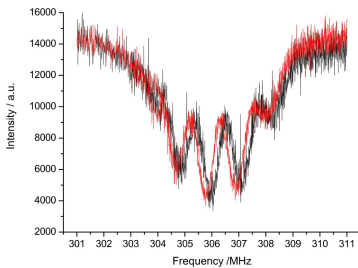
(b) Comparison of interference
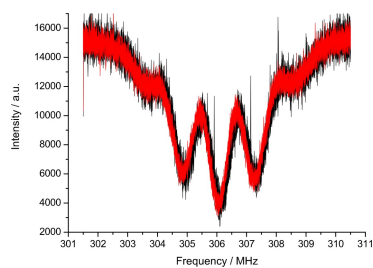
(c) Comparison of interference

Figure 5.4.: The phase stabilization records and the verification of no relaxation effects in the ground state population. 5.4(b) shows that the interference fringes recorded from PM1 and PM2 have a phase difference of 0.9 rad which corresponds to 180 kHz detuning. 5.4(c) shows that the interference fringes recorded from PM1 and PM2 have a phase difference of 0.4 rad which corresponds to 70kHz detuning.

5.2 on the right part. The frequency of the laser beams 1 and 2, which build up the Ramsey interferometer, is tuned through the transition. The power of the laser is kept constant and fulfills the $\pi/2$ condition of this transition. The frequency of the laser for the ground state detection is fixed to the center frequency of the desired hyperfine component, and the laser power is high enough to saturate the transition. The fluorescence intensity will be proportional to the molecule flux in ground state. After the two laser beam splitters 1 and 2, the population information in the ground state is detected immediately by photomultiplier tube the PM1. The distance between laser beam splitter 2 and PM1 is 1 cm, corresponding to a traveling time of 10 μs of K_2 matter wave. The molecules in excited state already decay spontaneously and will not add incoherent background to the detected signal in PM1. The same detection is made at the second observation zone by another photomultiplier PM2 30cm downstream of the molecular beam, the traveling time in between is $300\mu s$. Both photomultiplier tubes are R943-02 HAMAMATSU.

In order to avoid any influence of instabilities of the experimental setup, the interference patterns from both observation zones are recorded simultaneously for a certain frequency detuning. As shown in figure 5.2, the laser beam for the ground state detection is divided into two laser beams with equal intensity. The data acquisition is done alternatively in PM1 and PM2 synchronized by the shutter at each frequency detuning. The shutter is first opened, and the signal at PM1 is recorded. Then the shutter closes, the signal at PM2 is recorded. At next frequency step, the above process repeats. The scheme of the labview program for sequence controlling is given in the appendix B. Two scans, one with increasing frequency and one with decreasing frequency, are taken to be able to eliminate any phase shift that might come from the time constant delay of the program and electronics. With the stabilization scheme, 10 Ramsey interference patterns were recorded in 90 minutes and the superposition is shown in figure 5.4(a). For a single scan, the signal width corresponds to a phase uncertainty of 0.4 rad, the average process and usage of all data points for the fitting will reduce the uncertainty. The data treatment of this recording is discussed later in data processing section 5.2. Two conclusions for the curves in 5.4(a): 1. The interference patterns are not smeared out, the phase keeps constant. 2. The signal to noise ratio and the contrast of interference pattern do not change after traveling 30cm. A repopulation process of the ground state does not happen within this distance. Figure 5.4(b) and figure5.4(c) are examples of the interference signals recorded at PM1 and PM2 from different measurement days. All the image and data acquisition devices were as good as possible set identical in both observation zones PM1 and PM2. Different density filters are

used to get the same height of background level. Although all optical adjustments are performed in exactly the same way, the phase difference between the two interference fringes recorded at the different observation zones differ from day to day.
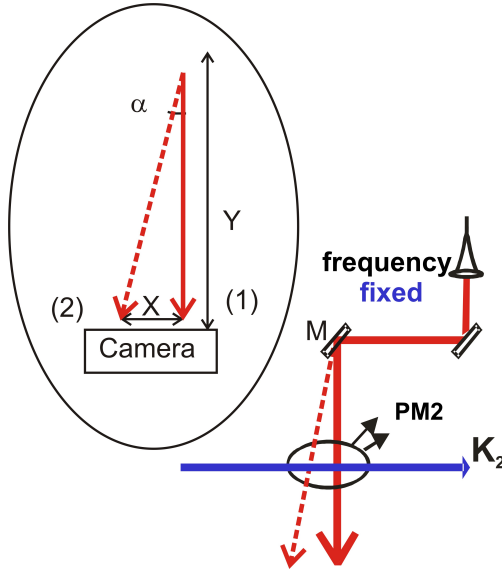

Figure 5.5.: Using Doppler effect to verify that the phase shift between interference fringes recorded from different exits in figure 5.4(b) and 5.4(c) comes from the alignment uncertainty of the detection beam.

A test was made to confirm that this phase difference comes from the Doppler shift of the transition which results from the uncertainty in the alignment of the detection laser beam. The angle between the laser beam and the molecular beam changes the resonance frequency. Different velocity components of the matter wave prepared by the interferometer are read out by the ground state detection laser beam which can result in the shift of the whole interference fringe. This angle was measured quantitatively. Ramsey fringes are first recorded by PM1 and PM2 as references. Then the laser beam at PM2 is tilted with a small angle to see the frequency shift of the interference pattern. Then this angle is measured by the position change of this laser beam spot in a cam-

era set far distance away as shown in figure 5.5. Angle α is calculated from Doppler shift

$$\alpha = \pi/2 - arccos(\frac{\Delta\omega}{k \cdot v}) \qquad (5.6)$$

For a phase difference of 0.4 rad corresponding to $\Delta\omega = 70$ kHz as in figure 5.4(c), a wave vector k corresponding to the laser wavelength 818 nm, a center molecular velocity v around 1×10^3 m/s, the angle calculated according to equation 5.6 is $\alpha = 5*10^{-5} rad$. The angle measured by the camera as indicated by the enlarged circle in figure 5.5 is $\alpha \approx tg\alpha = x/y$. It corresponds to the shift in x direction of 80 μm at a length of y = 600 mm, $\alpha' = 10*10^{-5} rad$. These two angles agree with each other, when we take into account the uncertainty of position reading of the laser beam spot with a diameter of 2 mm. In order to eliminate this phase shift, for the mirror mount marked as M in figure 5.5 with a size of 4.5 cm × 4.5 cm, a micrometer screw with step precision under 1 micrometer is required. For the investigation of relaxation effect in ground state population here, just the amplitude is considered, so such high precision step pointer is not implemented. When phase comparison is done for the detections at the same position (PM2) under different physical situations, this " permanent " phase difference between PM1 and PM2 needs not be considered neither as in the experiments in later sections.

5.1.3. Phase modulation to reduce the background

The interference signal sits always on a background from the transition line profile which depends on the laser power rather than on the laser phase. Equation 5.1 shows the phase dependence of the oscillation fringe on the phase of laser beams. In order to separate the Ramsey interference pattern from the background, a phase modulation method is used. When the laser beam wave front is modulated across the potassium molecular beam, the phase of the matter wave is also modulated, which results in a modulated interference fringe, and at any frequency detuning the detected fluorescence intensity by the photomultiplier is modulated. A lock-in amplifier can pick out this modulation to yield the pure interference pattern.

The experimental set-up is based on the phase stabilization scheme as shown in figure 5.6. A modulation voltage is added to the input of the high voltage amplifier (HV) which drives the piezo of mirror M2. The modulation frequency is 30 Hz. This frequency is chosen high enough, that the phase stabilization servo control is not influenced by it, but low enough, that it is still
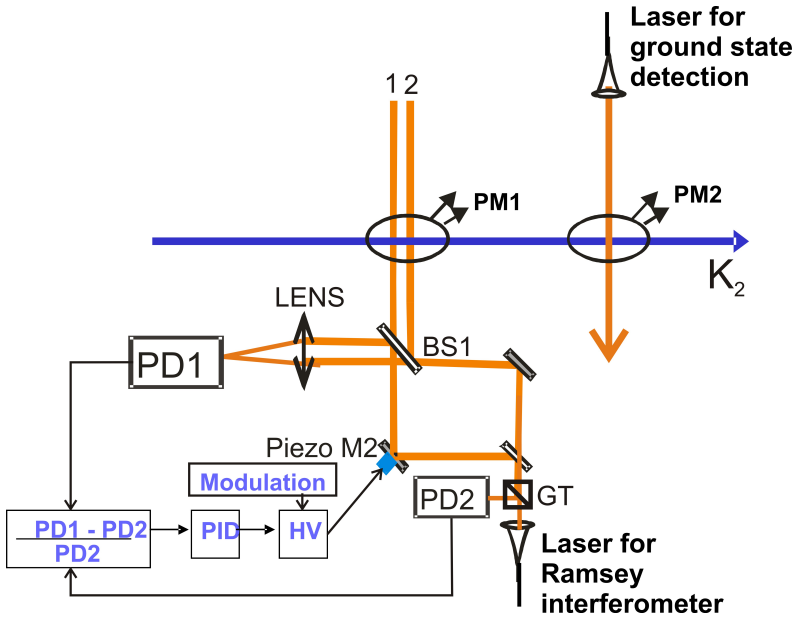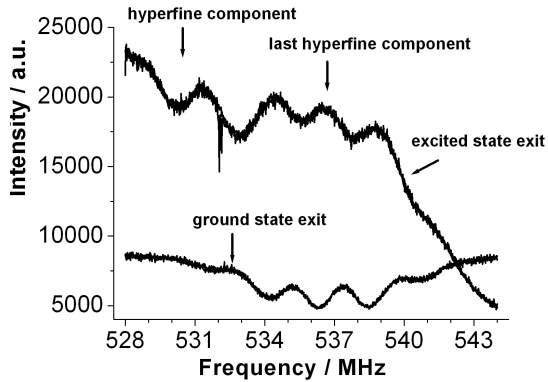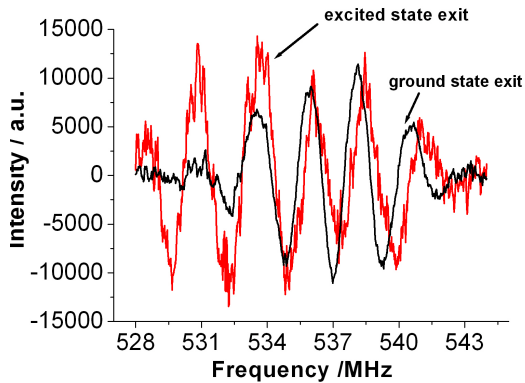
Figure 5.6.: Experimental setup for phase modulation and the comparison of detection scheme in excited and ground state exits
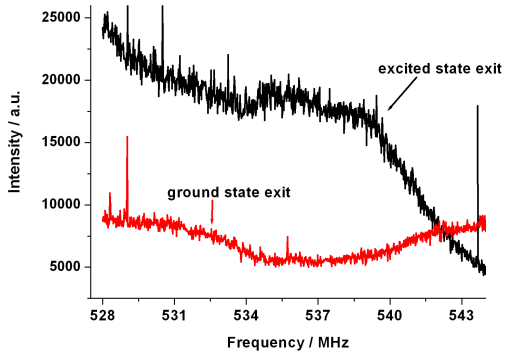
(a) Under small modulation amplitude: phase modulation smaller than 0.4π, the directly recorded interference signals from excited and ground state exits


(b) Signals detected by two lock-in amplifiers sensitive to the modulation on the signals of (a). Each lock-in filters out the interference fringe from the excited or ground state, respectively. The comparison gives the phase information between the interference fringe from the two exits.

Figure 5.7.: Phase comparison of interference fringes from ground and excited state exits with small modulation.

(a) Under larger modulation amplitude: phase modulation equals 2π, the directly recorded signals from excited and ground state exits, the interference contrast vanishes.
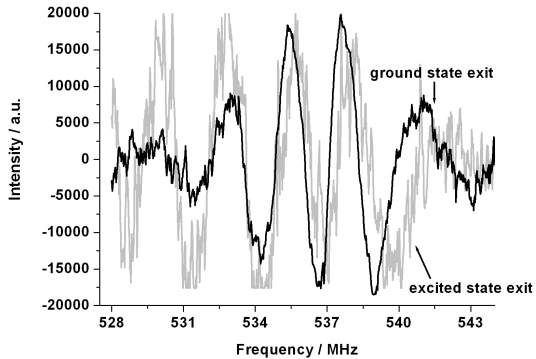
(b) Detection of the modulation: comparison of interference fringes from different lock-in amplifiers of the two signals from figure 5.8(a)

Figure 5.8.: Phase comparison of interference fringes from ground and excited state exits with large modulation amplitude.

within the bandwidth of the piezo and HV-amplifier. The fluorescence photon flux is $\approx 4 \times 10^4$/s. About 1000 photons are available for each modulation period. For the interference detection in section 5.1.2 it is proved that there is no changing of contrast for the interference pattern by relaxation. Now we use the two separated photomultiplier tubes to compare the signals from excited state exit and ground state exit. The Ramsey interference fringe from the excited state exit is detected by PM1. The signal of the ground state exit is read out in PM2 by applying a resonant laser as described in section 5.1.2. The current of the photomultiplier is transferred to voltage via a picoamperemeter, and then the voltage signal goes to either a data acquisition system (DAQ) or a lock-in amplifier respectively. The rising time within the photomultiplier tube and picoamperemeter are less than 30 ns and 1 ms respectively. The DAQ has an integration time of 1 s. The direct recordings of the DAQs are in figure 5.7(a). A modulation amplitude of 100 mV corresponds to a phase modulation of the interference pattern by 0.4π radian. The recorded signal in figure 5.7(a) shows that the interference patterns are not smeared out by the modulation, because of this modulation amplitude can be considered small. The interference fringe from ground state exit is the same as in last section. The one from excited state exit is on top of the overall fluorescence from the last two hyperfine components. The distance between the two hyperfine components depends on the energy splitting, thus the interference patterns from these two hyperfine components are not in phase with each other.

The interference patterns from lock-in amplifiers are in figure 5.7(b) with time constant 300 ms, sensitivity 10 mV. The phase of the lock-in amplifiers are so adjusted that the phases of interference patterns from both exits can be well compared. Since the energy splitting is the largest for the highest frequency hyperfine component, to compare the interference pattern observed on top of the hyperfine component, we look at the spectrum 5.7(b) starting from high frequency part. There is a clear appearance of out of phase between the interference patterns from ground and excited state exits. The appearance of out of phase reduces at the low frequency part. This is because: the signal from excited state exit is composed of two interference fringes not in phase with each other. This shifts the interference pattern from the excited state exit. For the interference pattern from ground state exit, only one hyperfine component is addressed, this symmetrical signal is better suited for the detection and later analysis.

Experiments are also done with large modulation amplitudes. In figure 5.8(a), the modulation amplitude is 500 mV, which results in a phase modulation of 2π. The modulation frequency is 30Hz, the time constant of data

acquisition (DAQ) is 1 s, so for each data point, there are 30 averaged scans, the average of a whole period of an interference pattern is 0, the average of laser induced fluorescence gives background. In the direct recording of DAQ in 5.8(a), the interference patterns are smeared out, only the transition profile as background remains. The lock-in amplifiers are with sensitivity 20 mV, time constant 300 ms, they still pick out the phase sensitive interference fringes on zero background as shown in figure 5.8(b). This method can be applied to smear out the signal from the embedded Ramsey interferometer in the Ramsey-Bordé configuration as given in chapter 7.2.

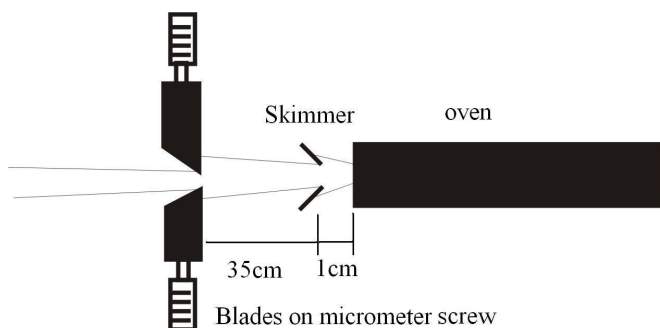## 5.1.4. Modifying the transverse coherence length

Figure 5.9.: Schematic view of blades on micrometer screws to change the coherence length of the matter wave

The Ramsey interference pattern comes from the transversely partial overlap of the wave packets. When the vertical displacement between the wave packets due to the recoil is constant, a size change of the matter wave packets in this direction leads to a change of the overlap area, and will influence the contrast of the interference fringes. The size of the wave packet is characterized by the coherence length which depends on the momentum distribution. $l_c = \hbar/2\Delta p$ [7]. The collimation controls the transverse velocity distribution. An experiment was performed to observe the interference contrast under different collimation ratios. For that two blades were introduced which could be moved symmetrically from outside the vacuum tank.

Figure 5.9 shows how the collimation is controlled. From right to left, the K_2 molecules are ejected out of the nozzle of the oven. The core is cut out
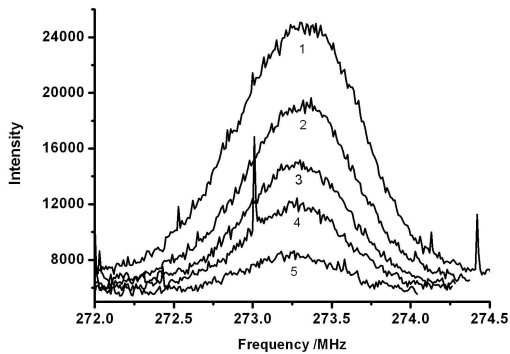
(a) Fluorescence profiles under different blade depths taken at PM2 by blocking the Ramsey interferometer laser beams. The integer numbers mark the different blade positions.
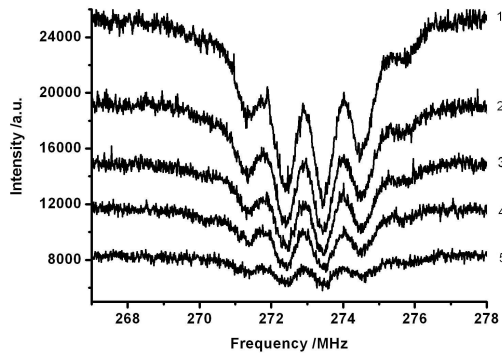
(b) The interference fringes under different blade shifts. Each integer number is with the same meaning as in figure 5.10(a). The decreasing signal level indicates the reduction of molecular number due to the cutting effect of blades.

Figure 5.10.: Varying the transverse coherence length.

by a skimmer 1 cm away. After the skimmer at a distance of 35 cm, two blades can be moved in to shape the molecular beam in the same plane common with the laser beam splitters. In this way, the velocity distribution of molecules in transverse direction can be narrowed, while the transverse coherence length increases. Another effect by the cutting of blades is the reduction of the molecule number. The observed signal is a statistic event of the whole ensemble so the interference amplitude must be renormalized to the reduced total molecule number to get the contrast.

The blades on micrometer screw has a precision of 0.1 mm. The starting point is chosen that the two blades just cut the edge of the molecular beam and initiate a population reduction. This is indicated as integer number 1 in figure 5.10(a). For each measurement, both blades shift with a step of 0.2 mm linearly symmetrically to the center of the molecular beam. To verify the position of the blades, fluorescence spectroscopy is done at PM2 by observing molecular population in the ground state. As shown in figure 5.10(a), the integer numbers mark the line profile taken under each blade position. With the assumption that the velocity distribution out of the oven is symmetrical in the horizontal plane, the symmetrical shape of the line profile indicates equal shift of the blades from both sides. From 1 to 5, transverse velocity distribution gets narrower linearly as the collimation ratio increases linearly. With each such velocity distribution, an interference fringe is recorded as shown in 5.10(b). The details of calculation for the contrast is in the next chapter ″data processing″.

5.2. Data processing of observed interferograms

Different from the excited state exit where the interference fringes from two hyperfine components can not be well separated, the interference fringes got from the ground state exit has only a single hyperfine component, which facilitates the fitting process. There are three methods to fit the data:

1. fit the oscillation fringe on zero background from the lock-in amplifier output by modulation method discussed in section 5.1.3.

2. fit the oscillation pattern from digital filtering as described in chapter 4.

3. fit the oscillation pattern sitting on the depletion dip, for example the experiment result of section 5.1.4.

In the following paragraphs, all three methods will be discussed and compared.

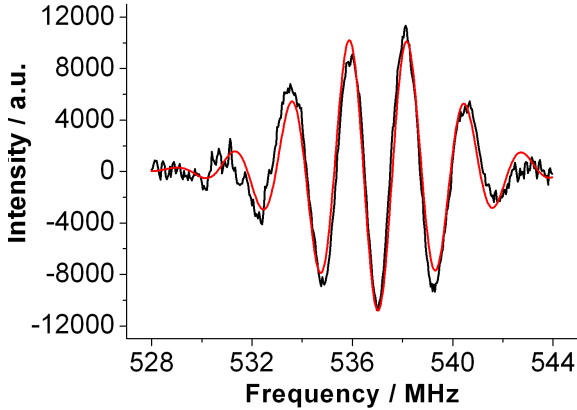## 5.2.1. Fitting method one

Figure 5.11.: Fitting result of the output signal from the lock-in amplifier. Within signal-to-noise ratio, the fitting in the center region is acceptable.

In the first approach, the pure oscillation fringe from the lock-in amplifier is fitted. Here the background does not need to be considered. The following formula is used,

$$G(\nu) = A \cdot cos[2\pi P(\nu - \nu_0) + \phi] \cdot exp[-(\frac{\nu - \nu_0}{\nu_w})^2] \qquad (5.7)$$

A is the oscillation amplitude, P is the oscillation period, ν_0 is the center frequency, ϕ is the phase. The Gaussian envelope $exp[-(\frac{\nu - \nu_0}{\nu_w})^2]$ is also centered at ν_0 with the Gaussian width ν_w. The cosine term describes the oscillation of the interference fringe. The Gaussian term describes the broadening of the wave packet by the velocity distribution if the homogeneous broadening by the focusing of the interferometer lasers is sufficiently wide.

The fit result of such interference pattern is shown in figure 5.11. The fitting is within signal-to-noise ratio (S/N) good in the middle area, while for the outer

regions, the measured oscillation period becomes larger. As the frequency is generated from a RF synthesizer, the linearity of the frequency scale is guaranteed. This variation of the period might come from the velocity distribution of the molecular ensemble.

The distribution of the deviations between fit and observation depends significantly on the weighting of the signals. If the weight in the center is high, the deviation in the wings shows up more strongly. Different weightings were not tried to check if a constant period P would be statistically acceptable.

Generally speaking, the relative simply formula 5.7 can describe the measured curve within the obtained S/N ratio. And it will be used to fit the oscillation for the following fitting process.

5.2.2. Fitting method two
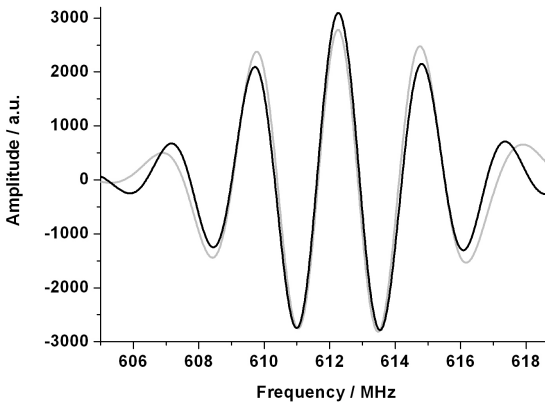
Figure 5.12.: The gray curve is the back transformed result after digital filtering with an effective time constant of seconds . The black curve is the fitting result using formula 5.7.

As discussed in the data analysis of chapter 4 section 4.5, the pure oscillation pattern can be mathematically separated from the low varying background and the high frequency noise. Formula 5.7 is used to describe the oscillation fringes obtained by digital filtering. A recording for 90 minutes with 10 spectra

as shown in figure 5.4(a) is analyzed by digital filtering and fitted by formula 5.7 to test the phase uncertainty. Every two spectra in sequence with scanning frequency up and down are compared for the time constant delay which is proved to be zero. Then these two spectra are averaged, all together there are five averaged curves for the same experimental condition. Such five averaged curves are treated with digital filtering method. The transformed back curves are fitted with all the parameters adjustable to get a reasonable good fitting. One of the fitting result is shown in figure 5.12. The high frequency noise as well as the low variation of background are suppressed by the band pass filter. That is the reason why the curve is so smooth. The fitting in the center part is quite good within signal-to-noise ratio. The deviation of the period in the wings is similar to that seen in figure 5.11.

In order to check the phase stability, the uncertainty from fitting procedure needs to be reduced. All parameters with the same experimental conditions are identical, like $P = D / v_0$, v_0, v_w. The dark zone length D and molecular velocity v_0 in longitudinal direction do not change during the whole recording time. v_0 is the center frequency of this transition and Gaussian width v_w is defined by the focus lens building the interferometer lasers. The average values of P, v_0, v_w are fixed and used to refit the data. The amplitude A is varied to allow for slow signal change from scan to scan due to long term drift. The standard deviation of phase from the fitting result shows that the phase uncertainty of the Ramsey interference fringe recorded for 90 minutes is smaller than 5 mrad.

5.2.3. Fitting method three

Based on the fitting experience from section 5.2.1 and 5.2.2, I want to compare the contrast of Ramsey fringes when varying the transverse coherent length. Here the total molecular population needs to be taken into account. The fitting method 1 and 2 can not give the information of particle number. To induce this information, which is contained in the depth of the dip, fitting method 3 is employed and the experiment result from figure 5.10(b) is fitted directly by the following formula 5.8.

$$G(v) = \frac{G(1 + AMP \cdot cos[2\pi P(v - v_0) + \phi] \cdot exp[-(\frac{v-v_0}{v_w})^2])}{1 + A \cdot [\frac{2(v-v_1)}{w_1}]^2 + (1 - A - B) \cdot [\frac{2(v-v_1)}{w_1}]^4 + B \cdot [\frac{2(v-v_1)}{w_1}]^6}$$
$$+ BG \qquad (5.8)$$

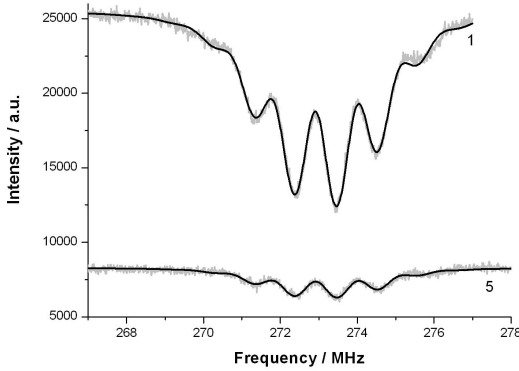The same formula as in the fitting method 1 and 2 from section 5.2.1 and

Figure 5.13.: Fitting results of the interference fringes on the depletion dip, the integer numbers mark the different blade positions as in figure 5.10(b). The gray line represents the direct recording, the black line represents the fitting curve.

5.2.2 is used to fit the interference term. The denominator describes the depletion dip produced by the interferometer laser. This is an empirical formula from the spectroscopic work. It describes a spectral line broadened by two types of mechanisms, one of which alone would produce a Gaussian profile (usually, as a result of the Doppler broadening), and the other would produce a Lorentzian profile. A and B are the coefficients to be adjusted, ν_1 is the center frequency of the depletion dip with a width w_1. They are set independent of the center frequency ν_0 and width ν_w of the interference term to allow for possible Doppler shift or broadening. The interference term is the modulation of the ground state population in the depletion process. G is the renormalization factor and AMP represents the contrast of the Ramsey interference fringe. BG is the total background composed of dark current from photomultiplier, scattered light and fluorescence signal from the ground state when there is no population depletion.

First, the curves 1-5 in figure 5.10(b) are fitted with all the parameters kept free. When only the blade position is shifted, the velocity distribution in transverse direction changes, but in longitudinal direction remains, so $P=D/\nu_0$ does not change. ν_0, ν_w, ν_1 and w_1 are the transition properties defined by the

molecular transition and laser beam splitter, they should stay the same value for all blade positions. The fitting result with all parameters kept free also shows that the standard deviations of these parameters are only a few percent of the averaged value. Within the signal-to-noise ratio, these parameters can be regarded as constants.

Comparing the values of ν_0 and ν_1, they differ only by a few percent, which means the depletion process happens at the same transition frequency as the interference fringe. But the value of w_1 is about 25% larger than ν_w, which means that at long distance, the Doppler boradening becasue of velocity distribution is larger than homogeneous broadening by the focusing of interferometer laser beam. Each average value of P, ν_0, ν_w, ν_1 and w_1 is taken as the fixed parameter to fit the curves to get the main parameters of interest AMP. Parameters G, AMP, ϕ, BG are varied because they will also depend on the setting of the blades, like the particle numbers. Figure 5.13 shows examples of the fitting result of the corresponding experimental curves 1 and 5 in figure 5.10(b). For no 1, the fit result is within the signal-to-noise ratio (S/N) good in the middle area, while for the outer region, especially at the wings the small discrepancy of the period is still visible. For no 5, since signal-to-noise ratio (S/N) is already small, there is no obvious discrepancy. For the comparison of contrast, this amplitude fit is already quite sufficient.

The area enclosed by the depletion dip to the background line is proportional to the total number N of molecules contributing to the interference process. It is the same as to integrate directly the area of the recorded fluorescence profile as given in figure 5.10(a) with respect to the background line.

5.3. Result and discussion

The results of comparing Ramsey fringe contrast at different transverse coherence lengths are shown in figure 5.14(a) and 5.14(b). These two figures are the measurements from different days. Figure 5.14(a) is the fitting result of experiment curves in figure 5.10(b), where the integer number representing the collimation is with the same meaning, the blade positions. The term AMP of formula 5.8, as contrast of the Ramsey fringe, is plotted as a function of the collimation ratio defined by the blade positions. Starting from the case of completely removed blades, position no 1, the blades are shifted in symmetrically, linearly with the step of 0.2 mm. Each blade position defines a collimation ratio, which confines the transverse velocity distribution of the molecular matter wave. As the transverse velocity distribution linearly gets narrower, the trans-

verse coherence length increases linearly, which should results in an increased contrast. As figure 5.14(a) and 5.14(b) show, the contrast indeed increases as the collimation ratio increases from 1 - 5, which agrees with the wave packet model of the Ramsey interferometer. Error bar is calculated as the noise renormalized to the signal. As collimation increases, the contrast should finally be a constant, since the lateral separation between the wave packet is negligible with the wave packet size. But because of small remaining particle number, the error bar is very large, this effect is not easy to recognize.
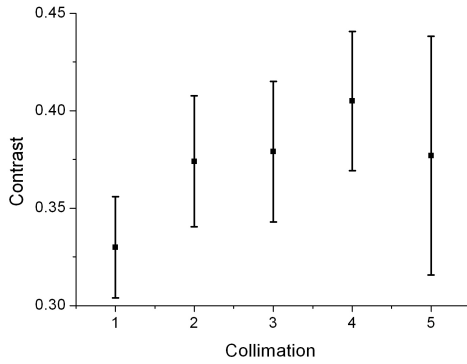
(a) The integer numbers mark the positions of the two blades, with the same meaning as in figure 5.10(b)
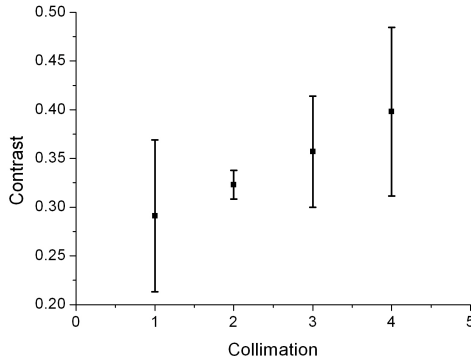
(b) Experimental result of the interference contrast from another experimental day

Figure 5.14.: Change of the interference contrast as a function of the collimation. The number in the collimation axis represents the blades position. As the collimation increases, the contrast increases.

6. Determination of transition dipole moment by matter wave interferometry employing the AC-Stark effect

Determination of transition dipole moments is of great importance in many applications of atomic or molecular systems. From them, a lot of parameters can be calculated, e.g. natural decay rate $\Gamma = |\mu|^2 \omega_0^3 / 3\pi\hbar c^3$ or Rabi frequency $\Omega_1 = \vec{\mu} \cdot \vec{E}/\hbar$. In this chapter, the Ramsey interferometer is employed to investigate the applicability of matter wave interferometry for the determination of molecular transition dipole moments. The experiment is focused on the transition $B^1\Pi_u - X^1\Sigma_g^+$ of K_2 employing the AC-Stark effect. By observing the phase shift and amplitude reduction of the interference fringe, the dipole moment can be calculated. Compared with spectroscopic work to measure the AC-Stark effect, the interferometer method has the advantage of separating the detection zone from the AC-Stark potential to avoid multi-photon effect. Another unique advantage is to select a certain transition for the dipole measurement. The spectroscopic work of using life time to calculate dipole moment sums over all the decay rate to the lower state, which requires a good understanding of the complete potential to the continuum region.

6.1. Theoretical aspects

6.1.1. AC-Stark effect and calculation of the phase shift of interference fringes using dressed state picture

When the matter wave undergoes the influence of a potential $U(x)$, the group velocity v changes locally and results in a phase difference $\Delta\phi_1$ compared with the situation without applying any field. This phase difference can be

expressed as [8]

$$\Delta\phi_1 = \frac{1}{\hbar v} \int_{x_1}^{x_2} U(x) dx \qquad (6.1)$$
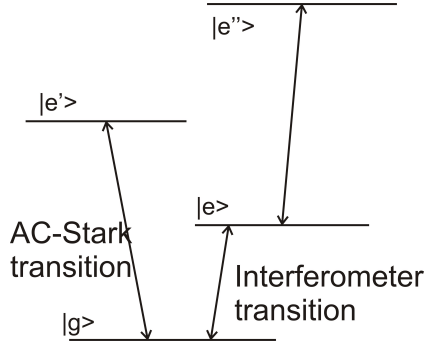
along the path from x_1 to x_2.

Figure 6.1.: Coupling diagram of the ground and excited states of the interferometer transition to higher levels by the AC-Stark effect.

As described in chapter 2 for the Ramsey interferometer without applying any potential, the phase difference between the two traveling paths of the matter waves at the exit is

$$\Delta\phi = \frac{D}{v_0}(\omega_L - \omega_0 - \delta) \qquad (6.2)$$

If the additional potential acts only on one of the interfering paths, the phase difference between the two matter waves at the exit is

$$\Delta\phi_{pot} = \frac{D}{v_0}(\omega_L' - \omega_0 - \delta) + \Delta\phi_1 \qquad (6.3)$$

the additional frequency detuning in order to compensate this phase shift is

$$\omega_L' - \omega_L = \Delta\omega = \frac{1}{D\hbar} \int_{x_2}^{x_1} U(x) dx \qquad (6.4)$$

In our experiment, we apply the potential $U(x)$ by a near resonant laser field. As shown in figure 6.1, the ground state $|g>$ of the interferometer transition is coupled by a near resonant laser field to a higher electronic level $|e'>$. In principle, the excited state of the interferometer transition can also be coupled

to another higher level $|e'' >$. By choosing the proper laser frequency one can switch between the two cases, assuming that for the other case the detuning is far more larger than for the desired case. The coupling between the molecule and the electro-magnetic field is called AC-Stark effect. In this experiment, the AC-Stark effect on the ground state $|g >$ is implemented. The scheme of applying AC-Stark potential on a Ramsey interferometer is shown in figure 6.2. Geometrically, the near resonant laser field and the laser fields for the interferometer have essentially no overlap. The molecular energy levels shift or split in the region of the near resonant laser field due to the Stark effect. Outside the potential region, the energy levels resume, only the phase shift introduced by the near resonant laser field on the matter wave remains and can be understood in the dressed state picture (see reference [30]).
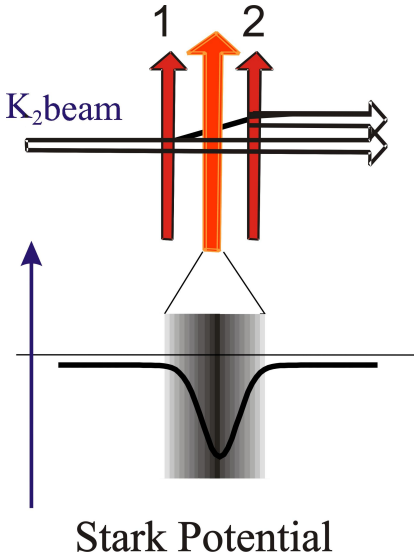

Figure 6.2.: Scheme of introducing a near resonant field as a Stark potential for the Ramsey interferometer

We begin by first neglecting the interaction between the molecule and the laser photons. The Hamiltonian of the global system is then $H_L + H_m$, where

$$H_L = \hbar\omega_{Lst}\left(a^+ a + \frac{1}{2}\right) \quad (6.5)$$

is the Hamiltonian of the laser mode, a^+ and a being the creation and annihilation operators for one photon with energy $\hbar\omega_{Lst}$, and

$$H_m = \hbar\omega_{0st}\left|e'\right\rangle\left\langle e'\right| \quad (6.6)$$

is the Hamiltonian of the molecule, having eigenstates $|e'\rangle$ and $|g\rangle$ with energies $E'_e = \hbar\omega_{0st}$ and $E_g = 0$. The eigenstates of $H_m + H_L$ are then labeled by two quantum numbers: the number M of laser photons in the mode ω_{Lst}, and the molecular quantum number e' or g.

The energies of states $|g, M+1\rangle$ and $|e', M\rangle$ are close to each other, when

6. AC-Stark effect

ω_{Lst} is near resonance, that is

$$\omega_{Lst} - \omega_{0st} = \Delta_{st} \ll \omega_{0st} \tag{6.7}$$

Δ_{st} is the detuning from resonance, and the manifold formed by these two levels is written as

$$E(M) = \{|g, M+1\rangle, |e', M\rangle\} \tag{6.8}$$

In the electric dipole representation, the interaction Hamiltonian V_{mL} couples the two states of each manifold $E(M)$ to each other. The corresponding matrix element is written as (details see reference book [30]).

$$< V_{mL} > = \langle e', M | V_{mL} | g, M+1 \rangle = \tilde{\mu} \cdot \tilde{E}/2 \tag{6.9}$$

μ is the transition dipole moment, and E is the electric field strength. The Rabi frequency Ω_1 is defined as the coupling strength

$$\vec{\mu} \cdot \vec{E} = \hbar\Omega_1 \tag{6.10}$$

When we take into account the coupling V_{mL} between the two states $|g, M+1\rangle$ and $|e', M\rangle$ of $E(M)$, two perturbed states $|1(M)\rangle$ and $|2(M)\rangle$ appear, these are called dressed states. They are separated by an energy interval [30].

$$\hbar\Omega = \hbar\sqrt{\Delta_{st}^2 + \Omega_1^2} \tag{6.11}$$

The eigen states and the eigen energies of the coupled dressed states are given as

$$
\begin{aligned}
|1(M)\rangle &= \cos\theta |g, M+1\rangle - \sin\theta |e', M\rangle & (6.12)\\
|2(M)\rangle &= \sin\theta |g, M+1\rangle + \cos\theta |e', M\rangle & (6.13)
\end{aligned}
$$

$$
tan2\theta = -\frac{\Omega_1}{\Delta_{st}} \qquad 0 \le 2\theta \le \pi \tag{6.14}
$$

$$
\begin{aligned}
E_{1M} &= (M+1)\hbar\omega_{Lst} - \frac{\hbar}{2}\Delta_{st} + \frac{\hbar}{2}\Omega & (6.15)\\
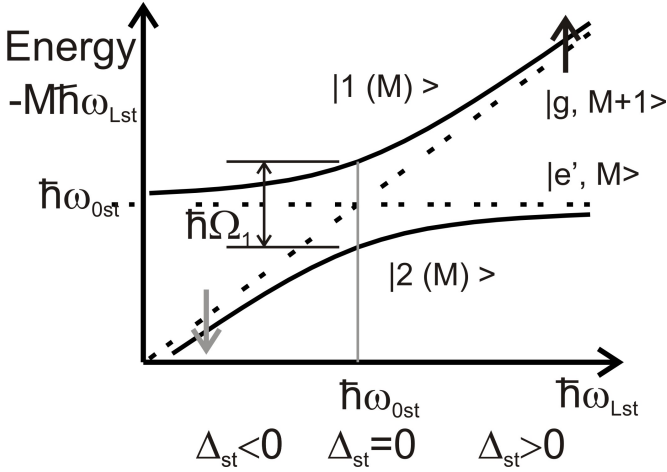E_{2M} &= (M+1)\hbar\omega_{Lst} - \frac{\hbar}{2}\Delta_{st} - \frac{\hbar}{2}\Omega & (6.16)
\end{aligned}
$$

Figure 6.3.: Energies of the dressed levels $|1(M)>$ and $|2(M)>$ (solid lines) versus $\hbar\omega_{Lst}$. The dashed lines represent the energies of the uncoupled states $|g, M+1>$ and $|e', M>$, cited from book [30]

The energies of different eigenstates as function of the detuning Δ_{st} are drawn in Figure 6.3. The dashed lines represent the energies of the uncoupled states $|g, M+1\rangle$ (straight line with slope 1) and $|e', M\rangle$ (horizontal line with ordinate $\hbar\omega_{0st}$). They intersect at $\hbar\omega_{Lst} = \hbar\omega_{0st}$. Because of interaction, the energy of dressed states is expressed by the solid lines. The energies of the dressed levels $|1(M)\rangle$ and $|2(M)\rangle$ form the two branches of a hyperbola having the dashed lines as asymptotes. The minimum distance between the two branches of the hyperbola occurs when $\hbar\omega_{Lst} = \hbar\omega_{0st}$ ($\Delta_{st} = 0$) and is equal to $\hbar\Omega_1$. The distance between the perturbed levels and their asymptotes represent the AC-Stark shifts of state g and e due to the coupling with the laser [30].

Without applying near resonant laser fields, the molecule is in state $|g, M+1\rangle$. When the near resonant laser field with positive detuning, $\Delta_{st} > 0$ and $|\Delta_{st}| \gg \Omega_1$ is applied, the molecule is in $|1(M)\rangle$ state, and the energy changes as the thick black arrow indicated in Figure 6.3, at large $\hbar\omega_{Lst}$. When a laser field with negative detuning, $\Delta_{st} < 0$ and $|\Delta_{st}| \gg \Omega_1$ is applied, the molecule is in $|2(M)\rangle$ state, and the energy changes as the thick gray arrow indicates in Figure 6.3, at small $\hbar\omega_{Lst}$. The energy shift is the additional potential energy

appearing when the matter wave enters the near resonant laser field. This is:

$$E_{|1(M)\rangle} - E_{|g,M+1\rangle} = -\frac{\hbar}{2}(\Delta_{st} - \Omega) \qquad \Delta_{st} > 0 \qquad (6.17)$$

$$E_{|2(M)\rangle} - E_{|g,M+1\rangle} = -\frac{\hbar}{2}(\Delta_{st} + \Omega) \qquad \Delta_{st} < 0 \qquad (6.18)$$

The frequency shift of the interference pattern is, using 6.4

$$\Delta\omega = \frac{1}{2D\hbar}\int\frac{\hbar}{2}(\Omega - \Delta_{st})\,dx \qquad (6.19)$$

$$= \frac{\Delta_{st}}{4D}\int\left(\sqrt{1 + \left[\frac{\vec{\mu}\cdot\vec{E}(x)}{\hbar\cdot\Delta_{st}}\right]^2} - 1\right)dx \qquad (6.20)$$

where the space dependence for the laser field was introduced. The calculation of the frequency shift with molecule in the excited state of the wave packet is similar, just with opposite sign compared with the ground state case.

6.1.2. Dependence of the transition dipole moment on M_F sublevels

As described by equation 6.20, the phase shift of the interference pattern is a function of the transition dipole moment μ. The interaction between the laser field and dipole moment written as $\vec{\mu}\cdot\vec{E}$ can be expressed as $\mu_0 E_z + \mu_{-1}E_{\sigma^+} + \mu_{+1}E_{\sigma^-}$, to take the different polarizations into account. The molecular state can be written as $|\gamma JM>$, J and M the total angular momentum and its projection on the space fixed axis, γ denotes the remaining quantum numbers like vibration and electronic ones [31].

An electronic dipole (E1) transition can occur only if the matrix element $<\gamma''J''M''|\vec{\mu}\cdot\vec{E}|\gamma J'M'>$ is non-zero. Because the electric dipole operator has odd parity, it follows that E1 transitions can occur only between states $\gamma''J''M''$ and $\gamma'J'M'$ of opposite parity [31]. Further selection rules follow by application of the Wigner-Eckart theorem which gives

$$E_{-q}<\gamma''J''M''|\mu_q|\gamma J'M'>=(-1)^{J''-M''}\underbrace{\begin{pmatrix} J' & J'' & 1 \\ M' & -M'' & q \end{pmatrix}}_{3j}<\gamma''J''||\mu_q||\gamma J'>E_{-q}[31]$$

$$(6.21)$$

the 3j-symbol describes the geometrical property of the transition: different M components carry different weights for this transition.

From the properties of the 3j-symbol we see that transitions can occur only if $(J', J'', 1)$ satisfy the triangle relation

$$\Delta J \quad \equiv \quad J'' - J' = 0, \pm 1 \qquad (6.22)$$

with   the   restriction   that

$$J'' \quad = \quad J' = 0 \quad is \quad not \quad allowed. \quad (6.23)$$

In addition, it is necessary that $M' - M'' + q = 0$, so that the only possible transitions are the three listed ones in the following table.

Δ M	μ	q	electric field polarization
$M'' = M'$	μ_0	0	linear, E_z, parallel to z-axis
$M'' = M'$ -1	μ_{-1}	+1	circular, $E_{\sigma+}$, clockwise in (x,y) plane
$M'' = M'$ +1	μ_{+1}	-1	circular, $E_{\sigma-}$,counterclockwise in (x,y) plane

Table 6.1.: The transitions allowed by the 3-j-Symbol

Application of 3j-symbol for near resonant light field

The linear polarization of the interferometer laser specifies the axis of quantization being parallel to the molecular beam axis.

The transition Q(25) (4-0)$B^1\Pi_u \leftarrow X^1\Sigma_g^+$ is used to introduce the near resonant field for the interferometer ground state. When the nuclear spin I does not change, the property on J can be transfered to F, the transition $\Delta F = \Delta J = 0$ is the strongest. If π polarization, parallel to the axis of quantization is used, $q = 0$, the square of 3j-symbol is

$$\begin{pmatrix} F & F & 1 \\ M_F & -M_F & 0 \end{pmatrix}^2 = \frac{M_F^2}{(2F+1)(F+1)F} \qquad (6.24)$$

If σ^+ polarization of the electric field is used, $q = 1$, μ_{-1} is selected, the square of 3j-symbol is written as

$$\begin{pmatrix} F & F & 1 \\ M_F & -M_F - 1 & 1 \end{pmatrix}^2 = \frac{-(M_F + \frac{1}{2})^2 + (F + \frac{1}{2})^2}{(2F+1)(F+1)F \cdot 2} \qquad (6.25)$$
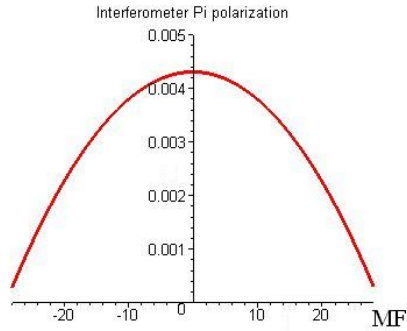
(a) Interferometer transition $R(25)(27-0)b^3\Pi_u \leftarrow X^1\Sigma_g^+$ with π polarization of electric field

(b) Transition Q(25) (4-0)$B^1\Pi_u \leftarrow X^1\Sigma_g^+$ for near resonant coupling, π polarization of electric field
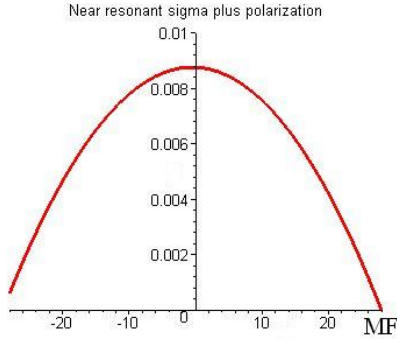
(c) Transition Q(25) (4-0)$B^1\Pi_u \leftarrow X^1\Sigma_g^+$ for near resonant coupling, σ^+ polarization of electric field
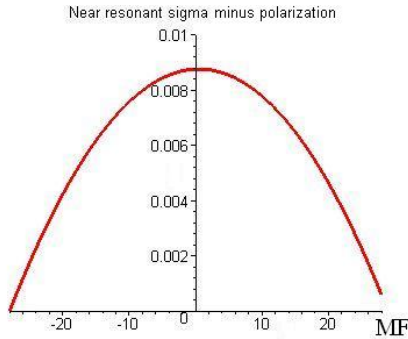
(d) Transition Q(25) (4-0)$B^1\Pi_u \leftarrow X^1\Sigma_g^+$ for near resonant coupling, σ^- polarization of electric field

Figure 6.4.: The plot of the square of 3j symbols as function of M_F for ground state F''=28 for interferometer transitions $R(25)(27-0)b^3\Pi_u \leftarrow X^1\Sigma_g^+$ F'=29 and near resonant transition $Q(25)(4-0)B^1\Pi_u \leftarrow X^1\Sigma_g^+$ F'=28 under different electric field polarizations.
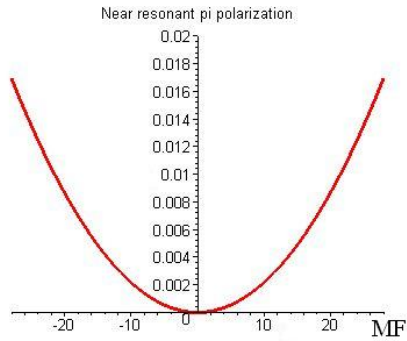
If σ^- polarization of electric field is used, $q = -1$, μ_{+1} is selected, the square of 3j-symbol is written as

$$\begin{pmatrix} F & F & 1 \\ M_F & -M_F+1 & -1 \end{pmatrix}^2 = \frac{-(M_F - \frac{1}{2})^2 + (F + \frac{1}{2})^2}{(2F+1)(F+1)F \cdot 2} \quad (6.26)$$

In the later experiment, we call the setting $\pi_{st} \parallel \pi_{IM}$, if the polarization of the coupling near resonant laser is parallel to that of the interferometer lasers; formula 6.24 should be applied. If we turn the polarization of the coupling near resonant laser perpendicular to that of the interferometer laser, we get the configuration $\pi_{st} \perp \pi_{IM}$. This linear polarization will project on to the quantization axis as σ^+ and σ^- polarization, each with half of the intensity and both contributions from 6.25 and 6.26 must be used.

The near resonant field couples $X^1\Sigma_g^+$ to $B^1\Pi_u$ state whose hyperfine splittings are known to be small [32], and single hyperfine components are not resolved in the spectrum. Thus an excitation involves all the hyperfine components simultaneously. Since the AC-Stark effect shares the same ground state $v'' = 0, J'' = 25, X^1\Sigma_g^+$ with the interferometer transition and only the highest hyperfine component is used for interferometer detection, all the phase shift introduced by near resonant laser field on the other nine components are not considered, we concentrate on the $F'' = 28$ of $X^1\Sigma_g^+$ state. All together there are $28 \times 2+1$ degenerate M_F subcomponents from -28 to 28. Depending on the electric field polarization, different states are coupled.

In the calculation of frequency shift by equation 6.20, the expectation value of each component of $| < \vec{\mu} \cdot \vec{E} > |^2$ can be written as
$(3j)_q^2 \cdot E_{-q}^2 | < \gamma'F'' ||\mu||\gamma'F' > |^2$

$(3j)_q$ is the 3j-symbol for the transition under different electric field polarization and the reduced matrix element contains the electric transition moment, the Franck-Condon Factor (FC) and the Hönl-London Factor (HL) and a factor F+1 for the renormalization of the reduced dipole moment.

The square of the 3j symbols gives the M_F dependence of the coupling strength for the three relevant cases, these functions are plotted from figure 6.4(b) to 6.4(d). Each M_F component corresponds to an expectation value $| < FM_F + q|\mu_q E_{-q}|FM_F > |^2$. For transition Q(25) (4-0)$B^1\Pi_u \leftarrow X^1\Sigma_g^+$ the square of transition dipole moment is $\sim 1.91(ea_0)^2$ [34], e and a_0 are the atomic units with e is the elementary charge, a_0 is Bohr radius. The dipole moment function got from [34] is scaled to the measured life time, where a constant scaling factor is used. Since the coupled state in our experiment is

deeply bound and far away from asymptote, the dipole moment is regarded as constant in this narrow internuclear distance. And the integration of this dipole moment over the vibration state is also taken into account.

Dependence on M_F for interferometer

The $R(25)(27-0)b^3\Pi_u \leftarrow X^1\Sigma_g^+$ transition is employed in the matter wave interferometry, since the nuclear spin does not change, $\Delta F = \Delta J = +1$ give the strong transitions, when π polarization is used, $q = 0$, the 3j symbol gives

$$\begin{pmatrix} F+1 & F & 1 \\ M_F & -M_F & 0 \end{pmatrix}^2 = \frac{(F+1)^2 - M_F^2}{(2F+3)(F+1)(2F+1)} \qquad (6.27)$$

As described in chapter 4, the $b^3\Pi_{u0^+}$ has predominantly magnetic hyperfine structure with a splitting of a few MHz while the hyperfine splitting in the ground state $X^1\Sigma_g^+$ is less than 100kHz from quadrupole and nuclear spin-rotation interaction [9]. In the spectroscopic work, only the hyperfine splitting in excited state is resolvable. For the level $v' = 27, J' = 26$ of state $b^3\Pi_u+$, the levels have total angular momenta F=J-I..J+I. For I=1, $F = 25, 26, 27$ there are three components and for $I = 3$, $F = 23, 24...28, 29$ seven components. The highest frequency hyperfine component $F' = 29$ is selected for the interferometer detection. In the ten hyperfine levels of $v'' = 0\ J'' = 25$ of ground state $X^1\Sigma_g^+$, the $F'' = 28$ is the corresponding lower state for the R transition, and a π polarization for this transition is used which means $\Delta M_F = 0$. So the transition starts from $M_F' = -28 \leftarrow M_F'' = -28$ to $M_F' = 28 \leftarrow M_F'' = 28$. The plot of the square of the 3j-symbol in formula 6.27 for this transition is in figure 6.4(a).

The observable contrast of the interference fringe results from the transition probability which depends on the dipole moment. Now for each M_F component, the same laser field does not work perfectly as 50% beam splitter as assumed before. For the transition probability P_{M_F}, the developement of the wave function for both ground and excited states through the laser beam splitters is drawn in figure 6.5.

Starting with wave function with amplitude 1, the transition probability P_{M_F} results in matter wave amplitude for excited state $P_{M_F}^{1/2}$, ground state $(1-P_{M_F})^{1/2}$. $\Delta\phi$ is the additional phase due to the recoil, and it is proportional to the time spent between the two laser beam splitters as discussed in chapter 2.
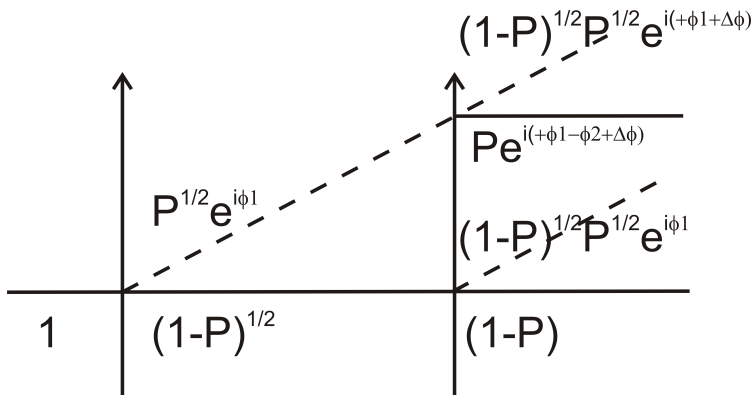
Figure 6.5.: The development of the wave function through the laser beam splitters. Solid lines stand for matter wave in ground state, dashed lines stand for excited state, lines with arrow stand for the laser beams. To simplify the drawing, P represents the P_{M_F} in the text.

ϕ_i is the phase added from the laser beam i during the interaction. The second laser beam splitter has the same transition probability P_{M_F}.

The recorded signal in the ground state exit for an individual M_F component is,

$$
\begin{aligned}
I_{M_F} \quad &\sim \quad |P_{M_F} e^{i(\phi1+\Delta\phi-\phi2)} + (1 - P_{M_F})|^2 \\
&= \quad P_{M_F}^2 + (1 - P_{M_F})^2 + 2P_{M_F}(1 - P_{M_F})cos(\Delta\phi + \phi1 - \phi2) \text{ (6.28)}
\end{aligned}
$$

$P_{M_F} \propto |<\mu>|^2$, $\Delta\phi \propto T$ (T = D/v_0).

$P_{M_F}^2 + (1 - P_{M_F})^2$ gives the incoherent background and $2P_{M_F}(1 - P_{M_F})$ is the contrast of the oscillation fringe. Because the data processing will digitally filter the oscillation pattern for the fitting process, only the oscillation fringe is discussed for the following calculation.

The recorded oscillation is the sum of interference patterns with different contrasts depending on M_F, but with the same phase $\Delta\phi$, and gives

$$
I \sim \tfrac{1}{2F+1} \Sigma_{M_F} 2P_{M_F}(1 - P_{M_F})cos(\Delta\phi + \phi1 - \phi2)
$$

Here I shortly discuss the dependence of contrast on M_F.

During the interaction between molecules and laser field, the population

probabilities with the molecular ground state and excited state experience an oscillation with a period of the reciprocal of Rabi frequency.

The Rabi frequency is defined in equation 6.10, and written out as

$\Omega_1 = \frac{1}{\hbar} < FM_F + q|\mu_q(M_F)E_{-q}|FM_F >$

The interaction time is defined by the geometrical width of the laser field with a fixed molecular velocity. And the intensity of interferometer laser is set so that the summation of the interference patterns has the largest contrast. Figure 6.6 shows the contrast $2P_{M_F}(1 - P_{M_F})$ as a function of M_F for the laser condition used in our experiment. The following list gives some qualitative analysis of the contrast.

- $M_F = 28$, $2P_{M_F}(1 - P_{M_F}) = 0.08$

- $M_F = 14$, $2P_{M_F}(1 - P_{M_F}) = 0.499$

- $M_F = 0$, $2P_{M_F}(1 - P_{M_F}) = 0.47$
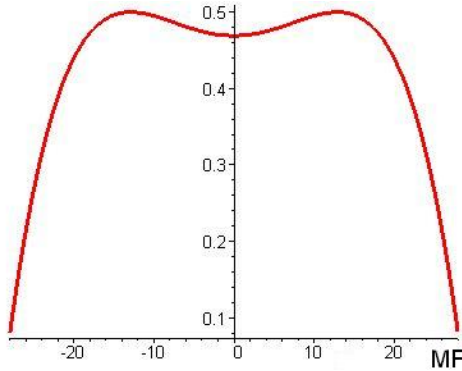
Figure 6.6.: The contrast of interference fringe as a function of MF, the highest possible contrast is 0.5

When the near resonant field is applied, an additional phase $\Delta\phi_{M_F}$ is added to the matter wave for each M_F subcomponent. This will appear as a shift of the interference pattern of the corresponding M_F subcomponent, the recorded signal is a summation of all M_F.

$I \sim \frac{1}{2F+1} \sum_{M_F} 2P_{M_F}(1 - P_{M_F})cos(\Delta\phi + \phi 1 - \phi 2 + \Delta\phi_{M_F})$

and $\Delta\phi_{M_F}$ appears as a detuning frequency shift

$$
\begin{aligned}
\Delta\omega &= \frac{\Delta}{4D} \int \sum_q \left(\sqrt{1 + \left[\frac{< FM_F + q|\mu_q E_{-q}|FM_F >}{\hbar \cdot \Delta} \right]^2} - 1 \right) dx \\
&= \frac{\Delta}{4D} \int \sum_q \left(\sqrt{1 + (\Omega_1/\Delta)^2} - 1 \right) dx
\end{aligned}
\tag{6.29}
$$

The Rabi frequency $\Omega_1/2\pi$ is 75 MHz, at a detuning $\Delta/2\pi = 300$ MHz, $(\Omega_1/\Delta)^2 \ll 1$, so using Taloy expansion, the formula 6.29 can be expressed out as

$$
\frac{\Delta}{4D} \sum_q \frac{1}{2} \frac{< \mu_q >^2}{(\hbar\Delta)^2} \int E^2 dx
\tag{6.30}
$$

The near resonant light field is provided by a Coherent CR599 dye laser with DCM dye. The size of the beam is determined by a camera, applying a Gaussian function fit for the beam profile. The waists of the Gaussian fit w_x and w_z are $(0.22mm, 1.64mm)$, which represents the width of Gaussian profile at $1/e$ of maximum intensity. The measured laser beam profiles viewed from different angles are presented in figure 6.7. In z direction, the recorded laser profile is not Gaussian but with a flat top, so the fitting is not such good, measured directly by the curse, the scale is marked in figure 6.7.

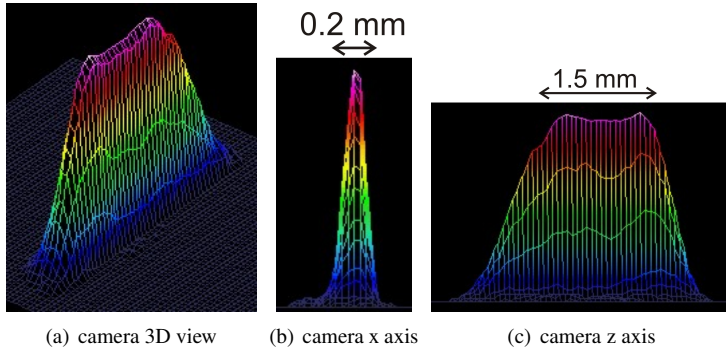(a) camera 3D view   (b) camera x axis   (c) camera z axis

Figure 6.7.: DCM laser beam profile captured by camera

The integration of the laser field in equation 6.30 can be replaced by $2I/zc\epsilon$,

I is the laser intensity, z is the length of the field distribution in z direction, c is the light speed and ε is the electric constant.

In the case of $\pi_{st} \parallel \pi_{IM}$,

$$\Delta\omega = (3j)^2_{\pi} \frac{\Delta}{4D} \frac{1}{2} \frac{<\mu>^2}{(\hbar\Delta)^2} \frac{2I}{zc\varepsilon}$$

for $(3j)^2_{\pi}$ figure 6.4(b) is used. The shift is transfered to the unit of radian.

- $M_F = 28$, $2P_{M_F}(1 - P_{M_F}) = 0.08$, $\Delta\omega_{\pi}(M_F = 28) = 3.3rad$

- $M_F = 14$, $2P_{M_F}(1 - P_{M_F}) = 0.499$, $\Delta\omega_{\pi}(M_F = 14) = 0.8rad$

- $M_F = 0$, $2P_{M_F}(1 - P_{M_F}) = 0.47$, $\Delta\omega_{\pi}(M_F = 0) = 0$

For large M_F, e.g. $M_F = 28$, the phase shift is large, but due to small contrast, the measurable contribution is small. By the middle value of M_F, e.g. $M_F = 14$, there is still a quarter of the phase contribution as the largest, and the contrast is the highest. By $M_F = 0$, the phase shift is zero, no change of the interference pattern.

In the case of $\pi_{st} \perp \pi_{IM}$,

$$\Delta\omega = [(3j)^2_{\sigma+} + (3j)^2_{\sigma-}]\frac{\Delta}{4D} \frac{1}{2} \frac{<\mu>^2}{(\hbar\Delta)^2} \frac{I}{zc\varepsilon}$$

Because the linear polarized near resonant laser project on to the quantization axis as σ^+ and σ^-, the field strength reduces to only half. For $(3j)^2_{\sigma+}$ and $(3j)^2_{\sigma-}$, figure 6.4(c) and figure 6.4(d) are used, The shift is transfered to the unit of radian.

- $M_F = 28$, $2P_{M_F}(1 - P_{M_F}) = 0.08$, $\Delta\omega_{\sigma^++\sigma^-}(M_F = 28) = 0.06rad$

- $M_F = 14$, $2P_{M_F}(1 - P_{M_F}) = 0.499$, $\Delta\omega_{\sigma^++\sigma^-}(M_F = 14) = 1.3rad$

- $M_F = 0$, $2P_{M_F}(1 - P_{M_F}) = 0.47$, $\Delta\omega_{\sigma^++\sigma^-}(M_F = 0) = 1.7rad$

For large M_F, e.g. $M_F = 28$, the phase shift is nearly zero. For middle value of M_F, e.g. $M_F = 14$, the phase shift is larger than the case of the parallel polarization, the contrast is the same as parallel case. For $M_F = 0$, the phase shift is the largest, and the contrast still keeps relatively high.

The following parameters are used to calculate the phase shift of the interference pattern under different polarization. And the calculated phase shift will be used to compare with measured value.

Term	value
μ	$1.15 * 10^{-29}$ C·m
P	7 mW
$\hbar$	$1.054571 * 10^{-34}$ J·s
D	400 μm
Δ	300 MHz
z	2 mm

Table 6.2.: Relative parameters to calculate the phase shift

	$\Delta_{st} = +300MHz$		$\Delta_{st} = -300MHz$	
polarization	$\pi_{st} \parallel \pi_{IM}$	$\pi_{st} \perp \pi_{IM}$	$\pi_{st} \parallel \pi_{IM}$	$\pi_{st} \perp \pi_{IM}$
phase shift /rad	-0.81	-1.2	+0.81	+1.2

Table 6.3.: Calculated frequency shift induced by the near resonant field

6.2. The experiment set-up and result

For the Ramsey interferometer the same optical arrangement as described in chapter 5 is used. In figure 6.8 the solid lines represent laser beams building the interferometer and the dashed line represents the near resonant laser beam. The polarizations are purified by Glan-Taylor(GT) crystals, the polarization of the interferometer laser beam is parallel to the x direction, the molecular beam direction. The polarization of near resonant laser can be rotated by a $\lambda/2$ plate. So it can be set either parallel or perpendicular to that of interferometer laser beam. The near resonant laser beam is introduced with a small angle θ with respect to the optical table. It travels above the mirror M2 and is transmitted by BS1, resulting in a waist $w = 200\mu m$ in x direction, at the crossing point of laser beam with the K_2 molecular beam. Geometrically it is introduced in the middle between the pair of interferometer laser beams and interacts with the K_2 molecules. The crossing point is shown enlarged in the encircled area in figure 6.8, which shows a cut view of y, z plane. The K_2 beam points out of the paper as indicated. The near resonant laser beam crosses the K_2 molecular beam at the same height as the interferometer laser beam but with a small angle $tan\theta = 1cm/60cm$ relative to the interferometer laser beam. At the crossing point, the polarization of the near resonant laser beam is either in x direction, i.e. parallel to that of interferometer laser beam, or in y-z plane perpendicular to that of interferometer laser.

As the molecule travels through the first laser beam splitter, the polarization of the electric field already defines the molecular axis for the transition. When the polarization of the near resonant field is parallel to that of the laser beam splitter, we have the case of $\pi_{st} \parallel \pi_{IM}$ transitions as discussed in section 6.1.2 and the coupling uses the selection rule $\Delta M_F = 0$. When the polarization of the near resonant field is perpendicular to that of the laser beam splitter $\pi_{st} \perp \pi_{IM}$, this linear polarization gives σ^+ and σ^- polarization for the already defined quantization axis being equal to the molecular axis. The coupling is described by the selection rule $\Delta M_F = \pm 1$
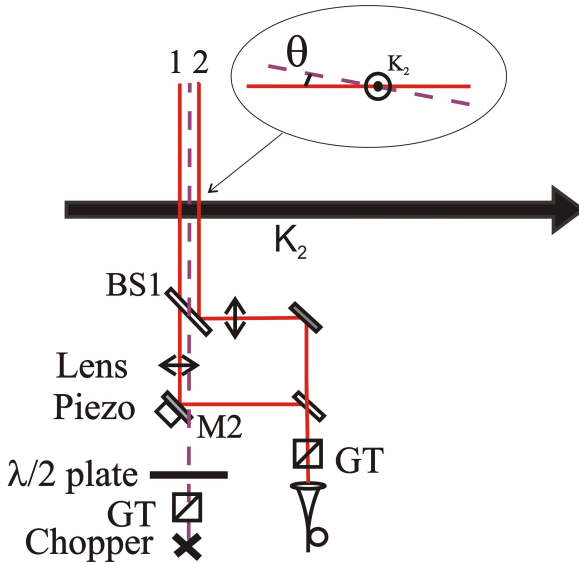
Figure 6.8.: Optical set-up for near resonant light field experiment

A DCM dye laser is used to generate the near resonant field. The frequency of Q(25) line of the (4-0) band $B^1\Pi_u \leftarrow X^1\Sigma_g^+$ is 15655.35 cm^{-1}. The DCM dye laser is frequency stabilized by locking it to a confocal Fabry-Pérot transfer cavity, which itself is locked to an iodine stabilized HeNe laser, as described in chapter 3.3. The spectral line width of this dye laser is about $2MHz$. The frequency of dye laser can be tuned by tuning the HeNe reference by an AOM. It is set at a value corresponding to the deepest depletion point in the fluorescence profile detected at the ground state exit when blocking interfer-

ometer laser beams. This frequency is the center of the B-X transition line and taken as the zero detuning position. The dye laser frequency can be set off resonant either by tuning the AOM or with steps of $150 MHz$, which is the free spectral range of the cavity for locking. The vertical position of the laser beam is fine adjusted for the deepest depletion dip produced at the detection position of the ground state exit. When the DCM dye laser beam interacts with the same ensemble of molecules as the laser beam for ground state detection, the depletion dip is the deepest. The horizontal position of the dye laser beam in the interferometer zone is adjusted and verified by a camera, by imaging a reflected set of beams 1 and 2 at the virtual position of the molecular beam. Far detuning $|\Delta| \gg \Omega_1$ is used to avoid population changes by optical pumping.

The phase difference between the pair of laser beams building the Ramsey interferometer is stabilized as described in chapter 5. In order to avoid any influence of long term instability of the experiment set-up, the interference pattern with and without near resonant field are recorded simultaneously at each frequency detuning. This is realized by synchronizing the chopper with the data acquisition and control system. At each frequency setting of the interferometer laser, the chopper opens and closes once to give a point of the interference pattern for the situation with and without near resonant field. Both excited state exit and ground state exit are detected. Examples of recorded spectra are shown in figure 6.9.

During the first measurements, there was in the first detection zone a problem of high near infrared background, which was obviously connected with the dye laser beam. Inspection of possible sources revealed finally, that fluorescence of the BK7 glass windows of the view ports of the vacuum system was responsible. Change of the windows to Quartz (fused silica) antireflection coated for infrared reduced the background in the near infrared region (wave length larger than 800 nm). With a filter RG750 to block the scattered laser light, the background is reduced by more than two orders of magnitudes, but it is still at the same magnitude as the signal amplitude. Further apertures were installed behind the window inside the vacuum chamber. The laser can still travel freely through the apertures, while the scattered light or fluorescence from windows at other angles are shielded from the detector. The apertures are painted black, to increase the absorption and reduce the reflection. By these means, the background in the first observation zone is further reduced to one tenth of the signal strength. In the second observation zone, the background is negligiblly small.

6.3. Data analysis and discussion

Figure 6.9 shows the interference fringes recorded with or without near resonant field applied. The upper sets of curves correspond to the ground state exit, the lower sets to the excited state exit of the interferometer. Each curve is an overlap of the cases of frequency scanning up and down and it is checked that there is no time constant delay in between. The experimental conditions for each figure are given in the following list, with P the laser power, Δ_{st} frequency detuning of the near resonant laser field. When the two polarizations are parallel to each other, it is denoted as $\pi_{st} \parallel \pi_{IM}$, when they are perpendicular, it is denoted as $\pi_{st} \perp \pi_{IM}$.

- a. P = 7 mW, Δ_{st} = +300 MHz, $\pi_{st} \parallel \pi_{IM}$

- b. P = 7 mW, Δ_{st} = -300 MHz, $\pi_{st} \parallel \pi_{IM}$

- c. P = 7 mW, Δ_{st} = -300 MHz, $\pi_{st} \perp \pi_{IM}$

- d. P = 7 mW, Δ_{st} = +300 MHz, $\pi_{st} \perp \pi_{IM}$

Take figure 6.9(a) as an example and the upper sets from ground state exit, the black line represents the interference fringes without near resonant laser field, the gray curve represent the one with near resonant field on. When both interference fringes are compared, in the center, an attenuation of the amplitude and a phase shift of the interference fringes are clearly seen. At the wings of the oscillation pattern, the two curves have almost the same height which indicates that there is no additional background from scattered laser light. For the lower sets from excited state exit, also the black line represents the interference fringes without near resonant laser field, the gray curve represent the one with. When the two curves are compared, there is a vertical shift between the interference patterns because of the scattered light from the near resonant laser. As discussed in section 5.1.3, the Ramsey interference fringes due to two hyper fine components in the excited state are not well separated. Additionally, the amplitude attenuation and phase shift of the interference fringes are not so obvious as in ground state exit. So the signal from ground state exit is used for further data analysis.

When figure 6.9(a) is compared with figure 6.9(b), for the same polarization of the near resonant laser field with the same power, at frequency detunings

positive, the interference fringe shifts to lower frequency side, at frequency detuning negative, the interference fringe shifts to high frequency side. The direction of the interference fringes shift is as expected. For determination of the phase, digital filtering method as discussed in chapter 4 and chapter 5 is employed to filter out the oscillation pattern.

Formula 5.7 is used for fitting. All the spectra taken without near resonant laser field are fitted individually with all the parameters variable to get a reasonable good fitting for each curve. Some parameters represent certain physical conditions e.g. P the fringe oscillation period, ν_0 the center frequency of the transition, ν_w the width of the Gaussian envelop, they are constant for the identical experimental condition. The individual fitting results also prove that the standard deviation of P, ν_0, ν_w are only a few percent of their average value. Within obtained experimental S/N they are regarded as constant. The average value of parameters P, ν_0, ν_w are fixed for the refit. The amplitude is varied for slow drift of the signal. The result of phase shifts is in table 6.4.

	Phase shift in unit of radian			
	$\Delta_{st} = +300MHz$		$\Delta_{st} = -300MHz$	
polarization	$\pi_{st} \parallel \pi_{IM}$	$\pi_{st} \perp \pi_{IM}$	$\pi_{st} \parallel \pi_{IM}$	$\pi_{st} \perp \pi_{IM}$
scanning up	-0.520	-0.584	0.643	0.982
scanning down	-0.545	-0.525	0.592	0.898

Table 6.4.: Phase shift induced by the near resonant field

Table 6.4 gives the phase shifts of interference fringes in units of radian. The experimental conditions are the same as given in figure 6.9. The frequency scanning up and down cases are treated separately to see the uncertainty of the results. Since there is no time constant delay between these two curves, they should deliver the same value of phase shift. The difference is just a few percent of the average value, so for the obtained experimental S/N it is acceptable.

From the simulation result in table 6.3, the sign agrees with the measured result. The absolute value of phase shift for $\pi_{st} \parallel \pi_{IM}$ case is 0.81 rad, for $\pi_{st} \perp \pi_{IM}$ is 1.2 rad. The calculated value is 25% larger than the measured value. The reason might be the laser field distribution. As shown in figure 6.7, at the edge of the laser beam profile, the molecules experience less intensity which corresponds to smaller phase shift. The measured result is a summation of all the molecules.

Conclusion:

- The shift of the interference pattern under the influence of AC-Stark effect from near resonant laser field is obvious.

- The interference fringes shift in the direction determined by the frequency detuning sign.

- Calculated value and the measured value are in the same order of magnitude.

- Large power is required to get π to 2π shift of the interference pattern.

- Further systematic analysis of the phase shift as the function of laser power and frequency detuning is needed.
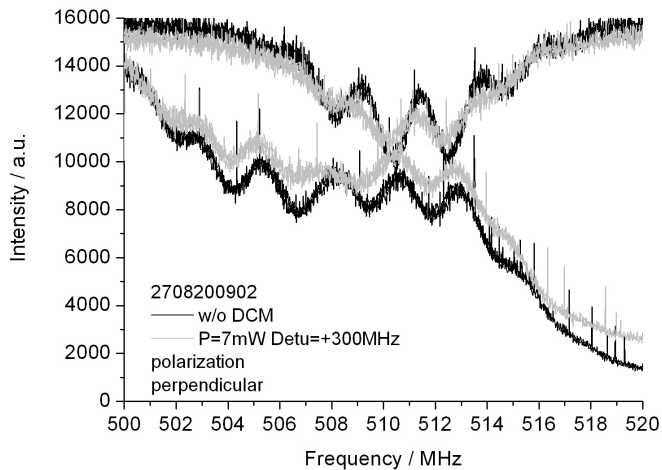
(a) P = 7 mW, $\Delta_{st} = +300$ MHz, $\pi_{st} \parallel \pi_{IM}$
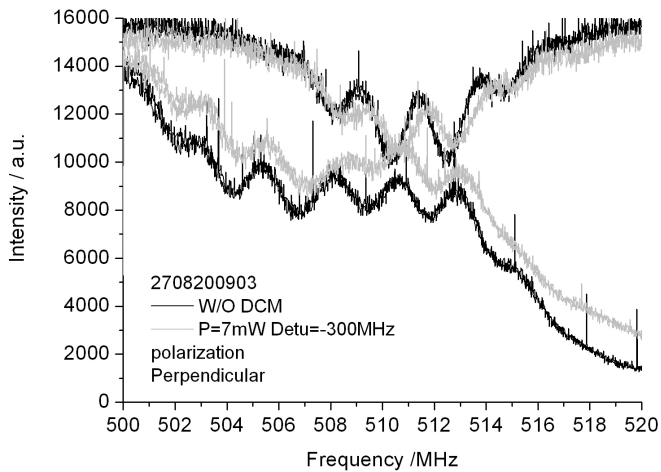
(b) P = 7 mW, $\Delta_{st} = -300$ MHz, $\pi_{st} \parallel \pi_{IM}$

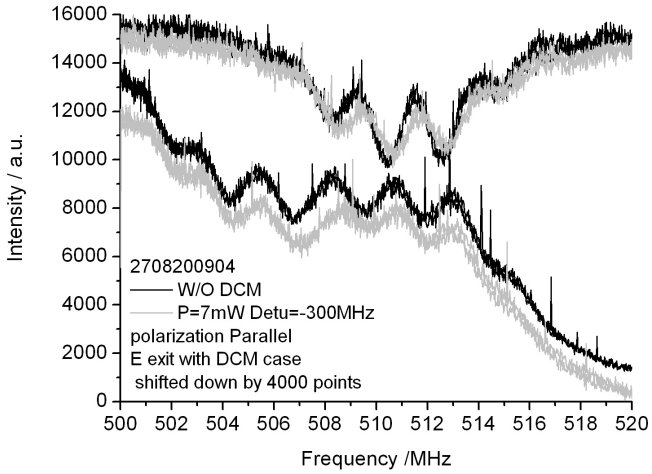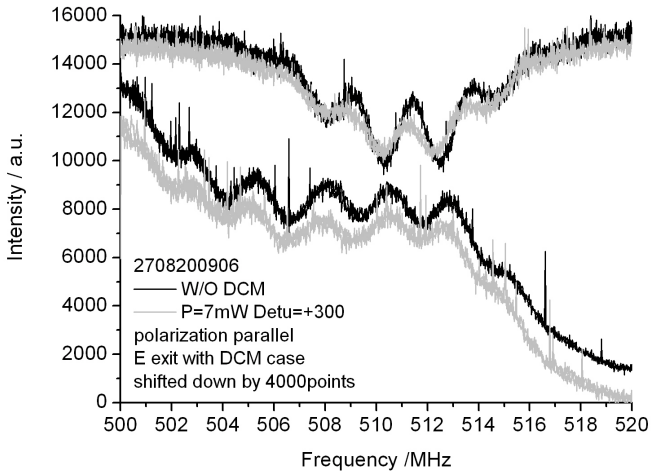(c) P = 7 mW, Δ_{st} = -300 MHz, $\pi_{st} \perp \pi_{IM}$

(d) P = 7 mW, Δ_{st} = +300 MHz, $\pi_{st} \perp \pi_{IM}$

Figure 6.9.: The phase shift under the near resonant field

6. AC-Stark effect

7. Cold collsion experiment

This chapter describes the suitability of Ramsey-Bordé interferometer for exploring low energy collisions between atoms and molecules in well defined quantum states. The particles are prepared in a supersonic potassium beam which provides a sample of colliding particles with small relative velocities in a fast moving frame of reference. By changing the properties of the medium, in which the molecular matter wave propagates, i.e. varying the density of the ^{39}K atoms in the beam, the shift of the interference patterns was investigated. The first section 7.1 of this chapter is a manuscript to be submitted for publication. The second section 7.2 describes the large amplitude modulation of the laser beam phase, which can be used to smear out the signal of the embedded Ramsey interferometer to improve the stability of the Ramsey-Bordé signal. This might increase the sensitivity of the interferometer for identifying the collisional effect.

7.1. Suppressing Ramsey interferences by phase modulation of the beam splitters

7.1.1. Introduction

In the field of Bose-Einstein condensates, collisions between atoms and molecules can contribute to unwanted loss mechanisms for the coherent systems. Thus investigation of collisions between atoms and molecules will give insight in the physical situation and a detailed understanding of the physical mechanisms can offer ways to avoid such losses. As a step in the direction of such experiments, we have set up an experiment which is dedicated to investigate collisions between potassium atoms and diatomic molecules in a supersonic beam. Expanding potassium vapor out of an oven into the vacuum yields a supersonic flow of atoms with a small fraction of K_2 molecules diluted in an environment of these K atoms. Due to the adiabatic expansion all particles acquire nearly the same speeds [13] yielding a narrow velocity distribution, representing a sample of atoms and molecules moving in a reference frame of high common

forward speed, in which the particles have low relative velocities and undergo "cold collisions".

As a sensitive detector for the collisions a matter wave interferometer with K_2 molecules is employed, which detects the influence of collisions by the phase shift observed in the interferograms in various physical situations.

When a matter wave propagates through a dilute medium, the wave that describes its propagation is modified by the interaction with the medium. This modification can be treated similarly to the case of propagation of a light wave in optics by introducing an index of refraction for the medium, in which the matter wave propagates. Important contributions to the theory were done by Vigué [35, 36], while pioneering experiments were performed by the Pritchard group by measuring phase shift and attenuation of the matter wave traveling through different mediums in order to determine the complex index of refractions [42, 37, 38, 39]. They used nanostructured mechanical diffraction gratings for physically separating the arms of their matter wave interferometer and successfully introduced a gas cell in one of the arms and observed the phase shift for various different gas pressures. Similar experiments were undertaken in the group of Vigué [40] with a matter wave interferometer of Li atoms in the ground state.

In our experiment a matter wave interferometer employing light fields as beam splitters is employed. This approach not only allows to split the matter wave coherently, but also provides selectivity regarding the choice and preparation of the inner state of the molecules. One major aspect of the experiment is to investigate the suitability of such matter wave interferometer for measurements of the index of refraction of the surrounding medium.

A Ramsey-Bordé interferometer based on four laser beams acting as splitters has been built and analyzed in details see chapter 4 and references [9, 12, 41]. In this chapter, we report on investigations of its suitability for measurements of the index of refraction seen by potassium dimer molecules prepared in different inner states traveling through a scattering medium of potassium atoms in the ground state.

In section 7.1.2, a summary of the theoretical background and an estimation of the magnitude of the expected phase shift of the interference patterns depending on the density of the medium will be presented. Then the experimental setup and measurement details are discussed. Section 7.1.5 describes the processing of the data. In section 7.1.6 the results of phase shift measurements will be presented and the uncertainty considerations will be discussed, followed by a conclusion in section 7.1.7.

7.1.2. Index of refraction picture in a Ramsey-Bordé matter wave interferometer

We will apply the index of refraction picture developed in [35, 36] and used e.g. in [42] to a molecular matter wave of molecules in different internal states. Due to the collision between environing atoms and the molecular matter wave, the wave packets will undergo phase shifts and will be attenuated compared to free propagation. Like in wave optics, assuming plane wave approximation the matter wave propagating in x direction can be described by $\Psi = A \cdot e^{ik_0 x}$, where k_0 is the free space wave vector $\vec{k}_0 = \vec{P}_0/\hbar$ given by the momentum $\vec{P}_0$ of the particle. When the wave propagates through some refractive medium, starting at $x = 0$, at some point L the wave function will have gained some additional phase and will be attenuated [2]. This can be described by

$$\Psi(x = L) = A \cdot e^{ik_0 L} e^{i\varphi NL} e^{-\frac{\sigma}{2}NL} \tag{7.1}$$

N denotes the density of scattering medium, φNL and $\frac{\sigma}{2}NL$ are phase shift and attenuation accumulated on the distance L. The quantities φ and σ are to be interpreted as cross sections. By introducing the new wave vector $k = nk_0$, the complex index of refraction n defining the properties of the scattering or refracting medium can be expressed as

$$n = 1 + \frac{N}{k_0}(\varphi + i\sigma/2) \tag{7.2}$$

In figure 7.1 the scheme of the Ramsey-Bordé matter wave interferometer is shown. The molecular beam is represented by the full horizontal line indicating the direction of the particles from left to right. Before crossing the first laser beam, indicated by the leftmost vertical arrow, the particles are in the ground state g and have no additional photon momentum, labeled by $|g,0\rangle$. The label $|g/e,m\rangle$ marks by g or e the molecular state, and by m the number of the transferred photon momenta in units of $\hbar$ **k**, where k is the modulus of the photon wave vector $\vec{k}$. The action of a laser beam as a beam splitter can be understood in a simple mechanical picture envoking energy and momentum conservation (see e.g. [43]). After the first beam splitter the particles are in a coherent superposition of ground state $|g,0\rangle$ and excited state $|e,+1\rangle$ with one additional unit of photon momentum. The path of the matter wave in the excited state is indicated by the broken line. The second beam splitter brings the excited component back to the ground state and removes the photon momentum.
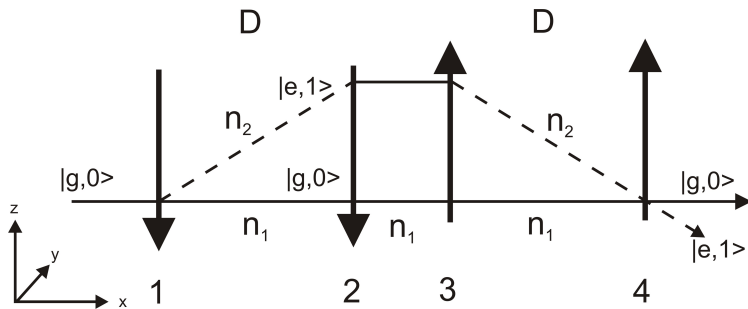
Figure 7.1.: Principle scheme of a Ramsey-Bordé matter wave interferometer. The four laser beams acting as splitters are indicated by the vertical arrows. The paths of molecules in the ground state are indicated by full horizontal lines, paths of excited molecules are marked by broken lines. The indexes of refraction are indicated as labels for the various paths, and distinguish as n_i the different inner molecular states. For details see text. Within this chapter the x, y and z directions are defined as in the figure.

In principle this second beam splitter will split the excited state path also into a superposition of ground and excited state, and similarly it will happen with the ground state path. This would finally lead to a closed interferometer path for a matter wave in the excited state. However, in our experiment the lifetime of the excited molecular state is so short, that the molecules will have decayed to other states before their matter wave will interfere. Thus this path is not realized in our setup, and was not drawn to keep the figure simple. The beam splitters 3 and 4, coming from the opposite direction with respect to 1 and 2, close the path of the interferometer, giving rise to matter wave interference inducing changes of the fluorescence from the excited state $|e, +1\rangle$ and of the population of the ground state $|g, 0\rangle$.

It will become obvious in the section 7.1.5, that the signal-to-noise ratio in the present experiment is limited. The signal-to-noise ratio presently prevents determination of small changes of the interference contrast due to attenuation of the matter wave. Thus in the following we will concentrate only on the comparison of phase differences of interferences due to high and low atomic density.

The indexes of refraction for the molecular waves in different inner states

are marked in figure 7.1 by n_i. For molecules in ground state, the index of refraction of the atom medium is n_1 and for molecules in the excited state it is n_2. Using $k = n_i k_0$ and the mechanical picture like in [43] we can calculate the phase difference $\Delta\phi$ of the matter waves along paths 1 and 2 when they travel through the medium and experience different indexes of refraction n_i.

$$\Delta\Phi = 2k_0 D[(n_2 - n_1) + n_2 \frac{1}{k_0 v_0}(\Delta - \delta)] \tag{7.3}$$

$\Delta = \omega_L - \omega_0$ is the frequency detuning of the laser frequency ω_L from the resonance frequency ω_0 of the molecule, $\delta = \frac{\hbar k^2}{2m}$ photon recoil shift, m being the mass of the particle, v_x is the molecular velocity parallel to the molecular beam direction.

We Modify equation 7.2 introducing ε

$$n_i = 1 + \varepsilon_i = 1 + \frac{N}{k_0}(\phi + \frac{i\sigma}{2}) \tag{7.4}$$

where ε is proportional to the density N of the medium, $\varepsilon \propto N$.

$$\Delta\phi(\varepsilon_i = 0) \quad = \quad \frac{2D}{v_x}(\Delta - \delta) \tag{7.5}$$

$$\Delta\phi'(\varepsilon_i \neq 0) \quad = \quad 2k_0 D[(\varepsilon_2 - \varepsilon_1) + (1 + \varepsilon_2)\frac{\Delta - \delta}{k_0 v_x}] \tag{7.6}$$

When the density of the medium changes from N to ηN ($0 \leq \eta \leq 1$), $\varepsilon_i' = \eta\varepsilon_i$.

Δ is the detuning at density N

Δ' is the detuning at density ηN.

$\Delta' = \Delta + \gamma(1 - \eta)$, γ is the collision induced resonant frequency shift due to the different medium density.

For Ramsey-Bordé interferometer, the phase change $\Delta\theta$ between the two different experimental situations can be expressed by

$$\Delta\theta = 2k_0 D(1 - \eta)[(\varepsilon_2 - \varepsilon_1) - \frac{1 + \varepsilon_2}{k_0 v_0}\gamma + \frac{\varepsilon_2}{k_0 v_0}(\Delta - \delta)] \tag{7.7}$$

While the first term and the second term on the right hand side of eq. 7.7 are of the same order of magnitude, the last term is many orders of magnitude smaller than those and can be neglected. Assuming typical values for ε_i in the order of 10^{-10} as was determined for various gases in [42], expected phase shifts are estimated to be about 90 mrad due to a change of about a factor of

10 of the atom density ($\eta \approx 0.1$) under the present experimental conditions for K_2 molecules of $v_x = 920$ m/s, a length $D \approx 400\ \mu m$ and $N \approx 10^{13}\ cm^{-3}$.

7.1.3. Experimental setup

A collimated particle beam out of an oven filled with potassium metal is formed by two skimmers separated by 1 m with open diameters of 2 mm. By means of the Doppler effect the molecular velocity distribution of K_2 has been determined, yielding a most probable longitudinal velocity $v_{prob} = 912 \pm 30$ m/s and a velocity width $\Delta v = 120$ m/s [41]. The density of the atomic medium in the supersonic beam was estimated to be in the order of $10^{13}\ cm^{-3}$ at the interferometer location. The background pressure in the vacuum chamber is 10^{-8} mbar.
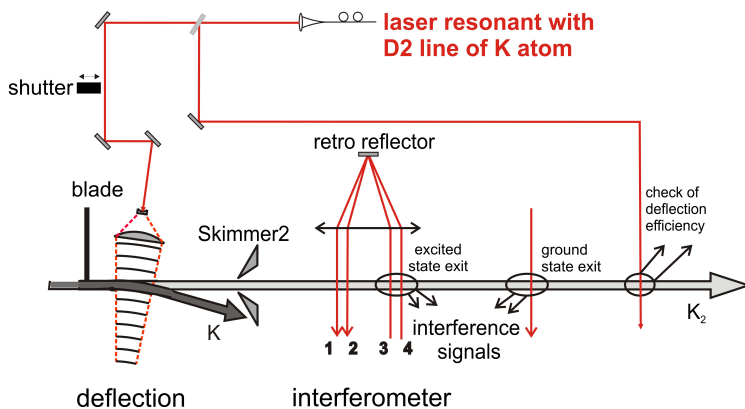

Figure 7.2.: The scheme of atom deflection and interferometer setup for the measurement of phase shift due to the different collision situations

To change significantly the atom density, the atoms are deflected out of the particle beam by a resonant laser interaction through the 4s-4p transition of K. As shown in Figure 7.2, after the first skimmer the particles pass a zone where the beam is shaped by a blade on one side and where two overlapping laser fields act as pump and repump beams of proper geometry and frequency to deflect the atoms such, that they do not pass any more through the second skimmer. Molecules are not affected. More details of the laser fields and the blade can be found in [44]. A small fraction of the light of the deflection laser

crosses the particle beam about 40 cm downstream of the interferometer zone to probe the atoms remaining in the beam after the deflection. Typically only 3% of ^{39}K (main isotope with abundance 93.3%) remain in the beam corresponding to a change of the atomic density by more than a factor of 10. After the deflection process, the nearly pure molecular beam enters the interferometer region.

The Ramsey-Bordé interferometer comprises two counter propagating pairs of two co-propagating laser beams. A retro reflector images the co-propagating pair of laser beams 3 and 4 into the opposite direction, beams 2 and 1, being mirror images of 3 and 4, respectively. During the interaction with the light field a phase $\phi_i, I = 1, 2, 3, 4$ is added to the phase of the matter wave, adding up to a total phase Φ of

$$\Phi = \phi_1 - \phi_2 + \phi_3 - \phi_4 \qquad (7.8)$$

taking into account the directions of propagation of the light fields. It is obvious that any change of the phase of an input beam 3 or 4 is compensated by an opposite change of its reflected counterpart 2 or 1, so that the total phase remains unaffected. This cancellation of phase shifts is a special property of stability of the Ramsey-Bordé setup.

The matter wave interference can be detected by observing the fluorescence out of the molecular state $|e, +1>$ as indicated in figure 7.1. This will be called the "excited state exit" of the interferometer. The detection zone is set directly above the interferometer lasers and indicated by the first oval mark in figure 7.2. The exit $|g, 0>$ can be inspected by the remaining population in the ground state and its change due to the matter wave interference. This exit, further on called "ground state exit" of the matter wave interferometer, is indicated by the second oval mark in figure 7.2.

7.1.4. Measurements

In order to observe small phase shifts in the interferograms, the stability of the whole apparatus has to be sufficient to exclude as much as possible any other unwanted sources of phase changes, e.g. by drift of the laser frequency of the beam splitters and by the optical setup. Therefore, the interferograms are recorded with the deflection process of the atoms switched on and off alternatively while the other experimental conditions and parameters are kept constant. In such sequence around 30 records of interference patterns are taken, 15 under low atom density, 15 under high atom density. Each such record

contains 1000 data points, with typical size of the frequency steps of 20 kHz and time constant per data point of 100 ms. Thus each spectrum takes 100 s, which is short enough to keep the experimental condition stable for the whole time of measurement. It turned out, that from day to day the setup had to be readjusted for optimum contrast of the interferences.

Equation 7.3 shows that $2D/v_0$ is the period of the observable interference pattern when tuning the laser frequency Δ. The reciprocal $v_0/2D$ gives the magnitude of the detuning for the laser frequency by which the phase shift varies by 2π. When the dark zone length D is increased, within the same frequency tuning range, more interference maxima and minima will appear. So a certain phase shift can be measured more precisely by the finer "ruler teeth". Of course, this is limited by the spectral width of the laser. The spectral width of diode laser system was determined to be less than 50kHz [10] . Additionally, a large D will reduce the influence of Ramsey interferences, which is not wanted in this experiment [41]. However, the maximum D is limited to about 1 mm by the life time of molecular excited state used here. For the present experiment, the dark zone length D was varied from $300\mu m$ to $800\mu m$ with $100\mu m$ steps. Due to the stability and reproducibility considerations above we measured the phase shifts at different separations within one day of experiment, where the adjustment is kept the same. So from a single day of experiment, we get an array of data at a series of different dark zone lengths D, which from the stability point of view, can be compared. Records of the same kind according to the atomic density are then averaged to improve the signal-to-noise ratio.

7.1.5. Data processing of observed interferograms

Under the present experimental conditions both interferometer exits show a superposition of different interference patterns due to the influence of transverse and longitudinal overlaps of the interfering matter waves. The interference patterns have been analyzed to be composed of a contribution caused by a two beam splitter Ramsey interference and a Ramsey-Bordé pattern with four beam splitters, see chapter 4 and reference [41]. The admixture of Ramsey interferences influences the stability of the phases from record to record and thus the suitability of the matter wave interferometer for phase measurements of the interferences. The intrinsic phase stability for the Ramsey-Bordé interferometer as discussed in section 7.1.3 is not valid for Ramsey interferometer since such cancellation does not exist chapter 4 and reference [41]. For reliable results it is necessary to separate the signals of both types of interference

from each other. Digital filtering has been used for that purpose. In principle the spectra taken are treated by a narrow band filter, which allows to extract the wanted spectral feature from the measured trace due to its limited frequency content. The details of this method is discussed in chapter 4 and refrence [41].

All scans from a series of records are sorted into two groups distinguished by the situation of low or high atomic density, in which they were recorded. For each situation, spectra are averaged point by point, a point corresponding to a fixed frequency of the laser. The standard deviation is calculated for each point of the averaged spectrum. Figures 7.3 show averaged curves (bold lines) with traces of 3σ deviations added and subtracted as thin curves above and below the corresponding average. The upper sets of curves correspond to the ground state exit, the lower sets to the excited state exit of the interferometer. Figure 7.3a shows records for a dark zone length $D = 400\mu$m, while figure 7.3b shows a similar result for $D = 800\mu$m. Both averaged curves are given for the case of atoms deflected out of the beam. Since any difference of interferograms between spectra of different atom density is not obvious in the figures, an examples of only one type are plotted. The excited state exit (lower curve in both panels) shows clearly matter wave interferences for two hyperfine components on top of the overall fluorescence profile, the signal from the ground state exit (upper curves) show the interference pattern in a dip corresponding to the transition of a single hyperfine component only. For the excited state exit in figure 7.3a at the last hyperfine component one can recognize clearly five oscillation periods. However, for the ground state exit at the corresponding frequency positions every second interference maximum has smaller amplitude or nearly disappears as indicated by the arrows. This is caused by the Ramsey interferences, which have twice the period length of the Ramsey-Bordé fringes, superimposed on the Ramsey-Bordé interferences. Moreover, one can also see a slight increase of the standard deviation curves with respect to the average at those pronounced maxima, indicating a larger scatter in the amplitudes of the individual records at those frequencies. This happens due to the small drift of the phase of the Ramsey pattern with respect to the Ramsey-Bordé fringes. In figure 7.3b the interferences of excited state and ground state exit are much more similar, they have the same number of oscillation periods and are essentially opposite in phase. The standard deviation curve follows the averaged curve well, indicating a more stable behavior.

The signals for both exits are a superposition of an incoherent background and interference fringes from different interference phenomena, Ramsey and Ramsey-Bordé interferences, with their interference periods differing by a factor of two. The next step of treating the data is digital filtering, in order to ex-
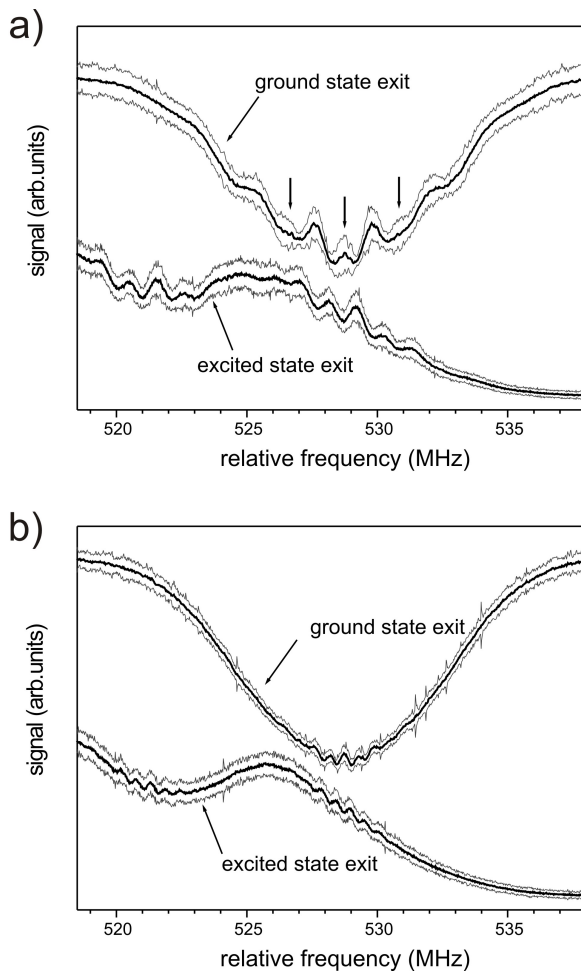
Figure 7.3.: Matter wave interferences observed at the high frequency hyperfine component part of the transition R(25) (25-0) of K_2 in a potassium molecular beam. The thick curves are averages of 15 individual records, the thin traces above and below the thick ones represent the 3σ standard deviations added and subtracted to the average for each frequency. The upper set of traces corresponds to the ground state exit of the matter wave interferometer, the lower set to the excited state exit. Panel a: $D = 400\ \mu$m, panel b: $D = 800\ \mu$m.
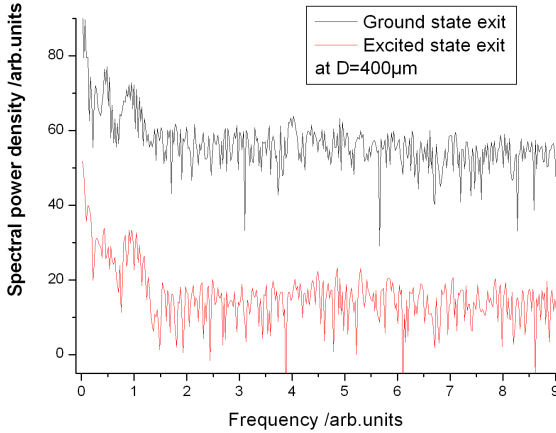
Figure 7.4.: Power spectrum of the recording 7.3a. The upper curve was shifted up by 30 dB for better visibility

tract the contribution of the Ramsey-Bordé interferences for comparison of the phases for the cases of high and low density of the atoms. For this discussion, in order to simplify the terminology, we regard the spectra as being recorded linearly in time, i.e. the frequency scale underneath the spectra being linear in time and the frequency steps during the recording are the steps in time. Then the Fourier transform can be regarded as a power spectral density as usual with a frequency scale according to the step unit in time.

The power spectrum after Fourier transformation of the average curve for the example in figure 7.3a for a dark zone length D=400μm is shown in figure 7.4 for both ground state exit and excited state exit. They are vertically shifted for better comparison. The frequency scale indicates the oscillation frequency of the interference fringe and the spectral power density indicates the amplitude of the frequency component. The spectra typically show a low frequency increase according to the slowly varying profiles and two main peaks (indicated by arrows in figure 7.4) on a noisy background. The low frequency peak corresponds to the Ramsey interference. This interference pattern is not used in this evaluation. The second peak corresponds to the Ramsey-Bordé interference, which is used to measure the collision induced phase shift. In the

power spectrum 7.4, the power density of the first peak is larger than the second peak, especially for the ground state exit. This explains the differences in figure 7.3a, where for the ground state exit the interference is obviously the addition of two oscillations. For the excited state exit, this phenomenon is not so obvious, resulting in a smaller Ramsey contribution to the power density.

For filtering a band pass is centered at the peak of the Ramsey-Bordé interference. The power density outside are set to zero, the low frequency part as well as high frequency part, in order to cut out only the Ramsey-Bordé interference pattern. This part is then Fourier transformed back and contains the pure Ramsey-Bordé interference pattern without background and noise. Here the question arises, how precise and reproducible can a phase be derived from an experimental signal using this procedure.

One problem is that for small D the tails of the two peaks overlap each other in the power spectra. Thus in such cases inevitably a part of the Ramsey power spectral density is included, which results in transfer of drifts to the processed signal. Inspecting the experimental signals we found that as the dark zone D is increased, the height of the first peak in the power density spectrum decreases faster than that of the second peak. It means that at large separation, the influence of Ramsey interferometer is less. The mechanism of signal decreasing of both kinds of interferometers is discussed in details in paper [41]. As the oscillation period of the Ramsey interferometer is twice that of Ramsey-Bordé interferometer, on the frequency scale the two peaks are further separated with larger D. So the larger the separation, the more stable will the interference pattern be.

Transforming the cut out band pass region back, clean interference fringes result, which are nearly free from background and high frequency noise, because of the filtering process. An example for D=400 μm is given in figure 7.5. The upper curve is the oscillation pattern from ground state exit, the lower curve from excited state exit has two oscillation patterns according to two hyperfine components. The variations of the upper curve outside the interference pattern indicates the remaining noise within the band pass.

Comparing the filtered oscillation patterns for different dark zone lengths D, we find the expected behavior. As D increases, the amplitude of oscillation decreases due to the loss of coherent molecules in excited state from spontaneous decay, while the period increases as $2D/v_0$.

As a simplified form of representation of the interference patterns the following form is used:
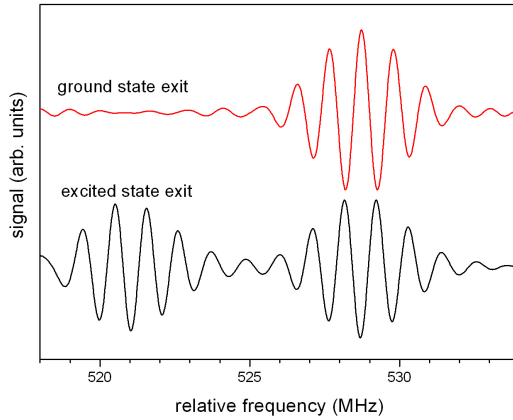
Figure 7.5.: Interference fringes after Fourier filtering (see text for details) for a separation of *D*=400 *μm*. The upper curve is vertically shifted up for better visibility
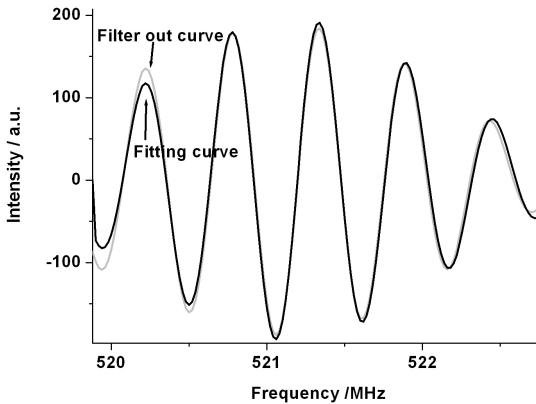

Figure 7.6.: Fitting result of one back transformed curve. The gray line represents the filtered and back transformed curve, the black line represents the fitting result.

$$I(\nu) = U + A \cdot \exp \frac{(\nu - \nu_0)^2}{\nu_w^2} \cdot \cos\left[2\pi P(\nu - \nu_0) + \varphi\right]. \qquad (7.9)$$

$I(\nu)$ describes an oscillation damped by a Gaussian envelope on a background U. The oscillation is centered at the transition frequency ν_0, with an oscillation period $P = 2D/v_x$ and a phase φ. The Gaussian envelope is centered also at ν_0 with a width ν_w. A is the common amplitude of the oscillation and Gaussian envelope. U accounts for any residual constant background after digital filtering. A result of such fitting is presented in figure 7.6. In the fitting process, the formula 7.9 does not perfectly describe the back transformed curve. In the center of the fringe there is a very good agreement, while in the wings deviations show up. The fitting process also reveals that all parameters are heavily correlated. The change of the starting or ending point of the fitted interval leads to different parameters. In order to reduce the error introduced by data processing for the measured spectra, the position of band pass filter and the starting/ending for fitted range are fixed for the same dark zone length D.

A numerical simulation is done to test the uncertainty introduced by this data processing. A series of 30 identical spectra with interference fringes were calculated using our simulation program [9] with parameters set to typical experimental values. Then Gaussian noise is added to each individual spectrum. The spectra are then treated in the same way as experimental data. The even curves are averaged as one group while odd curves are averaged as another group. The averaged curves are digitally filtered and transformed back, the filtered fringes are fitted as described before. Any resulting phase shift between even and odd labeled traces indicates the uncertainty of the data processing. For the simulated curves without noise, the fitting result for even and odd traces gives no phase difference. For the simulated curves with signal-to-noise ratio similar to the experimental one the phase difference between even and odd traces can have a standard deviation of up to 100 mrad. The influence of the band pass has been systematically analyzed. In the digital filtering, as far as the band pass filter covers the whole peak, a variation of the width of the bandpass and an asymmetry with respect to the center will not change the back transformed fringe.
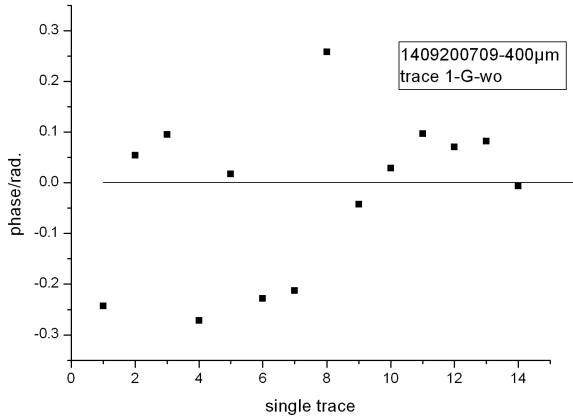
Figure 7.7.: The absolute phase of the individual fits of interference fringes under same experiment condition

7.1.6. Results and discussion

The absolute phase of each individual spectrum recorded under the same experimental condition in one long recording is fitted to test the uncertainty of the system. 14 interference fringes detected from ground state exit, under the condition without applying deflection laser beam at D= 400 μm from the same recording series are digitally filtered and fitted individually. Each spectrum is fitted by adjusting all parameters for a reasonable good fit. Then the average of parameters ν_0, w, P are fixed for the new fitting process for the identical experiment situations. U and A are varied for slow signal variations. Due to the fluctuation of molecule flux density the phase is considered to be a more reliable signal than amplitude attenuation. The phases of the 14 scans are plotted in figure 7.7. There is no obvious drift of the phase and the scattering of phase is larger than $\pm$ 200 mrad. The average process can help to reduce the error.

Then the phase difference of the averaged interference fringes under different atomic densities is calculated. In each recording, the interference fringes under the experiment situations with atom density low/high are averaged separatedly and digitally filtered. In order to reduce the error introduced by data
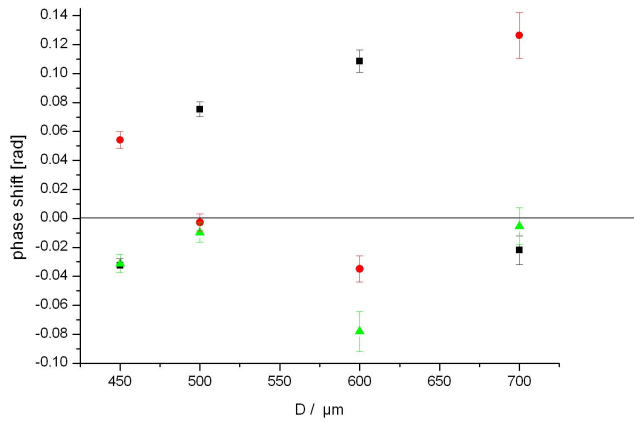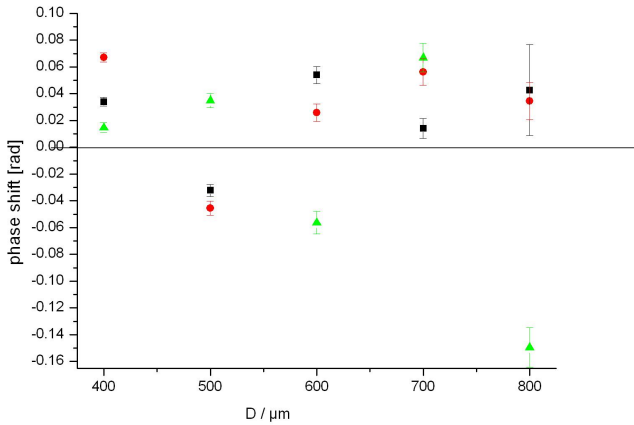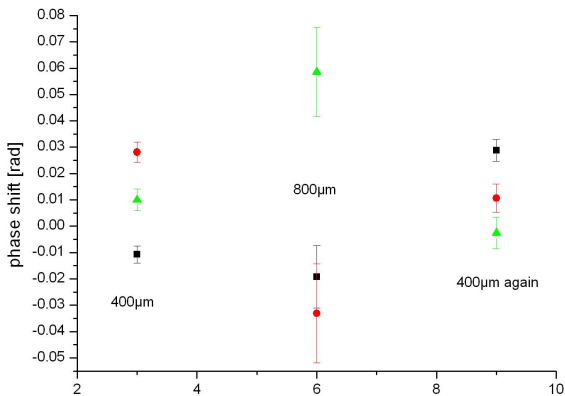
(a) Phase shift measured in one day, x-axis represents the dark zone length D
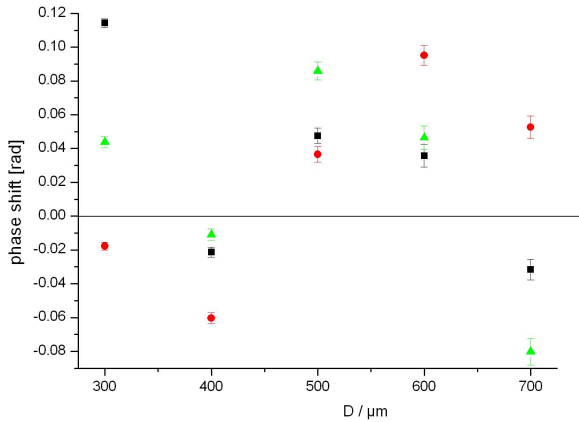
(b) Phase shift measured in one day, x-axis represents the dark zone length D

(c) Phase shift measured in one day, x-axis represents the dark zone length D

(d) phase shift measurement, this is the test starting from D = 400μm to 800μm and then back to 400μm. x-axis is chosen to display the data clearly.

Figure 7.8.: Phase shift between the interference fringes under low or high atomic density from different experiment days. The square, dot and triangle represent the phase shift by the fitting of interference pattern in ground state exit, the last hyperfine component in excited state exit, the second last hyperfine component in excited state exit.

processing for the measured spectra, the position of band pass filter and the starting/ending for fitting are fixed for the same dark zone length D. When all experimental conditions are kept the same, only the atom density is either low or high, the different index of refractions will only lead to an amplitude *A* and phase φ change, while all other parameters should be fixed for the comparison. So fitting is done by first adjusting all parameters for a reasonable good fit for low density case. Then parameters ν_0, ν_w and *P* are kept fixed in the analogous fit for the situation of high density case, the new amplitude and phase are determined. In order to exclude dependence of the result on starting parameters, the fitting sequence is reversed to check the phase shift. It is proved that the difference due to the order of fitting is much smaller than the statistical uncertainty of 10 mrad. At each dark zone length D, from ground state exit, a phase shift can be calculated. From the excited state exit, two hyperfine components give two phase shifts. From one day's measurement, the three phase shifts for each D and for a sequence of D can be compared.

Figures 7.8(a), 7.8(b), 7.8(c) and 7.8(d) represent such phase shifts measured at different days. The square, dot and triangle represent the phase shift by the fitting of interference pattern in ground state exit, the last hyperfine component in excited state exit, the second last hyperfine component in excited state exit. The error bars in the figure is the statistical error. In one measurement day, the dark zone length D starts from small value, increases with step of 100 μm. As D increases, the statistical error also increases because of the reduced signal-to-noise ratio. Take figure 7.8(a) as an example. The three data points marked by different symbols at D=450 μm represent the measured phase differences from the same recording, just read out from different exits or different hyperfine components. The scatter of these three points is around 100 mrad. The scatter of all data points is in the same order. Generally as the dark zone length D increases, the scattering of the phase difference increases because of the reduction of signal amplitude.

Figure 7.8(d) represents a test of the reproducibility of the phase shift. Starting from D = 400 μm, the dark zone length is set D = 800 μm directly and then set back to 400 μm. Comparing the phase shifts measured at D = 400 μm but at different time, no obvious drift of the value, it comes back to the original value with a scatter smaller than 50 mrad, the error bar is small. Comparing the phase shift measured at D = 400 μm and D = 800 μm, at D = 800 μm, the averaged value of all data points lifer the same shift as for D = 400 mrad, but the scatter is larger around 100 mrad and the error bar is larger.

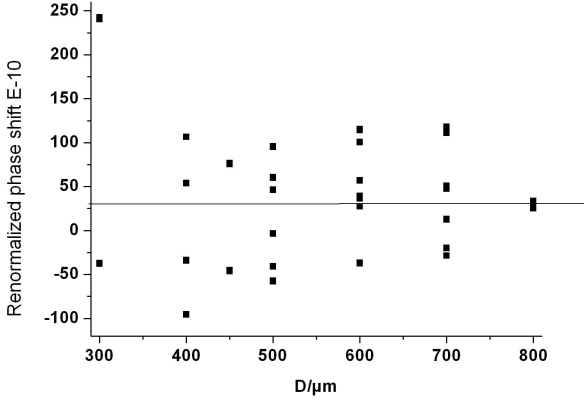As discussed in theory chapter given in equation 7.7, the renormalized phase

Figure 7.9.: Renormalized phase shift $\Delta\theta/k_0 D(1-\eta)$. The x-axis D just indicates at which dark zone length the data points were measured. y-axis is with the orders of magnitude 10^{-10}.

shift between the two different experimental situations is

$$\Delta\theta/k_0 D(1-\eta) = 2[(\epsilon_2 - \epsilon_1) - \frac{1+\epsilon_2}{k_0 v_0}\gamma] \tag{7.10}$$

All the renormalized phase shift at each dark zone length D are plotted in figure 7.9. They present the value of the right term in equation 7.10, which should be a constant and have no dependence on D. The measured value scattere positive and negative around zero, no obvious trend as D increases. The average value of $\Delta\theta/k_0 D(1-\eta)$ is 32×10^{-10} drawn as the black curve in figure 7.9. It represents the total effect of $(\epsilon_2 - \epsilon_1)$, the difference of index of refraction between excited and ground molecular state and $-\frac{1+\epsilon_2}{k_0 v_0}\gamma$, collision induced resonant frequency shift. As discussed in theory chapter, these two terms are of the same order of magnitude. Comparing the measured value with the reported value of indexes of refraction of the ground state atoms, they are ten times larger. Considering the excited state molecule, the collision happens between a P state atom and the ground state S atom. Perhaps this change of polarizability from 2S -> 2P increases the collisional cross section. This might explain the increased index of refraction value.

7.1.7. Conclusion

The cold collision experiment has been under exploration for long time in our group. Several improvements have been made:

1. Ground state exit has been implemented for detection. In one recording file, different exits and different hyperfine components give the possibility to compare the phase difference measured under the same experimental condition.

2. Different dark zone lengths are used varying from $300\mu m$ to $800\mu m$ with step of $100\mu m$. As D increases, in frequency space, the weight of first peak corresponding to Ramsey fringe decreases faster than the second peak corresponding to Ramsey-Bordé fringe, and they are further separated. But as D increase, the signal amplitude also decreases. The low signal-to-noise ratio results in big error bar. So there is a compromise in choosing D.

3. Previous results suffered from limited length of numbers in the fits [12]. This is eliminated by a new processing program which reads in all traces and saves the parameters for fitting with all digits, it improves the fitting result that the phase shift does not depend on the initial parameters and fitting sequence.

4. Phase shift derived from the measurement is in the same scale as the scattering. So we can not identify undoubtedly the collisional effect.

For the out look of this experiment, there are two points which can be improved based on the present work. The phase stabilization of the laser beam splitters described in section 5.1.1 can be implemented to get a stable embedded Ramsey interferometer. Based on the stabilization, large modulation amplitude can be applied to smear out the Ramsey interference pattern, while the Ramsey-Bordé interference pattern is not sensitive to the phase of laser beam. This method is discussed in next section 7.2.

7.2. Phase modulation for smearing out the Ramsey interference fringe inside a Ramsey-Bordé interferometer
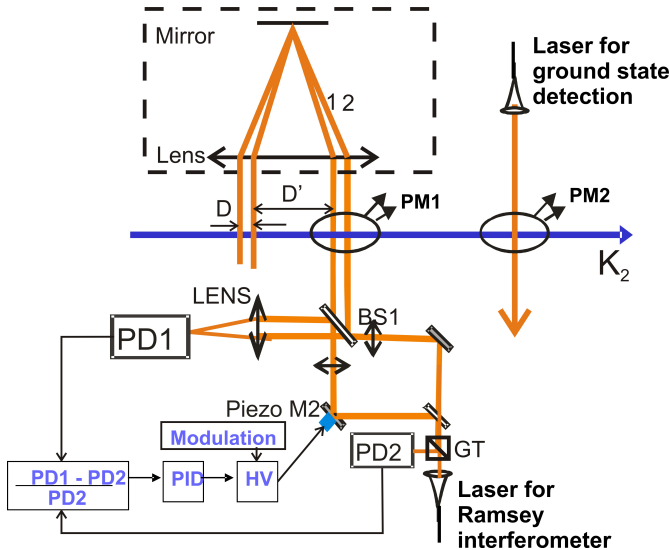

Figure 7.10.: Ramsey-Bordé interferometer with phase stabilization and phase modulation with large amplitude to smear out the signal of embedded Ramsey fringe.

As discussed in chapter 5, in the fluorescence spectrum, the interference patterns of the Ramsey setup are sensitive to the phase difference of laser beams. For a Ramsey interferometer, when a phase modulation is introduced at one laser beam with a modulation amplitude of 2π or more, the Ramsey signal will be suppressed. But for a Ramsey-Bordé interferometer, the phase modulation of the beam splitter will not influence the interference pattern. As already discussed in section 7.1, the retro-reflector results in a stable phase contribution from the laser beams on the matter wave for Ramsey-Bordé interference pattern. Any phase change from the laser beam on the matter wave will be canceled by the image of this laser beam. By this way, pure Ramsey-Bordé interference pattern can be realized experimentally.

7. Cold collision experiment

Figure 7.10 gives the whole setup of the Ramsey-Bordé interferometer with phase stabilization and modulation. The phase modulation is added to the high voltage amplifier (HV) with an amplitude to give a phase variation of 2π, and a modulation frequency of 30 Hz is applied. The retro-reflector (RR) enclosed in the box by the dashed lines produces the image of laser beam splitter 1 and 2 at $D' = 15$ mm away. The time of flight for K_2 molecule through D' is shorter than $15\mu s$. The wave front of laser beam can be viewed as static when the molecule travels through $D\prime$. Under the modulation frequency of $30Hz$, the molecule sees a static phase from the counter-propagating laser beams. So the phases imprinted from counter-propagating laser beams cancel. The distance D between a pair of laser beam is $400\mu m$.

This situation of large modulation amplitude is introduced already in section 5.1.3, and the smear out of Ramsey interference fringe is clearly seen in figure 5.8(a). As shown in Figure 7.11(a), the Ramsey-Bordé interference patterns are still clearly visible from both exits, in the Fourier transformation given in Figure 7.11(b), there appears just one frequency peak corresponding to Ramsey-Bordé interferometer.

This method can be well implemented to the experiment in section 7.1 of measuring cold collision induced phase shift on Ramsey-Bordé interferometer. The complicated data processing of separating the two interferometer signals can be avoided. Due to the lack of time, finally I did not make the systematic analysis using this method.
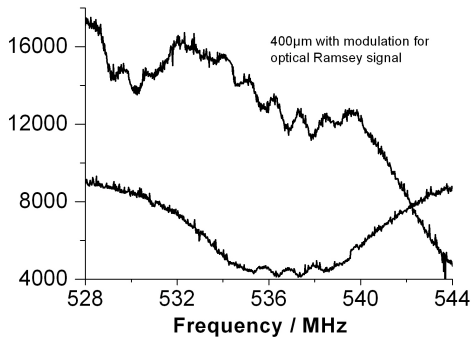
(a) Ramsey-Bordé interference signals remain when large ampli-
tude is applied for the phase modulation. The upper trace is from
excited state exit and the lower trace is from ground state exit.
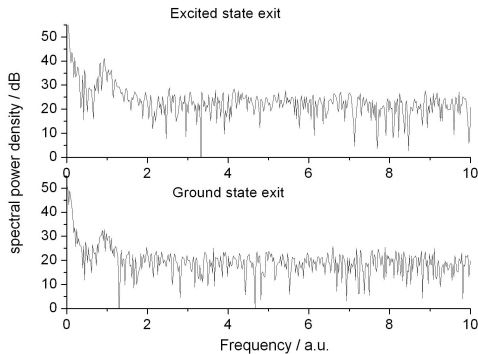
(b) Fourier transformation of interference signal from part (a).
There is just one peak corresponding to Ramsey-Bordé interfer-
ence signal for each exit.

Figure 7.11.: Using large amplitude ($\approx 2\pi$) for phase modulation to sup-
press the influence of embedded Ramsey interferometer in the
Ramsey-Bordé interferometer

7. Cold collsion experiment

8. Conclusion, open problems and outlook

8.1. Conclusion

In this thesis, I presented four experiments using two kinds of interferometers: Ramsey interferometer and Ramsey-Bordé interferometer. Each has its advantages and disadvantages. For Ramsey interferometer, the biggest advantage is the large signal-to-noise ratio. With a comparatively easy setup of two identical laser beam splitters, this interferometer preserves large molecule number. But the problem is the requirement of interferometric stability of the optical components. With our phase stabilization set-up, a stability of phase fluctuation better than 5 mrad is reachable. For Ramsey-Bordé interferometer, an intrinsic advantage is the separation of the two interaction zones, and due to a single retro reflector, the cancellation of the phases introduced from the laser beams. The problem is that the remaining molecule number for detection is small because of four laser beam splitters. After the 4th laser beam splitter, the total molecule number is less than 10% in the desired quantum state. An additional disadvantage of molecule detection compared to the atomic case is that the fluorescence detection cycle of molecule can be pathed only once. Although the wave packets fully overlap in transversal direction, which provides large contrast of the fringe, under present signal-to-noise ratio the phase measurement precision is limited to 100 mrad, since the uncertainty introduced by analysis of digital filtering is already 100 mrad. Another problem is the embedded Ramsey interferometer. This problem can be solved by either implementing multi-photon transition to incease the deflection angle or using transitions with longer life time to physically separate the two wave packets. Large amplitude modulation of the phase stabilization as discussed in section 7.2 can also be implemented to smear out the signal of Ramsey interferometer.

The first experiment describes the detection of the Ramsey-Bordé interferometer signal with ground and excited state exits. Different transitions are probed for the detection of ground state exit. The same transition for building

the interferometer is proved to be the best because of well resolved hyperfine components. Signal analysis reveals the embedded Ramsey interferometer. Digital filtering is used to separate the different oscillation signals from the two interferometers.

The second experiment is about the stabilization and the characterization of the Ramsey interferometer. The phase difference between the two laser beam splitters is stabilized and a signal analysis reveals a phase uncertainty smaller than 5 mrad. By comparing the interference fringes detected from ground state exits with separation of 30 cm, it is proved that there is no repopulation of the ground state exit within this distance. A phase modulation method is introduced, the comparison between excited and ground state exits is done and ground state exit is proved to be more suitable for signal detection. With the reduced transversal velocity distribution, the enlarged transversal coherent length results in increased interference contrast, which verifies our model of superposition of matter waves.

The third experiment investigated the possibility to measure the molecular transition dipole moment by AC-Stark effect. The transition dipole moment for $Q(25)$ $(4-0)$ $B^1\Pi_u \leftarrow X^1\Sigma_g^+$ is measured by coupling the ground state with a near resonant laser field. The phase shift imprinted on the matter waves are read out by the Ramsey interferometer. The sign of the phase shift agrees with the calculation. The magnitude of the shift is 0.5 rad, corresponding to a dipole moment two times larger than the calculated value.

The fourth experiment uses a Ramsey-Bordé interferometer to detect the cold collision between the molecules and ground state atoms within the particle beam. By deflecting the atoms out of the molecular beam, the density of the collision medium changes. The shift of the interference pattern due to the change of medium density corresponds to the difference of index of refraction of 3^{-10} for excited and ground states.

8.2. Open problems

The interference structures from excited state and ground state exits should be reversed to each other. But in the recorded spectrum, the Ramsey interference fringe is always much more dominant in ground state exit than in excited state exit. This needs further investigation to explain.

8.3. Outlook

Using AC-Stark effect to measure the transition dipole moment, smaller F state can simplify the analysis because of much less M_F components. But it concerns also the change of the interferometer transition. Since there are a lot of specific requirements of the interferometer transition e.g. long life time, well resolved hyperfine splitting, available laser system and detection range, a suitable transition was not readily found.

The transition dipole moment between interferometer ground state $X^1\Sigma_g^+$ and a higher level $B^1\Pi_u$ is measured. But for the transition dipole moment between interferometer excited state $b^3\Pi_u$ and higher levels $4^3\Delta_g$, $4^3\Sigma_g^+$, $3^3\Pi_g$ and $2^3\Delta_g$, the spectroscopic work published by other groups could not be repeated in our lab. Thus more spectroscopic work is needed to check the internal consistency of the spectroscopic data. This is a prerequisite for measurements of transition moments.

For an improvement of collision experiment, the Ramsey interferometer can be used to perform the collision experiment, due to its better signal-to-noise ratio. The stability of the phase difference between the two laser beam splitters is proved to be better than the uncertainty of Ramsey-Bordé interference pattern obtained by the complex numerical analysis. For the data analysis, one would not need to separate the two different kinds of interferometers.

The collision induced phase shift can be increased by enlarging the cross section between molecules and atoms. For this purpose the excitation to atomic Rydberg state is a good chance.

8. Conclusion, open problems and outlook

A. Interferometer set-up

A.1. The alignment of the molecular beam

In figure A.1, the vacuum chamber set-up is shown, for each assignment detail please see [12]. From right side, the K_2 will be produced through heating of the oven and expansion out of the nozzle. In order that the K_2 molecular beam can travel through both skimmer, a He-Ne laser, marked by the solid line in the middle, is used. The He-Ne laser injects from the left end view port of the interferometer chamber, passes both skimmers. Then, the oven is aligned such that the He-Ne laser goes through the nozzle and parallel to the oven body. The parallerity can be checked by leading the He-Ne laser through a long tube which is at the same height as the nozzle and attached to the end cap of the oven. A beam experiment is necessary to fine adjust the oven position to improve the fluorescence signal strength.
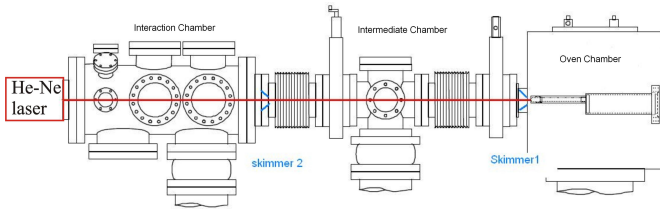

Figure A.1.: Scheme of alignment of the molecular beam

A.2. Perpendicular alignment of the laser beam

For the alignment of Ramsey Bordé interferometer, all four lasers need to cross the molecular beam at the same angle, the simpleset case is all perpendicular. So we first align one laser beam perpendicular to the molecular beam. In figure A.2(a) left, the retroreflector is composed of a lens and a high reflecting

mirror($R > 99\%$), sitting at the focus point of the lens. The laser goes through the center of the lens of the retroreflector, the reflected beam overlap with the incoming beam. When the laser is not perpendiuclar with the molecular beam, the incoming and outgoing beam meet the molecular beam at different angles, due to Doppler effect, the positions of the hyperfine components in the fluorescence spectroscopy have a shift. The direction of the incoming beam is adjusted so that, the positions of hyperfine components in fluorescence spectrum from both incoming and outgoing laser beams overlap with each other. When the intensity is lower than saturation intensity, a power effect can be clearly seen by blocking the reflected beam. Now the laser beam is perpendicular to the molecular beam. The height of the laser beam can be shifted up and down by lifting the fiber coupler to meet the center of the molecular beam.

A.3. Parallelity alignment over distance

A resonator built from two end mirrors is used to align a pair of counterpropagating laser beams parallel to each other. In figure A.2(a) right, on the base of the step before, a high reflecting mirror($T < 4\%$), is set at the other side of the K_2 beam than the retroreflector. Together with the end mirror of retroreflector, these two flat reflecting surfaces form a resonator. The peak spaced by free spectrum range can be observed in the oscilliscope. When the translation stage 1, which holds the retroreflector, is shifted out, the distance for the light travelling inside the resonator doubles and the free spectrum range decrease to a half, the peak intensity also decrease to a half. By reading the mark on the micro screw, the distance between the pair of counterpropagating laser beam can be set. The reflected laser beam hit the molecular beam with the same velocity ensemble at the same height. When molecules travel through the first laser beam, the laser intensity is so high that it drives all molecules to excited state. When the same ensemble of molecules with same velocity distribution is met by the second laser, there is no molecule to be excited, so a dip appears on the fluorescence line profile. The fine adjustment of the parallelity is done in fluorescence spectroscopy by observing the position of saturation dip. When both laser beams are perpendicular to K_2 beam, the saturation dip is in the middle of the line profile.

A.4. Parallelity alignment for a pair of laser beam

For Ramsey Bordé interferometer, we need two pairs of counterpropagating laser beams. We already got one pair from the method in last section, now we split the incoming laser into two, as show in figureA.2(b). The beam splitters BS1, BS2, and mirrors M1, M2 are arranged symmetrically to split and recombine laser beam. Out of fiber coupler, the laser beam is split by BS1, the laser beam travels through BS1, M1 and BS2 is aligned as discussed in A.2(a). This laser beam works as reference. Translation stage 2 is aligned to travel parallel to the laser beam, that is reflected by BS1. With translation stage 2 and mirror M2, the other laser beam is adjusted to overlap perfectly with reference laser beam so that the interference pattern of two laser wave fronts is totally dark. And later cylindrical lens are installed to focus the intensity at the plane where the laser beam across the K_2 beam. Laser beam goes through the optical axis of the lens. And one lens is fixed on translation stage 2(TS2), when TS2 moves, the alignment of TS2 makes sure the reflected laser beam from M2 always through the center of lens, so that it can reduced the angle distortion when setting the separation between a pair of coprapagating laser beams later. The parallelity of the pair of focused laser beams is fine adjusted by a camera at the virtual position of the molecular beam. The interference pattern of the two focused laser ellipse is totally dark.

A.5. Separation setting

As shown in figure A.2(b), by shifting translation stage 2 (TS2), the separation between a pair of coprapagating laser beams 3 and 4 can be fixed. Because the traveling direction of TS2 is parallel to laser beam reflected by BS1, the reflected laser beam from M2 goes through the center of the cylindrical lens, and keeps the plane of the wave front parallel with laser beam 4. The retroreflector makes the mirror image of laser beam 3 and 4 a certain distance upstream of the molecular beam. And the waists of laser beam 1 and 2 also lie at the molecular beam. For the experiment set-up of two zone optical Ramsey interferometer, the retroreflector is blocked.

Retroreflector Translation stage 1

Mirror

Lens

K_2 K_2

Interferometer laser beam

(a) Counterpropagating beam alignment

K_2 1 2 3 4 K_2

BS2 M1

M2 BS1

Translation stage 2

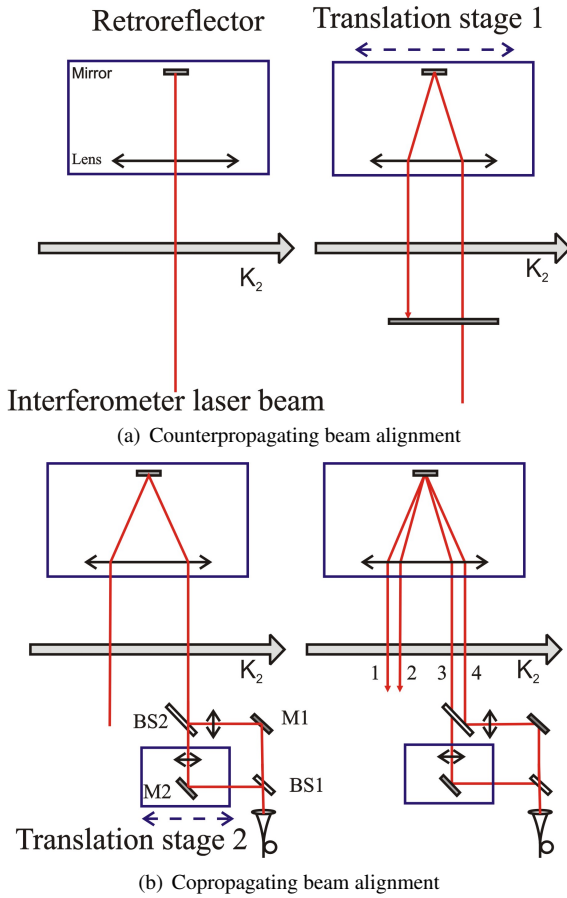(b) Copropagating beam alignment

Figure A.2.: The interferometer alignment

B. Labview program for sequence control

This is an extension work based on the labview program I used during my diplom work. The details please see appendix A in thesis [10].
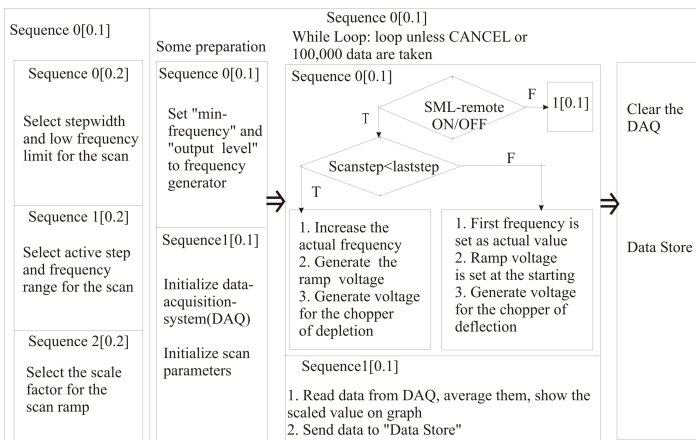

Figure B.1.: This is got from the appendix A in thesis [10].

The while loop in figure B.1 is modified. Instead of two sequence, it is divided into five different steps as shown in figure B.2.

Start from scan frequency increasing case

1. frequency increase by one step (in scan frequency decreasing case, decrease by one step)

2. wait 50 ms for RF generator reaches a stable output

3. set chopper open, check the status of chopper, when the open status is confirmed, read out and average the data from data acquisition system (DAQ) and save data

4. close chopper, check the status of chopper, when the closed status is confirmed, read out and average the data from DAQ and save data

5. check whether it reaches the full scan length. When no, go to item 0, repeat the five steps; when yes, go to item 0, decrease the frequency, repeat the following four steps till the end of the full scan length, change again

Sequence0	Sequence1	Sequence2	Sequence3	Sequence4
frequency setting	waiting 50ms	set chopper open	set chopper close	depends on the scan number odd or even
	wait for stable performance of frequency generator	check chopper condition	check chopper condition	set the frequency scanning step by +1 or -1
		average data and send data	average data and send data	

Figure B.2.: The five steps sequence program to synchronize the chopper with the frequency setting

C. Program to calculate phase shift

```
 > restart;
> q1:= abs((((F+1)^2-x^2)/((2*F+3)*(F+1)*(2*F+1))));
> q2:=subs(F=28,q1);
> q3:=simplify(sum(2*A*q2*(1-A*q2), x=-28..28)/(2*28+1));
> plot(q3,A=0..150);
> q4:=2*72.457*q2*(1-72.457*q2);
> plot(q4,x=-28..28);
#beamsplitter as function of M
> evalf(subs(x=28,q4));
  q4 := 144.914

> N1:= abs(x^2/((2*F+1)*(F+1)*F)*(F+1));
# 3j*(F+1) for phase shift
> N2:=subs(F=28,N1);
> N3:= abs(((F+1/2)^2-(x-1/2)^2)/(2*F*(F+1)*(2*F+1))*(F+1));
# 3j*(F+1) for phase shift
> N4:=subs(F=28,N3);
> N5:= abs(((F+1/2)^2-(x+1/2)^2)/(2*F*(F+1)*(2*F+1))*(F+1));
# 3j*(F+1) for phase shift
> N6:=subs(F=28,N5);

> I1:=sum(q4*cos(m),x=-28..28)/(2*28+1);
 #unperturbed interferometer
> plot(I1,m=1.57078..1.5708);

 Start detuning calculation
 Detu1:=(Delta/(8*D))*(mu^2*3/(hbar*Delta)^2)
        *(P/(z*C*epsilon));
```

C. Program to calculate phase shift

```
DetuTst:=mu^2*P/(4*hbar^2*D*Delta*C*epsilon*z);

tst:=simplify(Detu1/DetuTst);
Detu2:=subs(mu=1.15*10^(-29),P=0.007,
hbar=1.054571*10^(-34),pi=3.1415926,
D=400*10^(-6),Delta=2*3.1415926*300*10^6,
C=3*10^(+8),  epsilon=8.854*10^(-12),
 z=2*10^(-3),Detu1);
# experimental parameters

> phapi:=2*N2*Detu2/2315000;
 #M dependence for pi polarisation,
large factor in denominator period of fringe in Hz

> evalf(subs(x=14,phapi));

> I2:= sum(q4*cos(m+phapi),x=-28..28)/(2*28+1);
 plot(I2,m=0.7633..0.7634);
> evalf(subs(m=0.763,I2));

> phasig:=(N4+N6)*Detu2/2315000;
#M dependence for sigma polarisation,
large factor in denominator period of fringe in Hz

> evalf(subs(x=0, phasig));
> I3:= sum(q4*cos(m+phasig),x=-27..27);
> I4:=(I3+subs(x=-28,q4*cos(m+(N4)*Detu2/2315000))
+subs(x=28,q4*cos(m+(N6)*Detu2/2315000)))/(2*28+1);

> plot(I4,m=0.301..0.3025);
> evalf(subs(m=0.304,I4));
```

Bibliography

[1] C. Cohen-Tannoudji, B. Diu, F. Laloe, Quantum mechanics, Wiley, 2005

[2] T.D. Hammond, M.S. Chapman, A. Lenef, J. Schmiedmayer, E.T. Smith, R.A. Rubenstein, D. Kokorowski, D.E. Pritchard, Braz. J. Phys. **27**, 193 (1997).

[3] J. Schmiedmeyer, M.S. Chapman, C.R. Ekstrom, T.D. Hammond, S. Wehinger, D.E. Pritchard, Phys. Rev. Lett. **74**, 1043 (1995).

[4] M.S. Chapman, C.R. Ekstrom, T.D. Hammond, R.A. Rubenstein, J. Schmiedmeyer, S. Wehinger, D.E. Pritchard, Phys. Rev. Lett. **74**, 4783 (1995).

[5] B. Brezger, L. Hackermüller, S. Uttenthaler, J. Petschinka, M. Arndt, and A. Zeilinger, Phys. Rev. Lett. 88, 100404 (2002).

[6] K. Hornberger, S. Uttenthaler, B. Brezger, L. Hackermüller,M. Arndt, and A. Zeilinger, Phys. Rev. Lett. 90, 160401, (2003)

[7] P.R.Berman, Atom Interferometry. Academic press 1997

[8] K.Senstock, Ph.D thesis, Rheinishcen Friedrich-Wilhelms-Universität Bonn(1993)

[9] Ch.Lisdat, Ph.D thesis Leibniz Universität Hannover 2001 http://edok01.tib.uni-hannover.de/edoks/e01dh01/328751421.pdf

[10] Sha Liu: *Molecular matter wave interferometry: laser system, method of detection and application*, Diploma work, Leibniz Universität Hannover 2005.

[11] S.Jung: *Untersuchungen zur Manipulation von Stossbedingungen zwischen Atomen und Molekülen für ein Materiewelleninterferometer* Diploma work, Leibniz Universität Hannover 2002

[12] I.Sherstov Ph.D thesis 2006 Leibniz Universität Hannover http://edok01.tib.uni-hannover.de/edoks/e01dh06/515384828.pdf

[13] G.Scoles, Atomic and Molecular Beam methods. Oxford University Press 1988

[14] Ch.Salomon, Ph.D thesis, 1984 Université Paris-Nord, Laboratoire de physique des lasers

[15] Ch. M. Samuelis, Ph.D thesis, Leibniz Universität Hannover 2003, http://edok01.tib.uni-hannover.de/edoks/e01dh03/360554377.pdf

[16] S. Liu, I.Sherstov, C. Lisdat, H. Knöckel, E.Tiemann submitted to EPJD

[17] Ch. Lisdat, M. Frank, H. Knöckel, M.-L. Almazor, E. Tiemann, Eur. Phys. J. D **12**, 235 (2000).

[18] M. Jacquey, A. Miffre, G. Trénec, M. Büchner, J. Vigué, A. Cronin, Phys. Rev. A **78**, 013638 (2008).

[19] A. Miffre, M. Jaquey, M. Büchner, G. Trénec, J. Vigué, Phys. Scr. **74**, C15 (2006).

[20] A. Shelkovnikov, C. Grain, R.J. Butcher, A. Amy-Klein, A. Goncharov, C. Chardonnet, IEEE J. Quant El., **40**, 1023 (2004).

[21] Ch. J. Bordé, N. Courtier, F. du Burk, A.N. Goncharov, M. Gorlicki, Phys. Lett. A**188**, 187 (1994).

[22] S. Gerlich, L. Hackermüller, K. Hornberger, A. Stibor, H. Ulbricht, M. Gring, F. Goldfarb, T. Savas, M. Müri, M. Mayor, M. Arndt, Nature Physics **3**, 711 (2007).

[23] Ch. Lisdat, M. Frank, H. Knöckel, E. Tiemann Appl. Phys. B **73**, 99 (2001).

[24] Jacques Vanier and Claude Audoin, Metrologia 42 (2005) S31-S42

[25] Ch. Lisdat, O. Dulieu, H. Knöckel, E. Tiemann, Eur. Phys. J. D **17**, 319 (2001).

[26] Ch. Lisdat, H. Knöckel, E. Tiemann, J. Mol. Spectr. **199**, 81 (2000).

[27] R.A. Logan, R.E. Coté, P. Kusch, Phys. Rev. **86**, 280 (1952)

[28] J. Heinze, F. Engelke, J. Chem. Phys. **89**, 1 (1988).

[29] N. F Ramsey, Metrologia 42 (2005) S1-S3, doi:10.1088/0026-1394/42/3/S01

[30] C. Cohen-Tannoudji, J. Dupont-Roc, G. Grynberg, Atom-Photon Interactions, Basic Processes and application, John Weley & Sons, Inc, 1992.

[31] C. R. Duane, The theory of atomic structure and spectra, University of California Press, 1981.

[32] J. Heinze, F. Engelke, J. Chem. Phys. 89, 1 (1988)

[33] Hansson, Watson, A comment on Hönl-London factor, J.Mol.Spectr. 233 (2005) 169-173

[34] A. Gerdes, private communication (2009).

[35] J. Vigué, Phys. Rev. A **52**, 3973 (1995).

[36] C. Champenois, E. Audouard, P. Duplàa, J. Vigué, J. Phys. II France, **7**, 523 (1997).

[37] T.D. Hammond, M.S. Chapman, A. Lenef, J. Schmiedmayer, E.T. Smith, R.A. Rubenstein, D. Kokorowski, D.E. Pritchard, Braz. J. Phys. **27**, 193 (1997).

[38] M.S. Chapman, C.R. Ekstrom, T.D. Hammond, R.A. Rubenstein, J. Schmiedmayer, S. Wehinger, D.E. Pritchard, Phys. Rev. Lett **74**, 4783 (1995).

[39] Tony D. Roberts, Alexander D. Cronin, David A. Kokorowski, and David E. Pritchard Phys. Rev. Lett. 89, 200406 (2002).

[40] C. Champenois, M. Jacquey, S. Lepoutre, M. Büchner, G. Trénec, J. Vigué Phys. Rev.A **77**, 013621 (2008)

[41] Sh. Liu, I. Sherstov, Ch. Lisdat, H. Knöckel, and E. Tiemann EPJ manuscript No. submitted

[42] J. Schmiedmayer1, M. Chapman1, Ch. Ekstrom1, T. Hammond1, S. Wehinger, and D. Pritchard, Phys. Rev. Lett. 74, 1043 - 1047 (1995)

[43] U. Sterr et al. in Atom interferometry, edited by P.R. Berman, Academic Press (1997)

[44] I. Sherstov, S. Liu, Ch. Lisdat, H. Schnatz, S. Jung, H. Knöckel, and E. Tiemann, *Frequency measurements in the b* $^3\Pi(0_u^+) - X\ ^1\Sigma_g^+$ *system of* K_2, Eur. Phys. J. D 41, 485-492 (2007), highlight paper DOI: 10.1140/epjd/e2007-00013-1.

Bibliography

Curriculum Vitae

Name: Sha Liu
Date of Birth: 29.12.1980
Place of Birth: Hunan, China
Parents: Zhizhong Liu, Shujun Peng
Nationality: Chinese
Family Status: Single

Education:
- January 2006 - December 2009
  Ph.D student in Prof. Dr. Tiemann working group,
  Leibniz University Hannover, Germany
- January 2006 - December 2008
  member of European Graduate College 605,
  Interference and quantum application
- October 2003 - December 2005
  Diploma(MSc) of science in Physics,
  Leibniz University Hannover, Germany
- September 1999 - July 2003
  BSc degree in physics, microelectronic department,
  Sun Yat-Sen university, Guangzhou, China
- September 1993 - July 1999
  Changjun middle school, Changsha, Hunan, China
- September 1987 - July 1993
  Lirenpo primary school, Changsha, Hunan, China

Bibliography

Acknowledgements

Many contributions to the success of this this work for which I am sincerely grateful. My special thanks to:

- Mr.Prof.Dr.Eberhard Tiemann, that I could have the chance to make so many interesting experiments. I appreciate his patience in answering all the questions and his serious, honest attitude toward scientific research.

- Mr. Dr. Horst Knöckel for his long time and very useful help in solving the complicated problems in the lab. And also for the countless very valuable discussions of the experiment.

- Mr. (soon be Dr. when I am writing still yet Dipl.-Phys.) Andreas Gerdes. Sincerely thank you for your generous help that at any time any moment you are always so kind ready to help others. Also the countless discussion of all important things, experiment and life.

- Mr. Dr. Ivan Sherstov for his guide at the lab in the beginning of my research work and the attitude toward lab life.

- All present and former members of the working group: Dr. Olivier Allard, Dr. Sebastian Jung, Dr. Stephan Falk, Dr. Christian Lisdat, Dr. Asen Pashov, Dipl. Phys. Oleg Bucicov, Dipl. Phys. Alexander Stein for discussions and the everydayś lab life

- Mon cher ours, merci beaucoup pour ton aide et ton attention soucieuse tout au long de mon travail de thèse